

Universidade de São Paulo

Instituto de Física

Linear perturbations of black holes: stability, quasi-normal modes and tails.

Alexander Zhidenko

Orientador : Prof. Dr. Élcio Abdalla

Tese de doutorado apresentada no
Instituto de Física para a obtenção
do título de Doutor em Ciências.

Comissão Examinadora

Prof. Dr. Élcio Abdalla (Orientador, IFUSP)

Prof. Dr. Alberto Vasquez Saa (IMECC, Unicamp)

Prof. Dr. Laerte Sodré Junior (IAGUSP)

Prof. Dr. Vilson Tonin Zanchin (UFABC)

Prof. Dr. Patrício Aníbal Letelier Sotomayor (IMECC, Unicamp)

São Paulo

2009

FICHA CATALOGRÁFICA
Preparada pelo Serviço de Biblioteca e
Informação
do Instituto de Física da Universidade de São
Paulo

Zhydenko, Olexandr

Perturbações lineares de buracos negros: estabilidade, modos quase normais e caudas, São Paulo, 2009.

Tese (Doutorado) – Universidade de São Paulo.
Institutos de Física - Depto. de Física Matemática

Orientador: Prof. Dr. Élcio Abdalla

Área de Concentração: Física

Unitermos: 1. Relatividade (Física); 2. Física Teórica;
3. Teoria de Campos e Ondas; 4. Física computacional

USP/IF/SBI-046/2009

Abstract

Black holes have their proper oscillations, which are called the quasi-normal modes. The proper oscillations of astrophysical black holes can be observed in the nearest future with the help of gravitational wave detectors. Quasi-normal modes are also very important in the context of testing of the stability of black objects, the anti-de Sitter/Conformal Field Theory (AdS/CFT) correspondence and in higher dimensional theories, such as the brane-world scenarios and string theory.

This dissertation reviews a number of works, which provide a thorough study of the quasi-normal spectrum of a wide class of black holes in four and higher dimensions for fields of various spin and gravitational perturbations. We have studied numerically the dependance of the quasi-normal modes on a number of factors, such as the presence of the cosmological constant, the Gauss-Bonnet parameter or the aether in the space-time, the dependance of the spectrum on parameters of the black hole and fields under consideration. By the analysis of the quasi-normal spectrum, we have studied the stability of higher dimensional Reissner-Nordström-de Sitter black holes, Kaluza-Klein black holes with squashed horizons, Gauss-Bonnet black holes and black strings. Special attention is paid to the evolution of massive fields in the background of various black holes. We have considered their quasi-normal ringing and the late-time tails.

In addition, we present two new numerical techniques: a generalisation of the Nollert improvement of the Frobenius method for higher dimensional problems and a qualitatively new method, which allows to calculate quasi-normal frequencies for black holes, which metrics are not known analytically. Also we considered a possibility of construction of the acoustic analogue of the Schwarzschild black hole.

Contents

1	Introduction	11
2	Black hole perturbations	15
2.1	Equations of perturbations near a black hole	15
2.2	Time evolution of perturbations	18
2.3	Properties of the quasi-normal spectrum	20
2.3.1	Boundary conditions	20
2.3.2	Quasi-normal spectrum and black hole stability	22
2.3.3	Isospectrality	23
3	Numerical methods of calculation of the quasi-normal modes	25
3.1	Fitting time-domain data	25
3.2	Approximation by the Pöschl-Teller potential	26
3.3	WKB method	28
3.4	Frobenius method	31
3.4.1	Frobenius series	31
3.4.2	Method of a continued fraction	31
3.4.3	Nollert improvement	33
3.4.4	Continuation of the Frobenius series through midpoints	34
3.4.5	Generalisation of the Frobenius series	34
3.4.6	Frobenius series for the radial part of the charged field equation in the Kerr-Newman-de Sitter background	36
3.4.7	Frobenius series for the massive scalar field equation in the higher-dimensional Reissner-Nordström-de Sitter background	36
3.5	Horowitz-Hubeny method	38
4	Perturbations of four-dimensional black holes	39
4.1	Quasi-normal modes of Schwarzschild and Schwarzschild-de Sitter black holes	39
4.2	High overtones in the quasi-normal spectrum	40
4.3	Decay of charged scalar and Dirac fields in the Kerr-Newman-de Sitter background	41
5	Perturbations of higher-dimensional black holes	45
5.1	Stability and quasi-normal modes of Reissner-Nordström-de Sitter black holes	45
5.2	(In)stability of D -dimensional black holes in the Gauss-Bonnet theory	49
5.3	Quasi-normal modes of brane-localised Standard Model fields	52
5.3.1	Kerr black holes	53
5.3.2	Gauss-Bonnet black holes	56
5.4	Perturbations of squashed Kaluza-Klein black holes	59

5.4.1	Quasi-normal modes of the scalar field for rotating squashed Kaluza-Klein black holes	60
5.4.2	Gravitational quasi-normal modes for non-rotating squashed Kaluza-Klein black holes	62
6	Massive fields around black holes	65
6.1	Evolution of massive fields. Quasi-resonances	65
6.2	Quasi-normal spectrum of the massive scalar field around Schwarzschild black holes	66
6.3	Stability and quasi-normal modes of the massive scalar field around Kerr black holes	68
6.4	Quasi-normal modes of black strings and the Gregory-Laflamme instability	71
6.5	Late-time tails of massive fields	74
7	Quasi-normal modes of black holes, whose metrics are unknown analytically	77
7.1	Numerical methods	77
7.2	Quasi-normal modes of the scalar hairy black hole	79
7.3	Perturbations and quasi-normal modes of black holes in the Einstein-Aether theory	81
8	Perturbations of Schwarzschild black holes in laboratories	87
8.1	Acoustic analogue of gravity	87
8.2	de Laval nozzle	87
8.3	de Laval nozzle for the Schwarzschild black hole	90
9	Summary	93

List of Figures

2.1	The integration grid. Each cell of the grid represents an integration step. The thick points illustrate the choice of (S, W, E, N) for the particular step of the integration. The initial data are specified on the left and bottom sides of the rhombus.	19
2.2	The three stages of the evolution of the Schwarzschild black hole gravitational perturbations ($l = 2$ vector type, $\Lambda = 0$, $R = 22M$). Time is measured in units of the horizon radius.	20
3.1	The three regions separated by the two turning points $Q(x) = 0$	28
4.1	Real and imaginary parts of the fundamental quasi-normal frequency of the Schwarzschild-de Sitter black hole for scalar ($l = 2$), electromagnetic ($l = 2$), gravitational ($l = 2$), and Dirac ($\kappa = 2$) perturbations plotted with solid blue, dashed red, dot-dashed green and dotted black lines respectively.	40
4.2	Real part of the highly damping quasi-normal frequencies as a function of imaginary part ($\kappa_{\pm} = 1$ perturbations of the massless Dirac field in the Schwarzschild background). The frequencies are measured in inverse units of the black hole mass.	41
4.3	Real part of highly damping quasi-normal frequencies as a function of imaginary part for Schwarzschild-de Sitter black hole ($l = 1$ electromagnetic perturbations, $\Lambda M^2 = 0.02$). The frequencies are measured in inverse units of the black hole mass.	42
4.4	Real part of highly damping quasi-normal frequencies as a function of imaginary part ($l = 2$ metric perturbations of the Schwarzschild-de Sitter black hole, $\Lambda M^2 = 0.02$). The frequencies are measured in inverse units of the black hole mass.	43
4.5	Real part and imaginary part of the fundamental quasi-normal frequency of charged (q) scalar field ($l = 0$) for the charged (Q) black hole.	43
5.1	Effective potentials and time-domain profiles for scalar-type gravitational perturbations, $D = 5$ (blue) . . . $D = 11$ (red) ($l = 2$, $Q = 0$, $\Lambda = 0$). For higher D both the peak and the negative gap of the potential increase. Profile for higher D decays quicker. All quantities are measured in units of the event horizon r_+	47
5.2	Time-domain profiles for scalar-type gravitational perturbations of 11-dimensional Schwarzschild-de Sitter black hole ($Q = 0$, $D = 11$, $\rho = r_+/r_{\infty}$) for $\rho = 0.3$ (blue), $\rho = 0.5$ (green), $\rho = 0.7$ (yellow), $\rho = 0.8$ (orange), $\rho = 0.9$ (red). Profile for higher ρ decays slower. All quantities are measured in units of the event horizon r_+	47
5.3	Time-domain profile for gravitational perturbations of scalar type “-” of the Reissner-Nordström-de Sitter black hole ($D = 11$, $\rho = r_+/r_{\infty} = 0.8$, $l = 2$) for various values of the black hole charge $q = Q/Q_{ext}$: $q=0.4$ (brown) $q=0.5$ (blue) $q=0.6$ (green) $q=0.7$ (orange) $q=0.8$ (red) $q=0.9$ (magenta). The smaller q , the slower growth of the profile is.	48

5.4	The parametric region of instability in the right upper corner of the square ($\rho = r_+/r_\infty$, $q = Q/Q_{ext}$) for $D = 7$ (top, black), $D = 8$ (blue), $D = 9$ (green), $D = 10$ (red), $D = 11$ (bottom, magenta).	49
5.5	The picture of instability of tensor-type of gravitational perturbations of Gauss-Bonnet black holes, developing at large multipole numbers: $D = 6$, $l = 8$ (red), $l = 12$ (green), $l = 16$ (blue), $\alpha = 1.3$. All quantities are measured in units of the event horizon r_+	52
5.6	The threshold α as a function of the inverse multipole number l for tensor type of gravitational perturbations of Gauss-Bonnet black holes $D = 6$. The points $l = 16, 20, 32, 40, 50, 64$ were fit by the line $\alpha = 2.627l^{-1} + 1.005$. The theoretical result is $\alpha_t \approx 1.006$ (the value of α is measured in units of the event horizon r_+).	53
5.7	The picture of time-domain evolution for scalar-type gravitational perturbations of Gauss-Bonnet black holes $D = 10$, $l = 2$, $\alpha = 0.01$. One can see that two modes are dominating at the different stages. All quantities are measured in units of the event horizon r_+	54
5.8	Fundamental quasi-normal modes for the 6-dimensional black hole projected on the 4-brane.	55
5.9	A few higher overtones of the electromagnetic field for the 6-dimensional Kerr black hole projected on the 4-brane ($l = 3$, $m = 0$) for the range $(0, r_+)$ of the angular momentum parameter a with a step of $r_+/8$	56
5.10	Fundamental quasi-normal modes for the higher-dimensional Kerr black hole ($a = r_+$) projected on the 4-brane.	57
5.11	The quality factor of the scalar field localised on the 4-brane as a function of the Gauss-Bonnet parameter α ($D = 9$, $l = 1$).	58
5.12	The time-domain profiles of the brane-localised massless scalar field for the Gauss-Bonnet black hole ($D = 7$, $\alpha = 5$) for $l = 0$ (blue), $l = 1$ (green), $l = 2$ (orange), $l = 4$ (red). The bigger l corresponds to the longer life of quasi-normal ringing and the quicker tail decay.	59
5.13	Real and imaginary part of the fundamental quasi-normal frequency of the test scalar field ($l = 0$) for rotating squashed Kaluza-Klein black holes.	61
5.14	Real and imaginary parts of the fundamental quasi-normal frequency for metric perturbations ($M = J = 0$) $ K = 0$ (blue), $ K = 1$ (red), $ K = 2$ (yellow) of squashed Kaluza-Klein black holes. Higher values of K correspond to higher oscillation frequency and slower damping.	63
6.1	Three higher quasi-normal modes ($l = 0$) of the Schwarzschild black hole ($D = 6$) for the massive scalar field of various μ . The frequency for $\mu = 0$ has the largest imaginary part. The points were plotted with the step of $\Delta\mu r_+ = 1/2$. Solid lines mark the same overtone number.	67
6.2	Fundamental quasi-normal frequencies for the D -dimensional Schwarzschild black hole for the massive scalar field ($l = 0$) of various μ . The frequency for $\mu = 0$ has the largest imaginary part. The points were plotted with the step of $\Delta\mu r_+ = 1/10$. Solid lines mark the same number of D	68
6.3	Fundamental quasi-normal frequencies of the Schwarzschild black hole ($D = 6$) for the massive scalar field as function of the field mass μ for $l = 0, 1, 2$ (represented as dots, rhombuses and triangles respectively). The dashed line corresponds to $\text{Re}(\omega) = \mu$	69

6.4	High overtones of the Schwarzschild black hole for the massive scalar field ($D = 4$, $l = 0$) for $\mu r_+ = 0.6$ (dots) and $\mu r_+ = 6.0$ (boxes).	70
6.5	The fundamental quasi-normal frequency of Kerr black holes for the massive scalar field as a function of azimuthal number m for $l = 6$, $a = 0.15r_+$, $\mu r_+ = 0.2$	71
6.6	Time-domain profiles of black string perturbations for $kr_+ = 2.5$: $n = 2$ (red, top), $n = 3$ (orange), $n = 4$ (green), $n = 5$ (blue, bottom). Late-time decay of perturbations for $n \geq 3$ is $\Psi \propto t^{-(n+6)/2} \sin(kt)$	73
6.7	Time-domain profiles of black string perturbations for $n = 1$ $kr_+ = 0.84$ (magenta, top), $kr_+ = 0.87$ (red), $kr_+ = 0.88$ (orange), $kr_+ = 0.9$ (green), $kr_+ = 1.1$ (blue, bottom). We can see two concurrent modes: for large k the oscillating one dominates, near the critical value of k the dominant mode does not oscillate, for unstable values of k the dominant mode grows. The plot is logarithmic, so that straight lines correspond to an exponential growth or decay.	74
7.1	The effective potential for electromagnetic perturbations near the Schwarzschild black hole ($r_+ = 1$, $l = 2$) and the same potential interpolated numerically near its maximum.	78
7.2	Dependance of the real and imaginary parts of the quasi-normal frequency on Q for the scalar hairy black hole. The imaginary part quickly decreases as the “scalar charge” Q increases. The real part reaches its maximum and then quickly falls down to zero. It vanishes for some non-critical charge $Q_0 < \xi^{-1/2}$. For $Q \geq Q_0$ the real part remains zero and the frequency is purely imaginary (within numerical precision).	81
7.3	Dependance of the real and imaginary parts of the quasi-normal frequency on Λ for the scalar hairy black hole. The real part increases for relatively small “scalar charges” Q , but for large $Q = 2.2$ it also reaches maximum and then falls down and vanishes for $\Lambda \approx -0.292$. For larger values of Λ the real part remains zero and purely imaginary frequencies exist. The imaginary part decreases almost linearly as Λ grows.	82
7.4	Dependance of the real and imaginary parts of the quasi-normal frequency on $\xi < \frac{3}{16}$ for the scalar hairy black hole. The imaginary part decreases as ξ grows. The quickness of such decreasing depends on Λ and Q . For some Λ and Q (as presented on the bottom graphic) the real part can fall down to zero and purely imaginary frequencies appear for larger ξ	83
7.5	Dependance of the real and imaginary parts of the quasi-normal frequency on μ for the scalar hairy black hole. We consider only $0 \leq \mu^2 \leq -4\xi\Lambda$. The real part changes within comparatively small range. The imaginary part reaches its maximum remaining negative. For this value of μ the oscillations have the longest lifetime, but they still damp and we do not observe quasi-resonances. For larger scalar field masses the imaginary part of frequency decreases and the damping rate is higher.	84
7.6	First five quasi-normal frequencies for the scalar hairy black hole $\Lambda = -0.1$, $Q = 1$, $\xi = 0.1$, $\mu = 0$. The high overtones approach equidistant spacing.	85
7.7	Evolution of axial gravitational perturbations ($l = 2$) in time domain for non-reduced Einstein-Aether theory, $c_1 = 0.1$ (green line) and $c_1 = 0.4$ (red line), in comparison with the Schwarzschild case $c_1 = 0$ (blue line). The higher c_1 is the quicker decay of the observed perturbations.	86
8.1	The form of de Laval nozzles and the effective potential in the nozzle coordinates.	91

Acknowledgement

First, I would like to thank my supervisor Prof. Dr. Élcio Abdalla for all his help and support during my PhD study, for stimulating discussions and for the collaboration. I appreciate very much his invaluable help when reading and correcting Portuguese in the dissertation.

My special thanks are to Dr. Roman Konoplya, whose contribution to all the presented results is impossible to exaggerate. He was (and stays) not only the best collaborator, but also a good friend, whose help and advise are very important to me. He also helped me very much with preparing of the text of the dissertation.

Next, I thank Bárbara Idino Konoplya for all her help and, especially, for reading the first draft of the dissertation and correcting a lot of my mistakes in Portuguese.

Also I would like to thank Prof. Dr. Carlos Molina for the collaboration and for helping me with adaptation to the Brazilian lifestyle.

I am grateful to my collaborators Élcio Abdalla, K. H. C. Castello-Branco, Hideki Ishihara, Panagiota Kanti, Masashi Kimura, Roman Konoplya, Carlos Molina, Keijo Murata, Jiro Soda for their contribution to the presented results.

Many thanks to João da Silva Borges, Amélia Aparecida Ferrari Genova, Sybele Guedes de Paulo Groff and Simone Toyoko Shinomiya for the help, to all the staff of the Department of the Mathematical Physics of IFUSP for their work and to the Fundação de Amparo à Pesquisa do Estado de São Paulo (FAPESP) for the financial support.

Chapter 1

Introduction

The general relativity implies two qualitatively new phenomena, that cannot be described within Newton's gravity. First, there exist objects with masses so high, that the escape velocity from them exceeds the speed of light. These objects were called black holes. Second, the general relativity predicts gravitational waves, which appear due to finiteness of the gravitational interaction speed. These waves may be detected in the nearest future with the help of gravitational antennas. During last years there have been an advance in construction of the gravitational wave detectors, such as LIGO, GEO, VIRGO, TAMA and the planned space-based detector LISA, and the detection of gravitational waves is expected very soon [1].

One of the most promising sources of gravitational waves is collisions of black holes and/or of a star and a black hole. The result of these processes is a black hole with higher mass, which absorbs the gravitational waves. Therefore, the gravitational waves quickly decay and, at sufficiently late time, can be considered as small perturbations of the black hole metric. It means that one can study the linear perturbations, neglecting the higher order corrections. This approximation for the late-time behavior of the gravitational waves provides a good accuracy, which was checked by full non-linear simulations of collisions of two black holes [2].

It turns out that the late-time behavior of the gravitational perturbations does not depend on the way they were induced. At the late-time stage of the evolution of gravitational perturbations we observe the damping oscillations, which give way to asymptotic tails at very late time. The damping oscillations are characterised by complex frequencies, which are called *quasi-normal modes*. The real part of a complex frequency describes the actual oscillation frequency, while the imaginary part is the decay rate of the particular oscillation. The set of the quasi-normal frequencies form the spectrum. Being dependent only on the black hole parameters, the quasi-normal spectrum appears to be an important characteristic of a black hole, or as it is said its footprint. Therefore, detection of the quasi-normal modes allows us to determine the black hole parameters and compare them with those obtained by astronomical expectations [3].

Despite they are well described by linear approximation, the quasi-normal modes, when detected, can be used to check the general relativity as a full non-linear theory. This allows to study some aspects of the gravitational theory that cannot be experimentally confirmed without considering the regime of strong gravity. A good example is a phenomenon of violation of the local Lorentz symmetry. If we assume that there exist the locally preferred state of rest at each point of the space-time, we can describe this state by a unit time-like vector field. This vector field is called "aether" [4]. The parameters of the theory of the aether can be bounded by post-Newton corrections found from astronomical observations. Nevertheless, these bounds do not answer the question if the aether exists or not. Thus, one of the possible ways to observe the effect of the aether is the

determination of the corresponding shift in the quasi-normal spectrum of black holes.

Another motivation for study of the black hole perturbations is checking of stability of the black holes. This is a very important property for higher dimensional theories, such as the brane-world scenarios and string theory [5]. Since in higher than four dimensions there is no uniqueness theorem, stability may be the criteria which will select physical solutions among a variety of “black objects”: black holes, black branes, black rings etc. It is easy to understand that the quasi-normal spectrum of a stable configuration contains only damping modes, while black objects, unstable under small perturbations, must contain at least one growing mode in their spectrum.

In addition, the quasi-normal spectrum can be interpreted in the context of the anti-de Sitter/Conformal Field Theory (AdS/CFT) correspondence [6]. A black hole in the anti-de Sitter space-time corresponds to the thermal state in the dual Conformal Field Theory. The temperature of the thermal state coincides with the Hawking temperature of the black hole. Within the AdS/CFT duality the quasi-normal spectrum of the black hole in AdS corresponds to the poles of the retarded Green functions on the CFT side [7]. Due to the AdS/CFT correspondence we are able to calculate non-perturbative effects of the finite-temperature field theory at strong coupling by studying black holes in the anti-de Sitter space-times. The hydrodynamic parameters of the quark-gluon plasma were calculated within this approach, showing a good agreement with the results obtained in the experiments on the Relativistic Heavy Ion Collider (RHIC) [8].

Within the present work we provide the detailed study of the linear perturbations of a wide class of black holes and find the quasi-normal spectrum for scalar, Dirac, Maxwell fields and the gravitational perturbations. We have studied quasi-normal spectra of these fields in four and higher dimensions, within the Einstein, Einstein-Aether theories, brane-world scenarios with and without the Gauss-Bonnet corrections. We have considered the influence of the cosmological constant on the quasi-normal frequencies and on the asymptotic behavior of high overtones. We have calculated quasi-normal modes of charged scalar and Dirac fields in the Kerr-Newman-de Sitter background.

Also we have studied quasi-normal spectrum of the massive scalar field for Schwarzschild, Tangherlini and scalar hairy anti-de Sitter black holes and the massive vector field in the Schwarzschild background. We provided comprehensive discussions about properties of the quasi-normal spectrum and late-time tails of massive fields. We have considered appearing of the infinitely long-living oscillations (*quasi-resonances*) for particular values of the masses of the black hole and of the field.

We prove the instability of the higher dimensional Reissner-Nordström-de Sitter black holes for sufficiently large values of the black hole charge and of the cosmological constant. By the numerical analysis of the quasi-normal spectrum, we support the stability of the Kaluza-Klein black holes with squashed horizons, the instability region of the Gauss-Bonnet black holes and the long wavelength instability of black strings. We show the appearance of those instabilities in the time domain. Also we prove the stability of the massive scalar field in the background of the Kerr black hole.

We review the numerical methods used for our analysis: the time-domain simulation, the approximation by the Pöschl-Teller potential, the WKB approach and the Frobenius method.

We propose a generalisation of the Nollert improvement of the Frobenius method for higher dimensional problems. This improvement provides better convergence of the numerical procedure, which is crucial for the case when the imaginary part of the quasi-normal frequency is much larger than its real part and for the calculation of the quasi-normal modes of massive fields.

Also we describe a new numerical tool, which we developed for the calculation of the quasi-normal frequencies of a black hole, which metric is not known analytically, but can be found as a numerical solution of a set of differential equations. This technique supports the natural expectation that the dominant quasi-normal frequencies depend mainly on the region nearby the black hole and

do not depend on the behavior of the metric at large distance. We have also checked this method by the time-domain integration.

In addition, we discuss an interesting possibility of observation of the acoustic analogue of the Schwarzschild black hole in laboratories.

This work is aimed to clarify a number of questions about the behavior of perturbations of black holes. We provide a comprehensive analysis of the black hole perturbations in various theories in order to give the complete picture of quasi-normal modes, late-time tails and stability of black holes. The presented results were published in [9, 10, 11, 12, 13, 14, 15, 16, 17, 18, 19, 20, 21, 22, 23, 24, 25, 26].

Chapter 2

Black hole perturbations

2.1 Equations of perturbations near a black hole

The dynamics of the general relativity in D space-time dimensions is described by the Einstein-Hilbert action

$$S = \int \sqrt{|g|} \left(\frac{1}{16\pi} (R - 2\Lambda) + \mathcal{L}_M \right) d^D x, \quad (2.1)$$

where we use the geometrized unit system, so that the speed of light, c , and the gravitational constant, γ , are set equal to one. The metric signature is chosen as $(+ - - - \dots)$. R is the Ricci scalar, \mathcal{L}_M describes all matter fields $\phi_{(i)}$ appearing in the theory, and Λ is the cosmological constant.

The variation of the action (2.1) allows to find the Einstein equations

$$R_{ab} - \frac{1}{2} R g_{ab} + \Lambda g_{ab} = 8\pi T_{ab}, \quad (2.2)$$

and the field equations in the curved space-time

$$\frac{\delta \mathcal{L}_M}{\delta \phi_{(i)}} = 0. \quad (2.3)$$

The energy-momentum tensor T_{ab} in (2.2) is defined as

$$T_{ab} = -\frac{2}{\sqrt{-g}} \frac{\partial \sqrt{-g} \mathcal{L}_M}{\partial g^{ab}}.$$

The general solution of the equations (2.2, 2.3) is some metric and fields in the background this metric

$$ds^2 = g_{ab}(x) dx^a dx^b, \quad \phi_{(i)} = \phi_{(i)}(x). \quad (2.4)$$

We study a stationary black hole, for which g_{ab} and $\phi_{(i)}$ do not depend on time in the appropriate coordinate system and gauge.

Let us consider perturbations of the metric and fields as a sum of the unperturbed background g_{ab}^0 , $\phi_{(i)}^0$ and the actual perturbations δg_{ab} , $\delta \phi_{(i)}$

$$\begin{aligned} g_{ab} &\rightarrow g_{ab}^0 + \delta g_{ab}; \\ \phi_{(i)} &\rightarrow \phi_{(i)}^0 + \delta \phi_{(i)}. \end{aligned} \quad (2.5)$$

The perturbations are assumed to be small, i. e. we neglect the contributions of order $\mathcal{O}(\delta g_{ab})^2$, $\mathcal{O}(\delta g_{ab}\delta\phi_{(i)})$, $\mathcal{O}(\delta\phi_{(i)})^2$ and higher.

After substituting (2.5) into (2.2, 2.3) and taking into account that g_{ab}^0 and $\phi_{(i)}^0$ satisfy the equations (2.2, 2.3) as well, we are able to find the set of linear equations for the perturbations δg_{ab} and $\delta\phi_{(i)}$.

In this chapter we consider the stationary spherically symmetric solution of the equation (2.2) in 4 dimensions with $T_{ab} = 0$, which describes a black hole in vacuum. This solution is given by the well-known metric

$$ds^2 = f(r)dt^2 - \frac{dr^2}{f(r)} - r^2(d\theta^2 + \sin^2\theta d\phi^2), \quad f(r) = 1 - \frac{2M}{r} - \Lambda\frac{r^2}{3}, \quad (2.6)$$

where M is the black hole mass and Λ is the cosmological constant.

For $\Lambda = 0$ the metric (2.6) describes a Schwarzschild black hole. If the cosmological constant is positive ($\Lambda > 0$), we obtain a Schwarzschild-de Sitter black hole, while for negative values of the cosmological constant ($\Lambda < 0$) the black hole is called Schwarzschild-anti-de Sitter.

Since $T_{ab} = 0$, the field perturbations in such background are not coupled to the perturbations of the metric and, therefore, are equivalent to the test fields in the black hole background.

Let us describe the variable separation. As an example we consider the test scalar field which satisfies the Klein-Gordon equation in the curved space-time

$$\frac{1}{\sqrt{-g}} \frac{\partial}{\partial x^a} g^{ab} \sqrt{-g} \frac{\partial \Phi(x)}{\partial x^b} = \frac{1}{f(r)} \frac{\partial^2 \Phi}{\partial t^2} - \frac{\partial}{\partial r} f(r) \frac{\partial \Phi}{\partial r} - \frac{2f(r)}{r} \frac{\partial \Phi}{\partial r} - \frac{\Delta_{\theta,\phi} \Phi}{r^2} = 0, \quad (2.7)$$

where

$$\Delta_{\theta,\phi} = \frac{1}{\sin\theta} \frac{\partial}{\partial\theta} \sin\theta \frac{\partial}{\partial\theta} + \frac{1}{\sin^2\theta} \frac{\partial^2}{\partial\phi^2}$$

is the angular part of the Laplasian.

In order to separate the angular variables we choose the following ansatz:

$$\Phi(t, r, \theta, \phi) = \sum_{l=0}^{\infty} \sum_{m=-l}^l \frac{\Psi_{l,m}(t, r)}{r} Y_{l,m}(\theta, \phi), \quad (2.8)$$

where $Y_{l,m}(\theta, \phi)$ are the spherical harmonics, which are eigenfunctions of the operator $\Delta_{\theta,\phi}$

$$\Delta_{\theta,\phi} Y_{l,m}(\theta, \phi) = -l(l+1) Y_{l,m}(\theta, \phi). \quad (2.9)$$

The integers $l \geq 0$ and $|m| \leq l$ are called the multipole number and the azimuthal number respectively.

After substitution (2.8) into (2.7) we find the wave-like equation for the function $\Psi_{l,m}(t, r)$:

$$\left(\frac{\partial^2}{\partial t^2} - \frac{\partial^2}{\partial r_\star^2} + V_l(r) \right) \Psi_{l,m}(t, r) = 0, \quad (2.10)$$

where the effective potential has the form

$$V_l(r) = f(r) \left(\frac{l(l+1)}{r^2} + \frac{f'(r)}{r} \right), \quad l = 0, 1, 2, \dots \quad (2.11)$$

The variable r_\star is called the *tortoise coordinate*. It is defined up to an arbitrary constant as

$$dr_\star = \frac{dr}{f(r)}. \quad (2.12)$$

If $\Lambda \geq 0$ the tortoise coordinate maps all the region outside the black hole to the interval $(-\infty, \infty)$. In the anti-de Sitter space ($\Lambda < 0$) the interval becomes $(-\infty, r_{*\infty})$, where $r_{*\infty}$ is a finite value that depends on the integration constant of (2.12).

We can also consider other test fields near the black hole. In the most cases, after separation of the angular variables, we are able to reduce the equations of motion for such fields (2.3) to the set of the wave-like equations of the form (2.10).

One could find that the test massless Dirac field is described by the effective potentials [29]

$$V_{D\pm} = f(r) \frac{\kappa_{\pm}^2}{r^2} \pm \frac{d}{dr_*} \frac{\kappa_{\pm} \sqrt{f(r)}}{r}, \quad \kappa_{\pm} = 1, 2, 3 \dots \quad (2.13)$$

and the electromagnetic field is described by the potential [30]

$$V_{EM} = f(r) \frac{l(l+1)}{r^2}, \quad l = 1, 2, 3 \dots \quad (2.14)$$

The equation (2.2) allows us to find the equations of motion for the metric perturbations δg_{ab} (2.5). It is convenient to classify the tensor components δg_{ab} with respect to the transformation law under rotations on the sphere around the black hole. They can be of *scalar*, *vector* and *tensor* type, denoted by s , v and t respectively

$$\delta g_{ab} = \begin{pmatrix} s & s & v & v \\ s & s & v & v \\ v & v & t & t \\ v & v & t & t \end{pmatrix}. \quad (2.15)$$

In order to simplify the equations for the metric perturbations we can use the invariance under infinitesimal coordinate transformations. These transformations act as gauge transformations upon the metric perturbations

$$x^a \rightarrow x^a + \delta x^a \quad \Longrightarrow \quad \delta g_{ab} \rightarrow \delta g_{ab} + \delta x_{a;b} + \delta x_{b;a}.$$

The gauge freedom allows to simplify perturbation equations [31]. After the Regge-Wheeler gauge fixing, the perturbations are described by the potentials [30]

$$V_s(r) = \frac{2f(r) 9M^3 + 3c^2 M r^2 + c^2(1+c)r^3 + 3M^2(3cr - \Lambda r^3)}{r^3 (3M + cr)^2}, \quad (2.16)$$

$$V_v(r) = f(r) \left(\frac{l(l+1)}{r^2} - \frac{6M}{r^3} \right), \quad (2.17)$$

$$c = \frac{l(l+1)}{2} - 1, \quad l = 2, 3, 4 \dots$$

for the scalar and vector types respectively. The perturbations of the tensor type in 4 dimensions are eliminated by this gauge fixing. However, the perturbations of the higher dimensional black hole metric can be of all the three types [32].

According to the Chandrasekhar [33] classification, the perturbations of vector type are called *axial* because they impart the differential rotation to the black hole. Perturbations of scalar type are called *polar*. They are related with infinitesimal deformations of the event horizon. Any perturbations of a spherically symmetric black hole in 4 dimensions can be divided to its polar and axial part in any gauge [34].

One should note that the multipole numbers $l = 0, 1$ for gravitational perturbations and $l = 0$ for the electromagnetic field perturbations are not dynamical. For instance, $l = 0$ gravitational perturbations are spherically symmetric and, therefore, obey the Birkhoff theorem. They correspond to infinitesimal change of the black hole mass. Similarly, $l = 0$ perturbations of the electromagnetic field and $l = 1$ gravitational perturbations correspond, respectively, to the infinitesimal shift of the charge and the position of the black hole [31].

2.2 Time evolution of perturbations

In order to integrate the equation (2.10) numerically we use the technique developed by Gundlach, Price and Pullin [35]. We rewrite the wave-like equation (2.10) in terms of the so called light-cone coordinates $du = dt - dr_*$ and $dv = dt + dr_*$

$$\left(4\frac{\partial^2}{\partial u\partial v} + V(u, v)\right)\Psi(u, v) = 0. \quad (2.18)$$

Let us consider the operator of time evolution in these coordinates

$$\begin{aligned} \exp\left(h\frac{\partial}{\partial t}\right) &= \exp\left(h\frac{\partial}{\partial u} + h\frac{\partial}{\partial v}\right) = \exp\left(h\frac{\partial}{\partial u}\right) + \exp\left(h\frac{\partial}{\partial v}\right) - 1 + \\ &+ \frac{h^2}{2}\left(\exp\left(h\frac{\partial}{\partial u}\right) + \exp\left(h\frac{\partial}{\partial v}\right)\right)\frac{\partial^2}{\partial u\partial v} + \mathcal{O}(h^4). \end{aligned}$$

Acting by this operator on Ψ , and taking into account (2.18), we find

$$\Psi(N) = \Psi(W) + \Psi(E) - \Psi(S) - \frac{h^2}{8}V(S)(\Psi(W) + \Psi(E)) + \mathcal{O}(h^4), \quad (2.19)$$

where we introduced letters to mark the points as $S = (u, v)$, $W = (u + h, v)$, $E = (u, v + h)$, $N = (u + h, v + h)$.

The equation (2.19) allows us to calculate the values of Ψ inside the rhombus, which is built on the two null-surfaces $u = u_0$ and $v = v_0$ (see fig. 2.1), starting from the initial data specified on them.

Let us study, as a qualitative example, the time-domain profile of the vector type gravitational perturbations of the Schwarzschild black hole $\Psi(t, r = R)$ (fig. 2.2). We can divide the evolution of the perturbations into three stages. The first stage depends on the initial conditions and on the point R . At late time ($t \sim R$) we see exponential damping of the amplitude of the perturbations, which is followed by the so-called tails at asymptotically late time ($t \gg M$).

One can observe, that, after the initial outburst at the first stage, the behavior of the amplitude of the perturbations does not depend on the initial conditions. Being independent on the source of the perturbations, it depends only on the parameters of the field and the black hole. Therefore, the late-time damping law appears to be an important characteristic of the black hole.

The exponential damping of the perturbations is called *quasi-normal ringing*. It can be split to the superposition of exponentially damping oscillations, that can be represented as a set of complex frequencies, which are called *quasi-normal modes*. The real part of a quasi-normal frequency describes the actual frequency of the oscillation, while the imaginary part is its damping rate. In the next section we will study the basic properties of the quasi-normal spectrum of black holes.

In the case under consideration, the late-time tails decay according to the inverse power law. The qualitatively similar behavior is observed for the decay of all massless fields in asymptotically

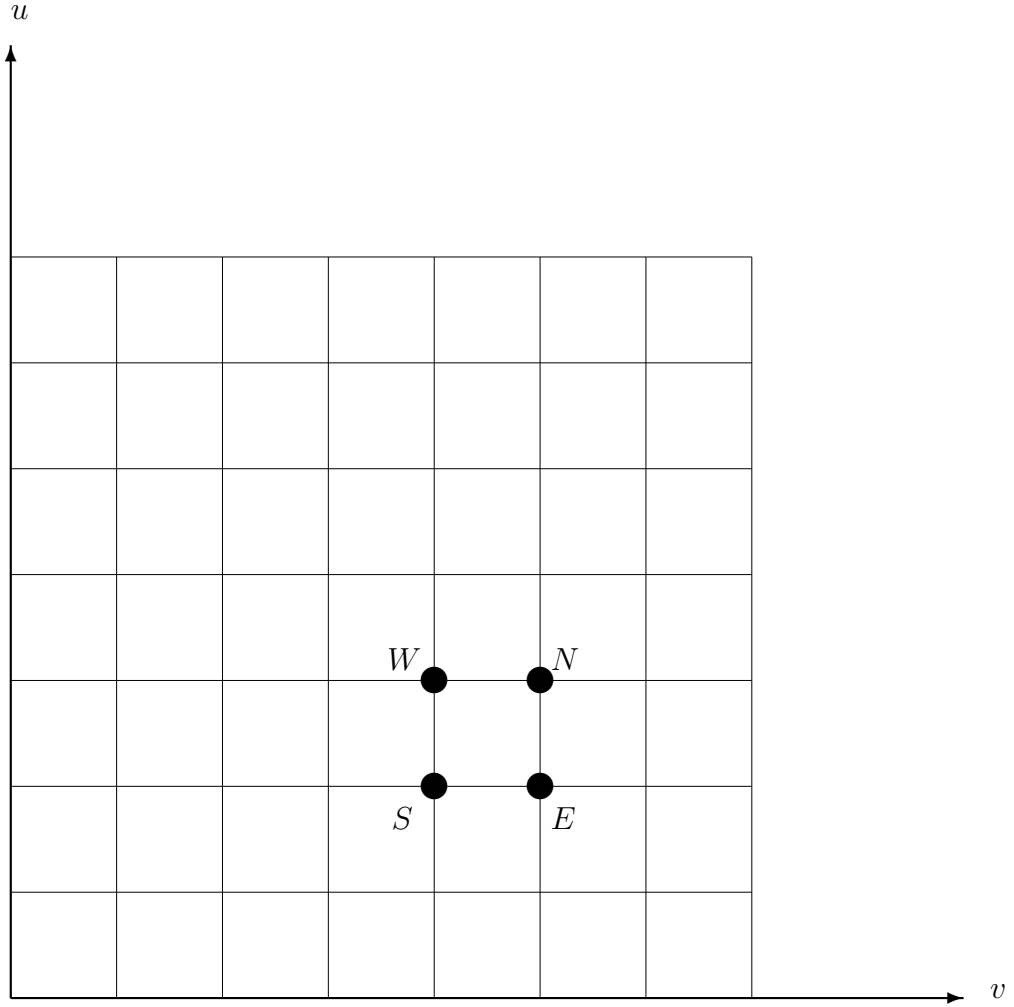


Figure 2.1: The integration grid. Each cell of the grid represents an integration step. The thick points illustrate the choice of (S, W, E, N) for the particular step of the integration. The initial data are specified on the left and bottom sides of the rhombus.

flat backgrounds. Yet, the late-time tails appear to be very sensitive to the asymptotical behavior of the potential: in the asymptotically anti-de Sitter space-times the quasi-normal ringing governs the decay of perturbations at all times [7]. The black hole perturbations in the de Sitter space-time have exponential tails, if the cosmological constant is large, and both power and exponential tails, if the cosmological constant is small [36, 37].

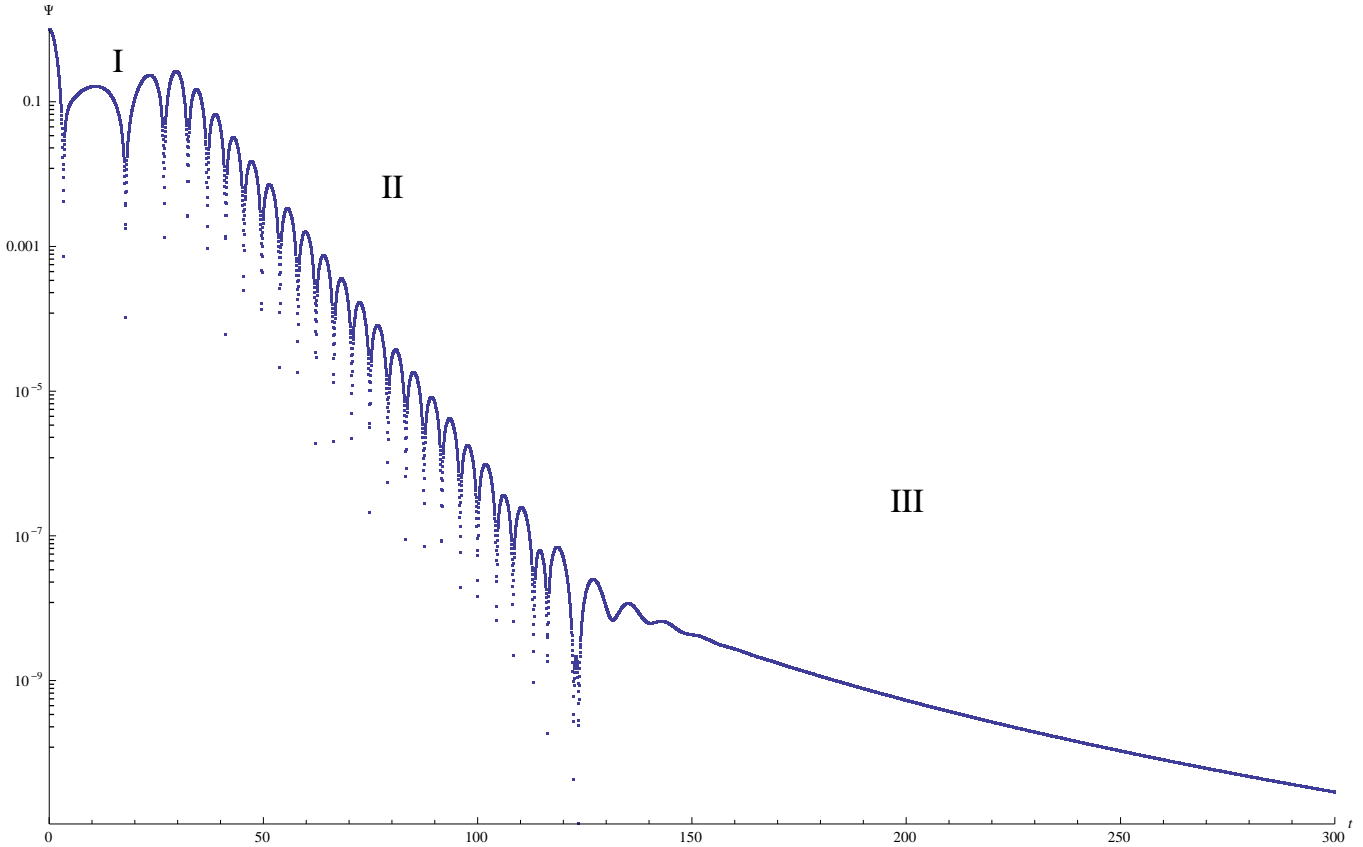


Figure 2.2: The three stages of the evolution of the Schwarzschild black hole gravitational perturbations ($l = 2$ vector type, $\Lambda = 0$, $R = 22M$). Time is measured in units of the horizon radius.

2.3 Properties of the quasi-normal spectrum

2.3.1 Boundary conditions

In order to study quasi-normal spectrum of a black hole it is convenient to make Fourier transform for the function

$$\Psi(t, r) = \sum_{n=0}^{\infty} \exp(-i\omega_n t) Q_{\omega_n}(r). \quad (2.20)$$

Let us note that generally the functions $\{\exp(-i\omega_n t)\}$, where $\{\omega_n\}$ is the quasi-normal spectrum, do not form basis in the vector space of the solutions of the equation (2.10). Therefore, the signal cannot be expanded in terms of these functions for all time. Indeed, as we see on fig. 2.2, the exponential decay is replaced by slower power-law decay at asymptotically late time. Yet, the expansion (2.20) is appropriate to describe the quasi-normal ringing epoch.

Henceforward, we will omit the index n of ω , implying that ω is any frequency from the quasi-normal spectrum.

The function Q_ω satisfies the linear equation

$$\left(\frac{d^2}{dr_\star^2} + \omega^2 - V(r) \right) Q_\omega(r) = 0. \quad (2.21)$$

Thus, the searching of the quasi-normal modes is reduced to the problem of finding eigenfrequencies of the equation (2.21). Since we are interested in what happens in the R -region outside the

black hole, we have to impose the boundary conditions at the event horizon and the cosmological horizon for $\Lambda > 0$ (or the spatial infinity for $\Lambda \leq 0$). In order to do this we must study the structure of the singularities of the equation (2.21) at those points.

Let us study the general properties of the singular points of the equation (2.21). First we note that at any horizon $r \rightarrow h$

$$V \propto f(r) = o\left(\frac{1}{r_\star}\right). \quad (2.22)$$

To prove (2.22) we consider two types of the horizon:

1. $f(r \rightarrow h) = (r - h)f'(h) + o(r - h)$

then

$$r_\star = \frac{1}{f'(h)} \ln \left| \frac{r}{h} - 1 \right| (1 + o(r - h)).$$

Thus, we find that the dominant contribution is

$$f(r \rightarrow h) \sim hf'(h) \exp(f'(h)r_\star) \sim hf'(h) \exp\left(\ln \left| \frac{r}{h} - 1 \right|\right) = o\left(\frac{1}{r_\star}\right)$$

This term decays exponentially with respect to r_\star because

$$\lim_{r \rightarrow h} \ln \left| \frac{r}{h} - 1 \right| = -\infty.$$

2. $f(r \rightarrow h) = A(r - h)^\alpha + o(r - h)^\alpha$, $\alpha > 1$ then

$$r_\star = -\frac{1}{A(\alpha - 1)(r - h)^{\alpha - 1}} (1 + o(r - h))$$

and

$$f(r \rightarrow h) = \frac{r - h}{(\alpha - 1)r_\star} + o(r - h)^\alpha = o\left(\frac{1}{r_\star}\right).$$

If $\Lambda = 0$, the condition (2.22) at spatial infinity is also satisfied for the potentials (2.11, 2.13, 2.14, 2.16, 2.17). Indeed, $r \sim r_\star$ and

$$V(r) = \mathcal{O}\left(\frac{1}{r^2}\right) = \mathcal{O}\left(\frac{1}{r_\star^2}\right) = o\left(\frac{1}{r_\star}\right).$$

Since the potential satisfies (2.22), the behavior of the eigenfrequency at the boundaries can be

$$Q_\omega \propto \exp(\pm i\omega r_\star). \quad (2.23)$$

The appropriate boundary conditions for the problem under consideration are purely ingoing wave at the event horizon and outgoing wave at the cosmological horizon (spatial infinity)

$$\begin{aligned} r_\star \rightarrow -\infty : & \quad Q_\omega \propto \exp(-i\omega r_\star), \\ r_\star \rightarrow +\infty : & \quad Q_\omega \propto \exp(+i\omega r_\star). \end{aligned} \quad (2.24)$$

This choice of the boundary conditions imply that, after the black hole is perturbed, there is no signal, which comes from the black hole or from any remote source [33]. It means that the source of the perturbations acts only before the first stage of the evolution. After this, we consider only the black hole response upon the perturbations.

For the 4-dimensional Schwarzschild-anti-de Sitter black hole ($\Lambda < 0$), one can find that the linear independent solutions at spatial infinity ($r \rightarrow \infty$) are

$$Q_1 \propto r, \quad Q_2 \propto r^{-2}.$$

Since we do not suppose to have an infinite amplitude of the perturbation at the spatial infinity, we must choose Q_2 as the appropriate boundary condition there, i. e. we impose the Dirichlet condition at the AdS boundary [7]

$$Q_\omega(r = \infty) = 0. \quad (2.25)$$

The Dirichlet boundary conditions are usually imposed at the spatial infinity in asymptotically anti-de Sitter backgrounds (see e. g. [38]).

2.3.2 Quasi-normal spectrum and black hole stability

Black holes do not exist in nature, that is why, the important property of any black hole solution is its stability against perturbations. Unfortunately, it is possible to prove stability analytically only of some relatively simple solutions of the Einstein equations. That is why the numerical test of stability is important for the black hole study. The instability implies the existing of growing modes in the quasi-normal spectrum. It is clear, that the linear approximation is enough for this test. Indeed, if the black hole is stable, any perturbations will decay until the linear approximation is valid. If the quasi-normal spectrum has a growing mode, the amplitude of perturbations will grow until we are compelled to consider the non-linear back reaction of the perturbations upon the metric. In this case, we state, at least, that in order to obtain the stable solution we must take into account this non-linear correction, which could be also non-stationary.

It is important to note that the black hole is unstable if there is only one growing mode in its spectrum. Therefore, in order to prove the black hole stability we must show that the quasi-normal spectrum does not contain any growing mode, i. e. frequency with positive imaginary part. It makes the numerical proof of the black hole stability extremely complicated.

Yet, in some cases we are able to prove the stability analytically. Let us multiply the equation (2.21) by the complex conjugated Q_ω^* and integrate the first term by parts

$$Q_\omega^*(r_*) \frac{dQ_\omega(r_*)}{dr_*} \Big|_{-\infty}^{\infty} + \int_{-\infty}^{\infty} \left(\omega^2 |Q_\omega(r_*)|^2 - V |Q_\omega(r_*)|^2 - \left| \frac{dQ_\omega(r_*)}{dr_*} \right|^2 \right) dr_* = 0.$$

Taking into account the boundary conditions (2.24) we find

$$i\omega A + \omega^2 B = \int_{-\infty}^{\infty} \left(V(r) |Q_\omega(r_*)|^2 + \left| \frac{dQ_\omega(r_*)}{dr_*} \right|^2 \right) dr_*, \quad (2.26)$$

where $A = |Q_\omega(r_* = \infty)|^2 + |Q_\omega(r_* = -\infty)|^2 > 0$, $B = \int_{-\infty}^{\infty} |Q_\omega(r_*)|^2 dr_* > 0$.

The imaginary part of (2.26) reads

$$\text{Re}(\omega)A + 2\text{Re}(\omega)\text{Im}(\omega)B = 0. \quad (2.27)$$

We can see that $\text{Im}(\omega) < 0$ except for the case $\text{Re}(\omega) = 0$. Thus, we conclude that *the growing modes do not oscillate* (see sec. 5.2).

If the potential is positive in the R -region outside the event horizon and $\text{Re}(\omega) = 0$, the real part of (2.26) implies that the imaginary part of the frequency remains negative

$$-\text{Im}(\omega)A - \text{Im}(\omega)^2B > 0 \quad \Rightarrow \quad \text{Im}(\omega) < 0.$$

It is clear, that the righthand side of (2.26) can be positive even though $V(r)$ is not positive everywhere. By introducing the new derivative $D = \frac{d}{dr_\star} + S(r_\star)$ we can rewrite the integral as

$$\int_{-\infty}^{\infty} \left(V(r) |Q_\omega(r_\star)|^2 + \left| \frac{dQ_\omega(r_\star)}{dr_\star} \right|^2 \right) dr_\star = \int_{-\infty}^{\infty} \left(\tilde{V} |Q_\omega(r_\star)|^2 + |DQ_\omega|^2 \right) dr_\star - \left[\begin{array}{c} r_\star = \infty \\ r_\star = -\infty \end{array} S(r_\star) |Q_\omega(r_\star)|^2 \right],$$

where $\tilde{V} = V + \frac{dS}{dr_\star} - S^2$. Thus, we conclude that if we find the function $S(r_\star)$ such as $S(r_\star = \infty) \leq 0$, $S(r_\star = -\infty) \geq 0$ and $\tilde{V} \geq 0$, the righthand side of (2.26) stays positive and, therefore, $\text{Im}(\omega) < 0$.

This technique is called S -deformation and allows us to prove stability for some cases, when the potential is not positive definite [39]. It is important to note that if we find an appropriate function S , we prove the black hole stability. Otherwise we do not know if the black hole is stable or not.

The same approach can be used in a similar way for anti-de Sitter black holes. We must just put $r_{\star\infty}$ as the upper bound in the integrals and use (2.25). Then we obtain $A = |Q_\omega(r_\star = -\infty)|^2 > 0$ and the requirement for S at the spatial infinity reads $S(r_\star = r_{\star\infty}) < \infty$.

Because we must guess the appropriate function S , the technique of S -deformation allows to proof stability only for relatively simple potentials. For more complicated cases we are able to prove the black hole stability only numerically.

2.3.3 Isospectrality

Let us consider two equations (2.21) with the effective potentials, taken as V^+ and V^- , with

$$V^\pm = W^2(r_\star) \pm \frac{dW(r_\star)}{dr_\star} + \beta, \quad (2.28)$$

where $W(r_\star)$ is some finite function and β is a constant. Then, if Q_ω^+ is an eigenfunction of (2.21) for the potential V^+ , the eigenfunction for the potential V^- is given (up to an arbitrary factor) by

$$Q_\omega^- = \left(W - \frac{d}{dr_\star} \right) Q_\omega^+, \quad (2.29)$$

corresponding to the same eigenvalue ω . Thus we conclude that the quasi-normal spectrum is the same for the potentials V^+ and V^- .

Let us consider the examples of isospectrality for 4-dimensional Schwarzschild((-anti)-de Sitter) black holes. One can check [33] that the potentials (2.16) and (2.17) can be obtained by taking

$$W = \frac{2M}{r^2} - \frac{3+2c}{3r} + \frac{3c^2+2c^3-9\Lambda M^2}{3c(3M+cr)} - \frac{1}{3M} \left(c^2 + c - \frac{3\Lambda M^2}{c} \right), \quad \beta = -\frac{c^2(c+1)^2}{9M^2}.$$

The potentials for the Dirac field (2.13) are, obviously, isospectral too.

It is clear that if one of the isospectral potentials is positive outside the event horizon, as one can notice for $V_s(r)$ ($c \geq 2$), both do not lead to growing modes, implying stability against the perturbations. The other possible case of stable potentials is $\beta \geq 0$, as it happens for (2.13). In order to prove the stability we just use the S -deformation technique with $S = \pm W$. In fact, all the potentials (2.11, 2.13, 2.14, 2.16, 2.17) are positive for $-\infty < r_\star < \infty$, thereby, the stability of the Schwarzschild black hole is evident.

Chapter 3

Numerical methods of calculation of the quasi-normal modes

3.1 Fitting time-domain data

The most direct approach to finding quasi-normal modes is the numerical integration of the equation (2.10) as described in the section 2.2. The result of the time-domain integration is a time profile data $\{\Psi(t = 0), \Psi(t = h), \Psi(t = 2h) \dots\}$, which can be used to calculate the quasi-normal modes.

Let us describe the simplest Prony method of fitting the profile data by superposition of damping exponents (see e. g. [40] and references therein)

$$\Psi(t) \simeq \sum_{i=1}^p C_i e^{-i\omega_i t}. \quad (3.1)$$

We suppose that the quasi-normal ringing epoch starts at $t = 0$ and ends at $t = Nh$, where integer $N \geq 2p - 1$. Then the formula (3.1) is valid for each value from the profile data

$$x_n \equiv \Psi(nh) = \sum_{j=1}^p C_j e^{-i\omega_j nh} = \sum_{j=1}^p C_j z_j^n. \quad (3.2)$$

The Prony method allows to find z_i in terms of known x_n and, since h is also known, to calculate the quasi-normal frequencies ω_i . In order to do this, we define a polynomial function $A(z)$ as

$$A(z) = \prod_{j=1}^p (z - z_j) = \sum_{m=0}^p \alpha_m z^{p-m}, \quad \alpha_0 = 1. \quad (3.3)$$

Let us consider the sum

$$\sum_{m=0}^p \alpha_m x_{n-m} = \sum_{m=0}^p \alpha_m \sum_{j=1}^p C_j z_j^{n-m} = \sum_{j=1}^p C_j z_j^{n-p} \sum_{m=0}^p \alpha_m z_j^{p-m} = \sum_{j=1}^p C_j z_j^{n-p} A(z_j) = 0.$$

Taking into account that $\alpha_0 = 1$, we find

$$\sum_{m=1}^p \alpha_m x_{n-m} = -x_n. \quad (3.4)$$

Substituting $n = p..N$ into (3.4) we obtain $N - p + 1 \geq p$ linear equations for p unknown coefficients α_m .

Let us rewrite these equations in the matrix form

$$\begin{pmatrix} x_{p-1} & x_{p-2} & \dots & x_0 \\ x_p & x_{p-1} & \dots & x_1 \\ \vdots & \vdots & \ddots & \vdots \\ x_{N-1} & x_{N-2} & \dots & x_{N-p} \end{pmatrix} \begin{pmatrix} \alpha_1 \\ \alpha_2 \\ \vdots \\ \alpha_p \end{pmatrix} = - \begin{pmatrix} x_p \\ x_{p+1} \\ \vdots \\ x_N \end{pmatrix}.$$

Such matrix equation

$$X\alpha = -x$$

can be solved in the least-squares sense

$$\alpha = -(X^+X)^{-1}X^+x, \quad (3.5)$$

where X^+ denotes the Hermitian transposition of the matrix X .

After the coefficients α_m of the polynomial function $A(z)$ are found, we can calculate numerically the roots z_j of the polynom and the quasi-normal frequencies

$$\omega_j = \frac{i}{h} \ln(z_j).$$

Because the quasi-normal stage is not a precisely defined time interval, in practice, it is difficult to determine when the quasi-normal ringing begins. In fact, when we observe explicitly damped oscillations, we usually see only the fundamental mode, while higher overtones, which damp quickly, are already exponentially suppressed. Being a small corrections to the signal, such higher damped oscillations are indistinguishable from numerical errors within the described approach. Thus, the higher overtones are difficult to find. Usually, the Prony method allows to calculate at most six roots of the polynom $A(z)$, including the complex conjugated ones, which correspond to the symmetry $\omega \leftrightarrow (-\omega^*)^*$. This symmetry exists just because the wave-like equation (2.10) is real. Therefore, in fact, we are able to calculate only two or, sometimes, three dominant frequencies.

In order to determine the beginning of the quasi-normal ringing epoch more precisely, we can use the following technique [41]. Let us find the dominant quasi-normal mode ω_1 and the corresponding coefficient C_1 at some late time interval. Then we can subtract this oscillation from the numerical data, and obtain the profile data without the contribution of the dominant mode. After this, one can see ringing for the first overtone. If the lifetime of the quasi-normal ringing is long enough, we are able to find, step by step, higher overtones, making sure, that the numerical error of the initial data is less than the signal after removing the contributions of the lower-damping modes.

3.2 Approximation by the Pöschl-Teller potential

The easiest method of calculation of the quasi-normal modes in frequency domain is approximation of the effective potential by the Pöschl-Teller potential. This method was suggested by Bahram Mashhoon [42, 43].

Suppose that the potential in the equation (2.21) is invariant under the following transformation

$$V(r^*, \alpha) = V(-ir^*, \alpha'),$$

where α is some parameter and α' depends on α .

Let us consider the solution of the equation with the inverse potential

$$\frac{d^2 Q_\Omega}{dr_*^2} + (-\Omega^2 + V)Q_\Omega = 0, \quad (3.6)$$

with the boundary conditions that are characteristic of bound states if $\text{Re}(\Omega) > 0$

$$Q_\Omega \propto e^{\mp \Omega r_*}, \quad r_* \rightarrow \pm \infty. \quad (3.7)$$

It is easy to see, that this solution is related with the solution of (2.21) with the quasi-normal boundary conditions (2.24) in a simple way

$$Q_\omega(r_*, \alpha) = Q_\Omega(-ir_*, \alpha'), \quad \omega(\alpha) = \Omega(\alpha'). \quad (3.8)$$

Thus, the quasi-normal mode problem is reduced now to the bound states problem for an inverse potential $V \rightarrow -V$, which is smooth potential gap, approaching zero at the infinite boundaries. This gap can be approximated by the Pöschl-Teller potential

$$V_{PT} = \frac{V_0}{\cosh^2 \alpha(r_* - r_*^0)}, \quad (3.9)$$

where V_0 is the height of the effective potential and $-2V_0\alpha^2$ is the curvature of the potential at its maximum. The bound states of the Pöschl-Teller potential are known in analytical form [44]

$$\Omega = \alpha \left(- \left(n + \frac{1}{2} \right) + \left(\frac{1}{4} + \frac{V_0}{\alpha^2} \right)^{1/2} \right), \quad n = 0, 1, 2, \dots \quad (3.10)$$

The potential (3.9) is obviously invariant under the transformation

$$V_{PT}(r_*, \alpha) = V_{PT}(-ir_*, i\alpha).$$

Therefore, the quasi-normal modes for the inverted Pöschl-Teller potential are

$$\omega(\alpha) = \Omega(i\alpha) = \pm \left(V_0 - \frac{\alpha^2}{4} \right)^{1/2} - i\alpha \left(n + \frac{1}{2} \right), \quad n = 0, 1, 2, \dots \quad (3.11)$$

Technically one has to fit a given effective potential to an inverted Pöschl-Teller potential. In the chapter 7 one shall see that in many cases the behavior of the effective potential only near the black hole is essential for determining the dominating quasi-normal modes. So that the fit of the height of the effective potential V_0 and of its curvature $-2V_0\alpha^2$ is indeed sufficient to estimate quasi-normal frequencies.

This method gives quite accurate results for the regime of high multipole numbers l . In particular, for gravitational perturbations of the $D = 4$ Schwarzschild black holes, the fundamental quasi-normal modes obtained by the Mashhoon method gives relative error of not more than 2% for the lowest multi-pole $l = 2$, and of about fractions of one percent for higher multipoles.

There are cases when the effective potential of a black hole is *exactly* the Pöschl-Teller potential. These are Schwarzschild-de Sitter [45] and Reissner-Nordström-de Sitter black holes with extremal value of the Λ -term in $D \geq 4$ space-time dimensions [46].

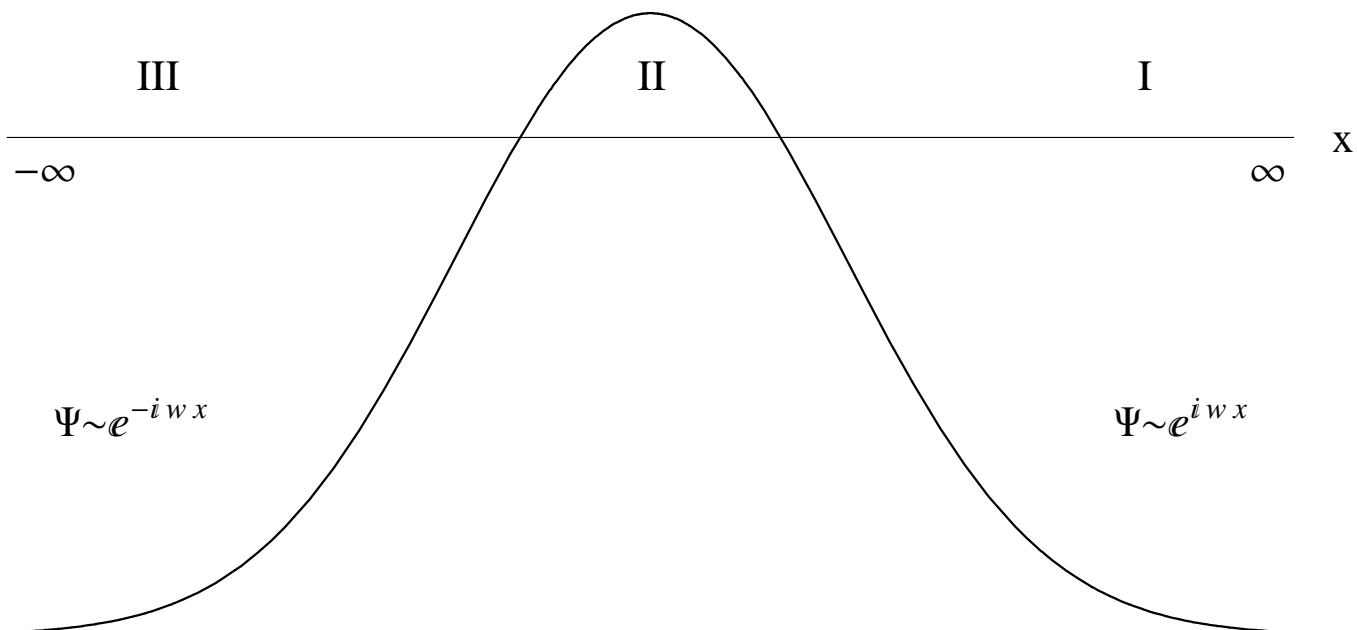


Figure 3.1: The three regions separated by the two turning points $Q(x) = 0$.

3.3 WKB method

In order to evaluate quasi-normal modes for more complicated effective potentials it is convenient to use the WKB (Wentzel, Kramers, Brillouin) method, which provides good accuracy. The WKB technique was applied to finding of the quasi-normal modes of black holes for the first time by Schutz and Will [47].

In order to simplify our notations, let us re-write the wave-like equation (2.21) in the following form

$$\frac{d^2\Psi}{dx^2} + Q(x)\Psi(x) = 0, \quad (3.12)$$

i.e. we identify $x \equiv r_*$, $Q \equiv \omega^2 - V$, and $\Psi \equiv Q_\omega$.

Let us introduce the WKB parameter ϵ in order to track orders of the WKB expansion. The asymptotic WKB approximation at both infinities has the following general form

$$\Psi(x) \propto \exp\left(\sum_{n=0}^{\infty} \frac{S_n(x)\epsilon^n}{\epsilon}\right). \quad (3.13)$$

Substituting the expansion (3.13) into the wave equation (3.12), and equating the same powers of ϵ , we find

$$S_0(x) = \pm i \int_{x_0}^x Q(\eta)^{1/2} d\eta, \quad (3.14)$$

$$S_1(x) = -\frac{1}{4} \ln Q(x). \quad (3.15)$$

The two choices of the sign in (3.14) correspond to either incoming or outgoing waves at either of the infinities $x = \pm\infty$.

Thus, at $x \rightarrow +\infty$ (region I), $Q(x) \rightarrow \omega^2$ in the dominant order, so that $S_0 \rightarrow +i\omega x$ for a wave outgoing at the infinity and $S_0 \rightarrow -i\omega x$ for a wave in-coming from infinity. In a similar fashion, at

the event horizon $x \rightarrow -\infty$ (region III), $S_0 \rightarrow +i\omega x$ is for wave in-coming from the event horizon, while $S_0 \rightarrow -i\omega x$ is for a wave out-going to the event horizon. We shall designate these four solutions as Ψ_+^I , Ψ_-^I , Ψ_+^{III} and Ψ_-^{III} respectively for plus and minus signs in S_0 in I and III regions (see fig. 3.1). Thus

$$\Psi_+^I \sim e^{+i\omega x}, \quad x \rightarrow +\infty, \quad \Psi_-^I \sim e^{-i\omega x}, \quad x \rightarrow +\infty \quad (3.16)$$

$$\Psi_+^{III} \sim e^{+i\omega x}, \quad x \rightarrow -\infty, \quad \Psi_-^{III} \sim e^{-i\omega x}, \quad x \rightarrow -\infty \quad (3.17)$$

The general solutions in the regions I and III are

$$\Psi = Z_{in}^I \Psi_-^I + Z_{out}^I \Psi_+^I, \quad (3.18)$$

$$\Psi = Z_{in}^{III} \Psi_+^{III} + Z_{out}^{III} \Psi_-^{III}, \quad (3.19)$$

The amplitudes at $x \rightarrow +\infty$ are connected with the amplitudes at $x \rightarrow -\infty$ through the linear matrix relation

$$\begin{pmatrix} Z_{out}^{III} \\ Z_{in}^{III} \end{pmatrix} = \begin{pmatrix} S_{11} & S_{12} \\ S_{21} & S_{22} \end{pmatrix} \begin{pmatrix} Z_{out}^I \\ Z_{in}^I \end{pmatrix}. \quad (3.20)$$

Now we need to match both WKB solutions of the form (3.13) in the regions I and III with a solution in region II, through the two turning points $Q(x) = 0$.

If the turning points are closely spaced, i.e. if $-Q(x)_{max} \ll Q(\pm\infty)$, then the solution in the region II can be well approximated by the Taylor series

$$Q(x) = Q_0 + \frac{1}{2}Q_0''(x - x_0)^2 + \mathcal{O}((x - x_0)^3), \quad (3.21)$$

where x_0 is the point of maximum of the function $Q(x)$, $Q_0 = Q(x_0)$, and Q_0'' is the second derivative with respect to x taken at the point $x = x_0$. Region II corresponds to

$$|x - x_0| < \sqrt{\frac{-2Q_0}{Q_0''}} \approx \epsilon^{1/2}. \quad (3.22)$$

The latter relation gives also the region of validity of the WKB approximation: ϵ must be small.

Let us introduce new functions

$$t = (2Q_0'')^{1/4} e^{i\pi/4} (x - x_0), \quad (3.23)$$

$$\nu + \frac{1}{2} = -iQ_0 / (2Q_0'')^{1/2}. \quad (3.24)$$

Then the wave equation (3.12) takes the form

$$\frac{d^2\Psi}{dt^2} + \left(\nu + \frac{1}{2} - \frac{1}{4}t^2 \right) \Psi = 0. \quad (3.25)$$

The general solution of this equation can be expressed in terms of parabolic cylinder functions $D_\nu(t)$,

$$\Psi = AD_\nu(t) + BD_{-\nu-1}(it). \quad (3.26)$$

Large $|t|$ asymptotics of this solution are

$$\begin{aligned} \Psi \approx & B e^{-3i\pi(\nu+1)/4} (4k)^{-(\nu+1)/4} (x - x_0)^{-(\nu+1)} e^{ik^{1/2}(x-x_0)^2/2} + \\ & (A + B(2\pi)^{1/2} e^{-i\nu\pi/2} / \Gamma(\nu+1)) e^{i\pi\nu/4} (4k)^{\nu/4} (x - x_0)^\nu e^{-ik^{1/2}(x-x_0)^2/2}, \quad x \gg x_2, \end{aligned} \quad (3.27)$$

$$\Psi \approx A e^{-3i\pi\nu/4} (4k)^{\nu/4} (x - x_0)^\nu e^{-ik^{1/2}(x-x_0)^2/2} +$$

$$(B - iA(2\pi)^{1/2} e^{-i\nu\pi/2} / \Gamma(-\nu)) e^{i\pi(\nu+1)/4} (4k)^{-(\nu+1)/4} (x - x_0)^{-(\nu+1)} e^{ik^{1/2}(x-x_0)^2/2}, \quad x \ll x_1, \quad (3.28)$$

where $k = \frac{1}{2}Q_0''$.

Equating the corresponding coefficients in (3.27), (3.28) and eliminating A and B , we obtain the elements of the S matrix,

$$\begin{pmatrix} Z_{out}^{III} \\ Z_{in}^{III} \end{pmatrix} = \begin{pmatrix} e^{i\pi\nu} & iR^2 e^{i\pi\nu} (2\pi)^{1/2} / \Gamma(\nu + 1) \\ R^{-2} (2\pi)^{1/2} / \Gamma(-\nu) & -e^{i\pi\nu} \end{pmatrix} \begin{pmatrix} Z_{out}^I \\ Z_{in}^I \end{pmatrix}, \quad (3.29)$$

where

$$R = (\nu + 1)^{(\nu+1/2)/2} e^{-(\nu+1/2)/2}. \quad (3.30)$$

When expanding in higher WKB orders, the S matrix has the same general form with just other R , still depending only on ν . Let us note that for a black hole there are no waves ‘‘reflected by the horizon’’, so that $Z_{in}^{III} = 0$, and due to quasi-normal mode boundary conditions, there are no waves coming from infinity, i.e. $Z_{in}^I = 0$. Both these conditions are satisfied by (3.29), only if

$$\Gamma(-\nu) = \infty, \quad (3.31)$$

and, consequently, ν must be integer. Then, from the relation (3.24) we find

$$n + \frac{1}{2} = -iQ_0 / (2Q_0'')^{1/2}, \quad n = 0, 1, 2, \dots \quad (3.32)$$

The latter relation gives us the complex quasi-normal modes labeled by an overtone number n with the accuracy of the first WKB order [47]. Later this approach was extended to the third WKB order beyond the eikonal approximation by Iyer and Will [48] and to the sixth order by Konoplya [49, 50]. In order to make the higher order WKB extension it is sufficient to take higher orders in ϵ WKB series (3.13) and to take appropriate number of consequent terms in the Taylor expansion (3.21). Since the S -matrix (3.20) depends only on ν , its elements S_{ij} can be found simply by solving the interior problem in region II at higher orders in ϵ [48], and without explicit matching of the interior solution with WKB solutions in regions I and III in each order.

Going over from Q to the effective potential V , the sixth order WKB formula has the form

$$\frac{i(\omega^2 - V_0)}{\sqrt{-2V_0''}} - \Lambda_2 - \Lambda_3 - \Lambda_4 - \Lambda_5 - \Lambda_6 = n + \frac{1}{2}, \quad n = 0, 1, 2, \dots \quad (3.33)$$

where the correction terms Λ_i depend on the value of the effective potential and its derivatives (up to the $2i$ -th order) in the maximum.

It was shown in [51] that WKB formula, extended to the sixth order, gives the relative error which is about two orders less than that of the 3rd WKB order. Yet one should remember that strictly speaking the WKB series converge only asymptotically and the consequent decreasing of the relative error in each WKB order is not guaranteed. Therefore it is reasonable to develop a modified WKB technique in the so-called optimal order [52]. The latter gives better results for moderately higher overtones n and especially when $n > l$. Yet, in many cases when $n \leq l$ the 6th order WKB formula gives better results than the optimal order treatment.

In some cases, the WKB approach needs modifications: for instance when considering a massive scalar field in a black hole background, the effective potential has a local minimum far from a black hole. This local minimum induces two changes in the WKB procedure. First, there are three turning points which separate all space into four regions, so that three matchings are required. Second, an influent subdominant term in the asymptotic WKB expansion at spatial infinity (3.19) appears (see sec. 3.4.7).

3.4 Frobenius method

3.4.1 Frobenius series

The most accurate method of searching of eigenvalues of the equation (2.21) is Frobenius method, which allows to find quasi-normal modes with arbitrary precision and does not require special form of the effective potential. This method allows to calculate also higher overtones of black holes. It was done for the first time by E. W. Leaver for Schwarzschild and Kerr black holes [53].

Let us consider the second order differential equation of more general form than (2.10)

$$\left(\frac{d^2}{dr^2} + p(r) \frac{d}{dr} + q(r) \right) R(r) = 0, \quad (3.34)$$

where the functions $p(r)$ and $q(r)$ depend on the eigenfrequency ω .

Let us start from the analysis of character of singular points of this equation. There are two points, which are always singular: the event horizon $r = r_+$ and the cosmological horizon (or the spatial infinity) $r = r_\infty$. Usually, there are also other singular points, that depend on $p(r)$ and $q(r)$. By definition, the quasi-normal modes are eigenvalues of ω with the boundary conditions that correspond to the outgoing wave at the cosmological horizon (spatial infinity) and the ingoing wave at the black hole event horizon. So, we are able to define the function $R(r)$ as a multiplication of some factor and the Frobenius series. The factor is divergent at these singular points. It is chosen in order to the series be convergent in the region $r_+ \leq r \leq r_\infty$. If $p(r)$ and $q(r)$ are rational functions of r , we can construct such series in terms of the rational functions,

$$R(r) = \begin{cases} \left(\frac{r - r_\infty}{r - r_0} \right)^{i\Omega} \left(\frac{r - r_+}{r - r_0} \right)^{-i\beta} \sum_{k=0}^{\infty} b_k \left(\frac{r - r_+}{r - r_0} \frac{r_\infty - r_0}{r_\infty - r_+} \right)^k, & r_\infty < \infty, \\ e^{i\Omega r} (r - r_0)^\sigma \left(\frac{r - r_+}{r - r_0} \right)^{-i\beta} \sum_{k=0}^{\infty} b_k \left(\frac{r - r_+}{r - r_0} \right)^k, & r_\infty = \infty. \end{cases} \quad (3.35)$$

The values Ω , σ and β are defined in order to satisfy (3.34) in the singular points $r = r_+$ and $r = r_\infty$. The quasi-normal boundary conditions fix $Re(\Omega)$ and $Re(\beta)$, which must be chosen of the same sign as $Re(\omega)$.

Let us consider the series

$$u(z) = \sum_{k=0}^{\infty} b_k z^k. \quad (3.36)$$

If all the singular points of the equation (3.34) satisfy $|z| > 1$, the series (3.36) are convergent at $z = 1$ ($r = r_\infty$), if and only if the value of ω is the eigenfrequency of the equation (3.34). If there is at least one singular point inside the unit circle, one has to continue the series (3.36) through some midpoints (see sec. 3.4.4) in order to test the convergence at the cosmological horizon or at the spatial infinity.

Note, that the definition of z contains an arbitrary parameter $r_0 < r_+$. In most cases, it can be chosen in order to move all the singularities outside the unit circle.

3.4.2 Method of a continued fraction

Substituting (3.35) into (3.34), one can obtain an N -term recurrence relation for the coefficients b_i

$$\sum_{j=0}^{\min(N-1,i)} c_{j,i}^{(N)}(\omega) b_{i-j} = 0, \quad i > 0, \quad (3.37)$$

where the coefficients $c_{j,i}^{(N)}(\omega)$ ($0 \leq j \leq \min(N-1, i)$) depend on ω .

We now decrease the number of terms in the recurrence relation

$$\sum_{j=0}^{\min(k,i)} c_{j,i}^{(k+1)}(\omega) b_{i-j} = 0 \quad (3.38)$$

by one, i. e. we find $c_{j,i}^{(k)}(\omega)$, which satisfy the equation

$$\sum_{j=0}^{\min(k-1,i)} c_{j,i}^{(k)}(\omega) b_{i-j} = 0. \quad (3.39)$$

For $i \geq k$, we can rewrite the above expression as

$$\frac{c_{k,i}^{(k+1)}(\omega)}{c_{k-1,i-1}^{(k)}(\omega)} \sum_{j=1}^k c_{j-1,i-1}^{(k)}(\omega) b_{i-j} = 0. \quad (3.40)$$

Subtracting (3.40) from (3.38) we find the relation (3.39) explicitly. Thus we obtain,

$$c_{j,i}^{(k)}(\omega) = c_{j,i}^{(k+1)}(\omega), \quad j = 0, \text{ or } i < k,$$

$$c_{j,i}^{(k)}(\omega) = c_{j,i}^{(k+1)}(\omega) - \frac{c_{k,i}^{(k+1)}(\omega) c_{j-1,i-1}^{(k)}(\omega)}{c_{k-1,i-1}^{(k)}(\omega)}.$$

This procedure is called *Gaussian eliminations*, and allows us to determine the coefficients in the three-term recurrence relation numerically for a given ω up to any finite i

$$c_{0,i}^{(3)} b_i + c_{1,i}^{(3)} b_{i-1} + c_{2,i}^{(3)} b_{i-2} = 0, \quad i > 1 \quad (3.41a)$$

$$c_{0,1}^{(3)} b_1 + c_{1,1}^{(3)} b_0 = 0. \quad (3.41b)$$

The complexity of the procedure is *linear* with respect to i and N .

If the the Frobenius series are convergent, we are able to find b_1/b_0 from (3.41b) and substitute it into (3.41a)

$$\frac{b_1}{b_0} = -\frac{c_{1,1}^{(3)}}{c_{0,1}^{(3)}} = -\frac{c_{2,2}^{(3)}}{c_{1,2}^{(3)}} - \frac{c_{0,2}^{(3)} c_{2,3}^{(3)}}{c_{1,3}^{(3)}} - \frac{c_{0,3}^{(3)} c_{2,4}^{(3)}}{c_{1,4}^{(3)}} \dots \quad (3.42)$$

Finally we find

$$0 = c_{1,1}^{(3)} - \frac{c_{0,1}^{(3)} c_{2,2}^{(3)}}{c_{1,2}^{(3)}} - \frac{c_{0,2}^{(3)} c_{2,3}^{(3)}}{c_{1,3}^{(3)}} \dots, \quad (3.43)$$

what can be inverted n times

$$c_{1,n+1}^{(3)} - \frac{c_{2,n}^{(3)} c_{0,n-1}^{(3)}}{c_{1,n-1}^{(3)}} - \frac{c_{2,n-1}^{(3)} c_{0,n-2}^{(3)}}{c_{1,n-2}^{(3)}} \dots - \frac{c_{2,2}^{(3)} c_{0,1}^{(3)}}{c_{1,1}^{(3)}} = \frac{c_{0,n+1}^{(3)} c_{2,n+2}^{(3)}}{c_{1,n+2}^{(3)}} - \frac{c_{0,n+2}^{(3)} c_{2,n+3}^{(3)}}{c_{1,n+3}^{(3)}} \dots \quad (3.44)$$

The equation (3.44) with the *infinite continued fraction* on the right-hand side can be solved numerically by minimising the absolute value of the difference between the left- and right-hand sides. The equation has an infinite number of roots (corresponding to the quasi-normal spectrum), but for each n , the most stable root is different. In general, we have to use the n times inverted equation to find the n -th quasi-normal mode. The requirement that the continued fraction be itself convergent allows us to restrict its depth by some large value, always ensuring that an increase in this value does not change the final results within the desired precision.

3.4.3 Nollert improvement

It turns out, that the convergence of the infinite continued fraction becomes worse, if the imaginary part of ω increases with respect to the real part. It means that in order to calculate the higher overtones correctly, we must increase the depth of the continued fraction, what dramatically increases the time of calculation. The convergence is bad also if r_0 in (3.35) is not a singular point. Such fixing of r_0 is necessary to move all the singular points outside the unit circle for higher-dimensional Schwarzschild black holes.

The problem of slow convergence was circumvented in [54] for the three-term recurrence relation and generalised for higher N in [18]. Let us consider

$$-\frac{b_n}{b_{n-1}} = R_n = \frac{c_{2,n+1}^{(3)}}{c_{1,n+1}^{(3)}} \frac{c_{0,n+1}^{(3)} c_{2,n+2}^{(3)}}{c_{1,n+2}^{(3)}} \dots, \quad (3.45)$$

that for large n can be expanded as

$$R_n(\omega) = C_0(\omega) + \frac{C_1(\omega)}{\sqrt{n}} + \frac{C_2(\omega)}{n} + \dots \quad (3.46)$$

In order to find the coefficients C_j of (3.46), we divide the equation (3.37) by b_{i-N+1} and use the definition $R_n = -b_n/b_{n-1}$. We find the equation with respect to R_n

$$\sum_{j=0}^{N-1} (-1)^j c_{j,i}^{(N)}(\omega) \prod_{k=0}^{N-2-j} R_{i-k} = 0. \quad (3.47)$$

For large n , $c_{j,n}^{(N)}(\omega) \propto n^2$. Thus, substituting the expansion (3.46) into (3.47), we find

$$\lim_{n \rightarrow \infty} \frac{1}{n^2} \sum_{j=0}^{N-1} (-1)^j c_{j,n}^{(N)}(\omega) C_0^{N-1-j}(\omega) = 0. \quad (3.48)$$

In general, the equation (3.48) has $N - 1$ roots (in fact there are multiple roots). One of the roots (also multiple) is *always* $C_0 = -1$, implying the unit radius of convergence of the series (3.35). Other roots appear due to the existing of additional singular points of the equation (3.34). Thus we choose $C_0 = -1$.

After fixing $C_0 = -1$ one can find an equation with respect to C_1^2 . In order to fix the sign of C_1 we can use the convergence of the series (3.35) at $z = 1$. Therefore,

$$\lim_{n \rightarrow \infty} b_n = 0, \quad \text{i. e. } \nexists N : \forall n > N \quad |b_n| > |b_{n-1}|.$$

Since for large n we have

$$\frac{b_n}{b_{n-1}} \sim -R_n \sim -C_0 - \frac{C_1}{\sqrt{n}} = 1 - \frac{C_1}{\sqrt{n}},$$

we find out that the real part of C_1 *cannot be negative*.

After the sign of C_1 is fixed, the other coefficients in (3.46) can be found step by step from (3.47) without encountering indeterminations.

Since we can calculate the coefficients C_j , the expansion (3.46) could be used as an initial approximation for the “remaining” infinite continued fraction. In order to ensure the convergence of (3.46) for a given value of ω , one has to start from the found approximation deeply enough inside the continued fraction (3.44). The expansion gives a good approximation for R_n . Therefore, the required depth is less than it would be, if we started from some arbitrary value.

3.4.4 Continuation of the Frobenius series through midpoints

Let us consider the case when we are unable to fix the parameter r_0 in (3.35) in such a way that all the singularities, except $r = r_+$ and $r = r_\infty$, move outside the unit circle. In this case there is at least one singularity, for which $|z| < 1$. This singularity implies smaller radius of convergence for the series (3.36). In order to test that the function $u(z)$ is convergent at $z = 1$, we must continue the series analytically, by constructing iteratively the expansions of $u(z)$ at some midpoints [55].

Namely, we equate the series expansion at two points

$$u(z) = \sum_{n=0}^{\infty} b_n z^n = \sum_{n=0}^{\infty} \tilde{b}_n (z - z_0)^n, \quad (3.49)$$

where $z = z_0$ is a midpoint inside the radius of convergence of (3.36).

The coefficients \tilde{b}_n also satisfy the N -term recurrence relation, which could be reduced to the three-term one

$$\tilde{c}_{0,i}^{(3)} \tilde{b}_i + \tilde{c}_{1,i}^{(3)} \tilde{b}_{i-1} + \tilde{c}_{2,i}^{(3)} \tilde{b}_{i-2} = 0, \quad i > 1. \quad (3.50)$$

In order to find \tilde{b}_1/\tilde{b}_2 , we must use the condition at the event horizon by taking into account (3.49),

$$\tilde{b}_0 = \sum_{n=0}^{\infty} b_n z_0^n, \quad \tilde{b}_1 = \sum_{n=1}^{\infty} n b_n z_0^{n-1}. \quad (3.51)$$

From (3.41b) and (3.41a) we find the coefficients b_n and substitute them into (3.50). If $z = 1$ is the closest singular point to $z = z_0$, we obtain the equation with respect to ω as

$$\frac{\tilde{b}_1}{\tilde{b}_0} = -\frac{\tilde{c}_{2,2}^{(3)}}{\tilde{c}_{1,2}^{(3)}} - \frac{\tilde{c}_{0,2}^{(3)} \tilde{c}_{2,3}^{(3)}}{\tilde{c}_{1,3}^{(3)}} - \frac{\tilde{c}_{0,3}^{(3)} \tilde{c}_{2,4}^{(3)}}{\tilde{c}_{1,4}^{(3)}} \dots \quad (3.52)$$

Otherwise one has to repeat the procedure, by constructing the series (3.49) for the next midpoints z_1, z_2, z_3, \dots , until the cosmological horizon (or spatial infinity) appears to be inside the radius of convergence.

One should note, if the convergence of the continued fraction on the right-hand side of (3.52) is slow, one can use the Nollert improvement. Since the radius of convergence of the Frobenius series is now less than one ($R < 1$), we must choose $C_0 = -R^{-1}$ in (3.46).

3.4.5 Generalisation of the Frobenius series

The series expansion (3.36) is not necessarily to be done in terms of power of a rational function of r . For some purposes, the more convenient choice is expansion in terms of an other full set of functions in the appropriate Hilbert space. Here we consider, as an example, a Kerr-Newman-de Sitter black hole, that is described by the line element

$$ds^2 = -\rho^2 \left(\frac{dr^2}{\Delta_r} + \frac{d\theta^2}{\Delta_\theta} \right) - \frac{\Delta_\theta \sin^2 \theta}{(1 + \alpha)^2 \rho^2} [adt - (r^2 + a^2)d\varphi]^2 + \frac{\Delta_r}{(1 + \alpha)^2 \rho^2} (dt - a \sin^2 \theta d\varphi)^2, \quad (3.53)$$

where

$$\begin{aligned} \Delta_r &= (r^2 + a^2) \left(1 - \frac{\alpha}{a^2} r^2 \right) - 2Mr + Q^2, \\ \Delta_\theta &= 1 + \alpha \cos^2 \theta, \quad \alpha = \frac{\Lambda a^2}{3}, \end{aligned} \quad (3.54)$$

M is the black hole mass, Q is the charge, a is the rotation parameter, and Λ is the cosmological constant.

After separation of the variables, the angular part of the massless (charged) field equation of motion can be reduced to [56]

$$\begin{aligned} & \left(\frac{d}{dx}(1+\alpha x^2)(1-x^2) \frac{d}{dx} + \lambda - s(1-\alpha) + \frac{(1+\alpha)^2}{\alpha} \xi^2 - 2\alpha x^2 + \right. \\ & \left. \frac{1+\alpha}{1+\alpha x^2} \left(2s(\alpha m - (1+\alpha)\xi)x - \frac{(1+\alpha)^2}{\alpha} \xi^2 - 2m(1+\alpha)\xi + s^2 \right) - \right. \\ & \left. - \frac{(1+\alpha)^2 m^2}{(1+\alpha x^2)(1-x^2)} - \frac{(1+\alpha)(s^2 + 2smx)}{1-x^2} \right) S(x) = 0, \end{aligned} \quad (3.55)$$

where λ is the separation constant $\xi = \alpha\omega$, $x = \cos(\theta)$, s is the field spin and m is the projection of the angular momentum of the field onto the axis of the black hole rotation, $0 \leq s \leq 2$ and m are (half)integers.

The appropriate series for the function S are [56]

$$S(z) = z^{A_1} (z-1)^{A_2} (z-z_s)^{A_3} (z-z_\infty) \sum_{n=0}^{\infty} b_n u_n(z), \quad (3.56)$$

where

$$\begin{aligned} z &= \frac{\sqrt{\alpha} - i}{2} \frac{x+1}{x\sqrt{\alpha} - i}, & z_s &= -\frac{i(1+i\sqrt{\alpha})^2}{4\sqrt{\alpha}}, & z_\infty &= -\frac{i(1+i\sqrt{\alpha})}{2\sqrt{\alpha}}, \\ A_1 &= \frac{|m-s|}{2}, & A_2 &= \frac{|m+s|}{2}, & A_3 &= \pm \frac{i}{2} \left(\frac{1+\alpha}{\sqrt{\alpha}} \xi - \sqrt{\alpha} \xi - is \right), \end{aligned}$$

and the expansion is done in terms of the Jacobi polynomials

$$u_n(z) = F(-n, n + \bar{\omega}; \gamma; z) = (-1)^n \frac{\Gamma(2n + \bar{\omega})n!}{\Gamma(n + \gamma)} P_n^{(\bar{\omega}-\gamma, \gamma-1)}(2z-1),$$

where $\bar{\omega} = 2A_1 + 2A_2 + 1$ and $\gamma = 2A_1 + 1$.

The coefficients b_n in (3.56) satisfy the three-term recurrence relation (3.41a, 3.41b) with

$$c_{0,n}^{(3)} = \pm \frac{i}{\sqrt{\alpha}} \xi \frac{n(n + A_1 + A_2 \mp s)(n + 2A_2)}{2(2n + 2A_1 + 2A_2 + 1)(n + A_1 + A_2)}, \quad (3.57)$$

$$\begin{aligned} c_{1,n}^{(3)} &= \frac{i}{\sqrt{\alpha}} \left\{ \pm \xi \frac{J_n}{2(n + A_1 + A_2)(n + A_1 + A_2 - 1)} \right. \\ &+ \frac{(n-1)(n + 2A_1 + 2A_2)}{4} \\ &\left. - \frac{1}{4} \left[\lambda - 2A_1 A_2 - A_1 - A_2 + 2(m + s \mp (2A_1 + 1))\xi - \frac{m^2 - s^2}{2} - s \right] \right\}, \end{aligned} \quad (3.58)$$

$$c_{2,n}^{(3)} = \mp \frac{i}{\sqrt{\alpha}} \xi \frac{(n-1 + A_1 + A_2 \pm s)(n-1 + 2A_1)(n-1 + 2A_1 + 2A_2)}{2(2n + 2A_1 + 2A_2 - 3)(n-1 + A_1 + A_2)}, \quad (3.59)$$

where

$$J_n = (n-1)(n+2A_1+2A_2)(A_1-A_2) + (A_1+A_2 \pm s+1) \left((n-1)(n+2A_1+2A_2) + (2A_1+1)(A_1+A_2) \right).$$

Since the series (3.56) must be convergent at $z = 1$, we can solve numerically the equation (3.44), and find, thereby, the separation constant as a function of frequency.

In the Reissner-Nordström-de Sitter limit ($a \rightarrow 0$) the equation (3.44) is reduced to $c_{1,n}^{(3)} = 0$. In this case the value of λ does not depend on ω

$$\lambda = (l - s + 1)(l + s), \quad l = n + A_1 + A_2 \geq \max(|m|, |s|).$$

3.4.6 Frobenius series for the radial part of the charged field equation in the Kerr-Newman-de Sitter background

The radial part of the massless (charged) field equation of motion is of the form (3.34) and reads [56]

$$\left\{ \Delta_r^{-s} \frac{d}{dr} \Delta_r^{s+1} \frac{d}{dr} + \frac{1}{\Delta_r} \left(K^2 - isK \frac{d\Delta_r}{dr} \right) + 4is(1 + \alpha)\omega r - \frac{2\alpha}{a^2} (s + 1)(2s + 1)r^2 + 2s(1 - \alpha) - 2isqQ - \lambda \right\} R(r) = 0, \quad (3.60)$$

where $K = [\omega(r^2 + a^2) - am](1 + \alpha) - qQr$, q is the field charge.

The appropriate Frobenius series are found to be [22]

$$R(r) = \left(\frac{r - r_+}{r - r_-} \right)^{-s - 2iK(r_+)/\Delta_r'(r_+)} e^{iB(r)} r^{-2s-1} u \left(\frac{r - r_+ r_\infty - r_-}{r - r_- r_\infty - r_+} \right) \quad (3.61)$$

Note, that, in order to obtain the recurrence relation for both types of the boundaries (asymptotically flat and de Sitter), we introduce the exponent $e^{iB(r)}$ such that $\frac{dB(r)}{dr} = \frac{K}{\Delta_r}$. This exponent describes an outgoing wave at the horizons and spatial infinity. Thus we have to compensate the outgoing wave at the event horizon. That is why the factor 2 appears in the power of the first multiplier in (3.61). The parameter r_0 is fixed to be the inner horizon r_- , in order to move all the singularities outside the unit circle and, at the same time, to provide the best convergence of the infinite continued fraction (3.44).

Since λ can be calculated numerically as a function of ω (see section 3.4.5), we are able to solve the equation (3.44) with respect to ω .

In the Reissner-Nordström-de Sitter limit ($a = 0$) for neutral field ($q = 0$) we obtain $K = \omega r^2$ and

$$R(r) = \left(\frac{r - r_+}{r - r_-} \right)^{-s - i\omega/\kappa} e^{i\omega r_\star} r^{-2s-1} u \left(\frac{r - r_+ r_\infty - r_-}{r - r_- r_\infty - r_+} \right). \quad (3.62)$$

The tortoise coordinate is defined by $dr_\star = \frac{r^2 dr}{\Delta_r}$, and $\kappa = \frac{\Delta_r'(r_+)}{2r_+^2}$ is the surface gravity on the event horizon.

3.4.7 Frobenius series for the massive scalar field equation in the higher-dimensional Reissner-Nordström-de Sitter background

A D -dimensional Reissner-Nordström-de Sitter black hole is described by the metric

$$ds^2 = f(r) dt^2 - \frac{dr^2}{f(r)} - r^2 d\Omega_{D-2}, \quad (3.63)$$

where $d\Omega_{D-2}$ is the line element of a $(D - 2)$ -dimensional sphere,

$$f(r) = 1 - \frac{2M}{r^{D-3}} + \frac{Q^2}{r^{2D-6}} - \frac{2\Lambda r^2}{(D-1)(D-2)}. \quad (3.64)$$

After separation of the angular and time variables, the radial part of the massive scalar field equation of motion $(\square + \mu^2)\Psi = 0$ is reduced to the wave-like equation

$$\left(\frac{d^2}{dr_*^2} + \omega^2 - f(r) \left(\mu^2 + \frac{l(l+D-3)}{r^2} + \frac{f'(r)(D-2)}{2r} + \frac{f(r)(D-2)(D-4)}{4r^2} \right) \right) r^{\frac{D-2}{2}} R(r) = 0, \quad (3.65)$$

where integer $l = 0, 1, 2, \dots$ parameterises the angular separation constant.

The Frobenius series for this case are

$$R(r) = \left(\frac{r-r_+}{r-r_0} \right)^{-\frac{i\omega}{\kappa}} e^{iA(r)} r^{-\frac{D-2}{2}} u \left(\frac{r-r_+}{r-r_0} \frac{r_\infty-r_0}{r_\infty-r_+} \right), \quad (3.66)$$

where $\kappa = \frac{1}{2}f'(r_+)$, $e^{iA(r)}$ describes the outgoing wave for the spatial infinity and the horizons $\frac{dA(r)}{dr} = \frac{\sqrt{\omega^2 - \mu^2 f(r)}}{f(r)}$. The sign in the exponent is fixed by the quasi-normal boundary condition: the real part of $A(r \rightarrow r_\infty)$ must be of the same sign as the real part of the eigenfrequency ω . This choice of the sign makes the wave outgoing at the cosmological horizon (or spatial infinity).

For massless field ($\mu = 0$) this exponent is $e^{i\omega r_*}$ [20] and the Frobenius series read

$$R(r) = \left(\frac{r-r_+}{r-r_0} \right)^{-\frac{i\omega}{\kappa}} e^{i\omega r_*} r^{-\frac{D-2}{2}} u \left(\frac{r-r_+}{r-r_0} \frac{r_\infty-r_0}{r_\infty-r_+} \right). \quad (3.67)$$

Since for $D = 4$ we can choose $r_0 = r_-$, we come to (3.62) ($s = 0$).

At the cosmological horizon we can observe the same asymptotical behavior of the exponent

$$e^{iA(r)} \sim e^{i\omega r_*}, \quad r \rightarrow r_\infty < \infty.$$

If $\Lambda = 0$, $D \geq 5$, $f(r) = 1 + o(r^{-1})$ we can write the Frobenius series as [18]

$$R(r) = \left(\frac{r-r_+}{r-r_0} \right)^{-\frac{i\omega}{2\kappa}} e^{ir\sqrt{\omega^2 - \mu^2}} r^{-\frac{D-2}{2}} u \left(\frac{r-r_+}{r-r_0} \right). \quad (3.68)$$

For $D = 4$ the term of order $\sim r^{-1}$ in $f(r)$ leads to the non-trivial contribution [57]

$$R(r) = \left(\frac{r-r_+}{r-r_0} \right)^{-\frac{i\omega}{2\kappa}} e^{ir\sqrt{\omega^2 - \mu^2}} (r-r_0)^{ir + \sqrt{\omega^2 - \mu^2} + 2\mu^2/2\sqrt{\omega^2 - \mu^2}} r^{-\frac{D-2}{2}} u \left(\frac{r-r_+}{r-r_0} \right). \quad (3.69)$$

The same approach could be applied for the equations of motion for the Maxwell field and the gravitational perturbations, because their radial part can be reduced to the form (3.34) [58, 59]. Practically, the continued fraction coefficients appear to be so complicated for such cases, that we are unable to compute quasi-normal modes with this method during reasonable time.

3.5 Horowitz-Hubeny method

In order to find quasi-normal modes in the asymptotically anti-de Sitter space-times, usually we need to impose the Dirichlet boundary conditions at the spatial infinity. Thus, we can find the appropriate expansion for the function $R(r)$ in (3.34) without consideration of the singularity point at the infinity. This method was proposed by Horowitz and Hubeny [7]. Namely, we define

$$R = z^{-i\omega/(2\kappa)}\psi(z), \quad z = \frac{r - r_+}{r - r_-}, \quad (3.70)$$

where κ is the surface gravity at the event horizon.

If we substitute (3.70) into (3.34), we find that $\psi(z)$ satisfies the equation

$$s(z)\psi''(z) + \frac{t(z)}{z}\psi'(z) + \frac{u(z)}{z^2}\psi(z) = 0, \quad (3.71)$$

where

$$s(z) = \sum_{n=0}^{N_s} s_n z^n, \quad t(z) = \sum_{n=0}^{N_t} t_n z^n, \quad u(z) = \sum_{n=1}^{N_u} u_n z^n,$$

are polynomial functions of z .

Since the function $\psi(z)$ is regular at the event horizon $z = 0$, we can expand it as

$$\psi(z) = \sum_{n=0}^{\infty} a_n z^n. \quad (3.72)$$

The Dirichlet boundary condition at the spatial infinity $\psi(1) = 0$ reads

$$\sum_{n=0}^{\infty} a_n = 0. \quad (3.73)$$

Substituting (3.72) into (3.71), we can find the recurrence relation for the coefficients a_n

$$a_n = - \sum_{k=0}^{n-1} a_k \frac{k(k-1)s_{n-k} + kt_{n-k} + u_{n-k}}{n(n-1)s_0 + nt_0}. \quad (3.74)$$

The equation (3.74) allows to calculate all a_n starting from an arbitrary a_0 , which fixes the scale of $\psi(z)$. Substituting a_n into (3.73), we find the equation with respect to the eigenvalue ω . Practically, since the series (3.73) are convergent, we sum over some finite number of terms and solve (3.73) with respect to ω . In order to ensure that this truncation does not cause incorrect result we have to increase the number of terms until the value of ω does not change within the required precision.

Note, that, for the sum (3.73) to be convergent, r_- has to be a singular point of the equation (3.34), and all the other singularities, except $r = r_+$ and $r = r_\infty$, must lay outside the unit circle $|z| > 1$. If both of these conditions are impossible to satisfy, we must use the continued fraction method with the appropriate fixing of the behavior of R at spatial infinity.

Chapter 4

Perturbations of four-dimensional black holes

4.1 Quasi-normal modes of Schwarzschild and Schwarzschild-de Sitter black holes

Perturbations of four-dimensional black holes were studied extensively in the context of possibility to observe quasi-normal ringing with the help of gravitational wave detectors (see reviews [34, 60]). Since in our Universe the cosmological constant appears to be positive, its correction to the quasi-normal spectrum must be taken into account. Gravitational perturbations of spherically symmetric black holes in the de Sitter background were studied for the first time by the numerical integration (see sec. 2.2) in [30].

In [9] we study for the first time quasi-normal modes of massless Dirac and electromagnetic field in the Schwarzschild-de Sitter background. Also we study massless scalar and gravitational perturbations of Schwarzschild-de Sitter black holes, using the 6-th order WKB approach (see sec. 3.3), which provides more accurate results. Namely, we substitute the effective potentials for the scalar, electromagnetic, Dirac and gravitational perturbations (2.11, 2.13, 2.14, 2.16, 2.17) into the WKB formula (3.33) and find, that the presence of the cosmological constant leads to decrease of the real oscillation frequency and to a slower decay (see fig. 4.1).

For large l the following analytical expressions were found [9]

$$\omega = \frac{\sqrt{1 - 9M^2\Lambda}}{3\sqrt{3}M} \left(l + \frac{1}{2} - \left(n + \frac{1}{2} \right) i \right) + \mathcal{O} \left(\frac{1}{l} \right), \quad (4.1a)$$

$$\omega = \frac{\sqrt{1 - 9M^2\Lambda}}{3\sqrt{3}M} \left(\kappa_{\pm} - \left(n + \frac{1}{2} \right) i \right) + \mathcal{O} \left(\frac{1}{\kappa_{\pm}} \right). \quad (4.1b)$$

As the black hole mass approaches its extremal value, the effective potentials (2.11, 2.13, 2.14, 2.16, 2.17) look like the Pöshl-Teller potential (see sec. 3.2). Thus, using the Pöshl-Teller approach, it was found in [45] that in the near-extremal limit of the Schwarzschild-de Sitter black hole the quasi-normal frequencies are proportional to the surface gravity at the event horizon $\kappa = \frac{1}{2}f'(r_+)$

$$\omega = \kappa \left(\sqrt{(l+1-s)(l+s) - \frac{1}{4}} - i \left(n + \frac{1}{2} \right) \right) + o(\kappa), \quad (4.2a)$$

$$\omega = \kappa \left(\sqrt{\kappa_{\pm}^2 - \frac{1}{4}} - i \left(n + \frac{1}{2} \right) \right) + o(\kappa). \quad (4.2b)$$

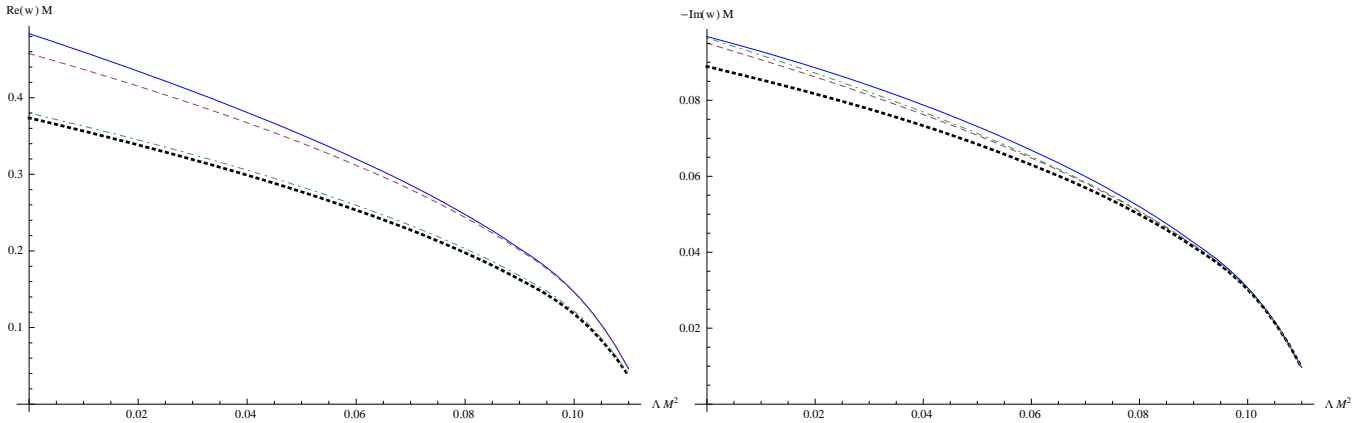


Figure 4.1: Real and imaginary parts of the fundamental quasi-normal frequency of the Schwarzschild-de Sitter black hole for scalar ($l = 2$), electromagnetic ($l = 2$), gravitational ($l = 2$), and Dirac ($\kappa = 2$) perturbations plotted with solid blue, dashed red, dot-dashed green and dotted black lines respectively.

Despite the dominant contribution of the imaginary part does not depend on the field spin s , the metric perturbations decay slower among the considered perturbations for all values of Λ .

4.2 High overtones in the quasi-normal spectrum

Though, practically, we can observe only low-damping oscillations, the frequencies with large imaginary part attracted some attention in the context of the black hole thermodynamics. Such frequencies are called high overtones. Since their imaginary part is very large, the WKB approach is not appropriate and one should use the more accurate Frobenius method (see sec. 3.4).

It has been suggested in [61] that the asymptotic value of the real part of the quasi-normal frequency (i. e. when the imaginary part approaches infinity) coincides with the so-called Barbero-Immirzi parameter [62, 63]. This parameter must be fixed in order to predict the Bekenstein-Hawking formula for entropy within the framework of Loop Quantum Gravity. For Schwarzschild black holes it was found numerically [54] and analytically [64] that the asymptotical behavior of the quasi-normal frequency is given by

$$\omega_n r_+ = \frac{\ln(3)}{4\pi} - \frac{i(n + 1/2)}{2} + \mathcal{O}(n^{-1/2})$$

for the gravitational perturbations and for the test scalar field, while for the electromagnetic perturbations the real part asymptotically approaches zero

$$\omega_n r_+ = -\frac{in}{2} + \mathcal{O}(n^{-1/2}).$$

We have shown numerically in [11] that for perturbations of the massless Dirac field, the asymptotical value of the real part of the highly damping quasi-normal frequencies is also zero (see fig. 4.2). The correct spacing of the imaginary part was found later in [65], with an alternative form of the effective potential for the Dirac perturbations. The asymptotical formula for the high overtones of the massless Dirac field in the Schwarzschild background reads

$$\omega_n r_+ \sim -\frac{in}{2}.$$

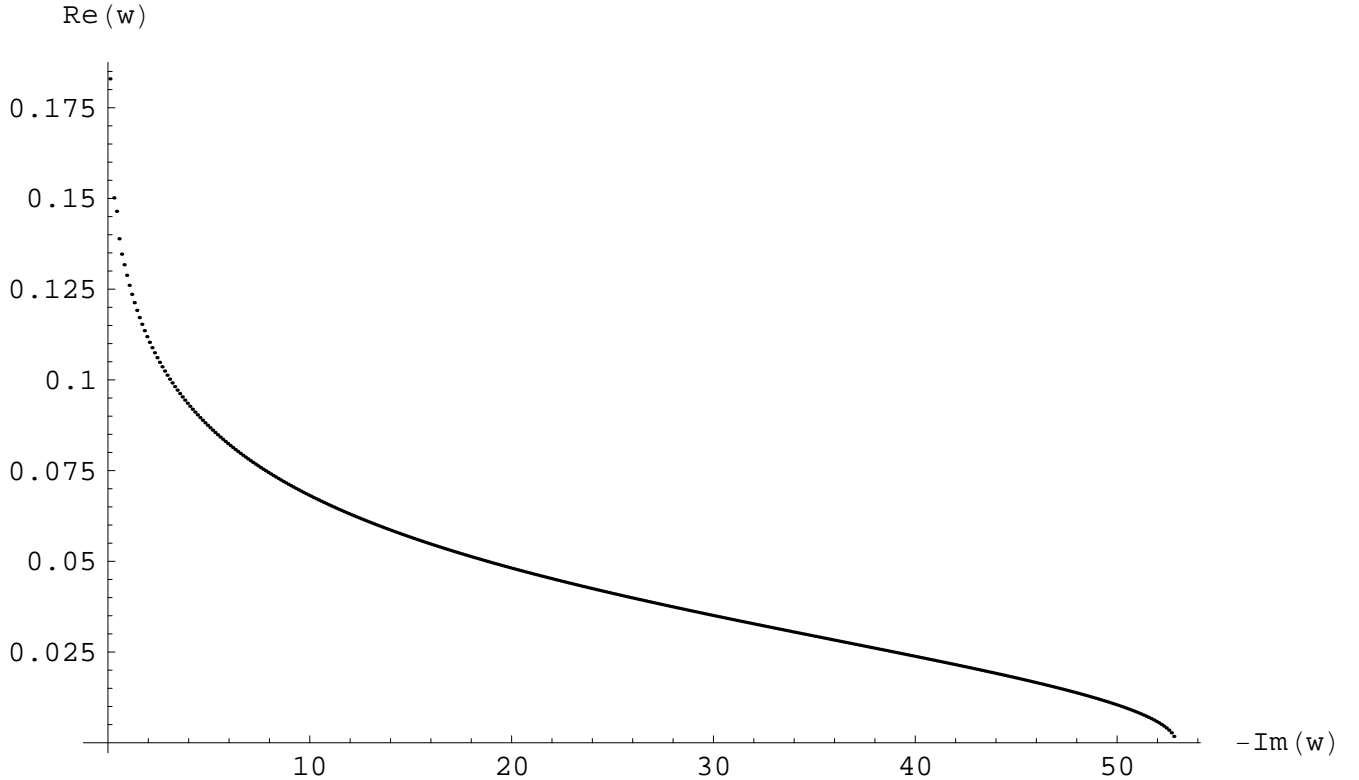


Figure 4.2: Real part of the highly damping quasi-normal frequencies as a function of imaginary part ($\kappa_{\pm} = 1$ perturbations of the massless Dirac field in the Schwarzschild background). The frequencies are measured in inverse units of the black hole mass.

Using the Frobenius method (see sec. 3.4), for Schwarzschild-de Sitter black holes we have found for the first time in [10] that again the real part of the quasi-normal frequencies for electromagnetic perturbations asymptotically approaches zero, satisfying

$$\omega_n \sim i\kappa n \quad \cup \quad \omega_n \sim i\kappa_{\infty} n,$$

where $\kappa = \frac{1}{2}f'(r_+)$ and $\kappa_{\infty} = \frac{1}{2}f'(r_{\infty})$ are the surface gravities at the black hole horizon and the cosmological horizon respectively (see fig. 4.3). This result was later confirmed analytically in [66].

The real part of the quasi-normal modes for metric perturbations does not approach a constant. Frequencies with high imaginary part satisfies the non-algebraic equation

$$\cosh\left(\frac{\pi\omega}{\kappa} - \frac{\pi\omega}{\kappa_{\infty}}\right) + 3 \cosh\left(\frac{\pi\omega}{\kappa} + \frac{\pi\omega}{\kappa_{\infty}}\right) \sim 0,$$

which implies oscillation of the real part as a function of the imaginary part (see fig. 4.4).

4.3 Decay of charged scalar and Dirac fields in the Kerr-Newman-de Sitter background

For charged black holes, the scalar field electrodynamics can describe the interaction of a charged field with the electromagnetic background of the black hole. When the influence of the spin of

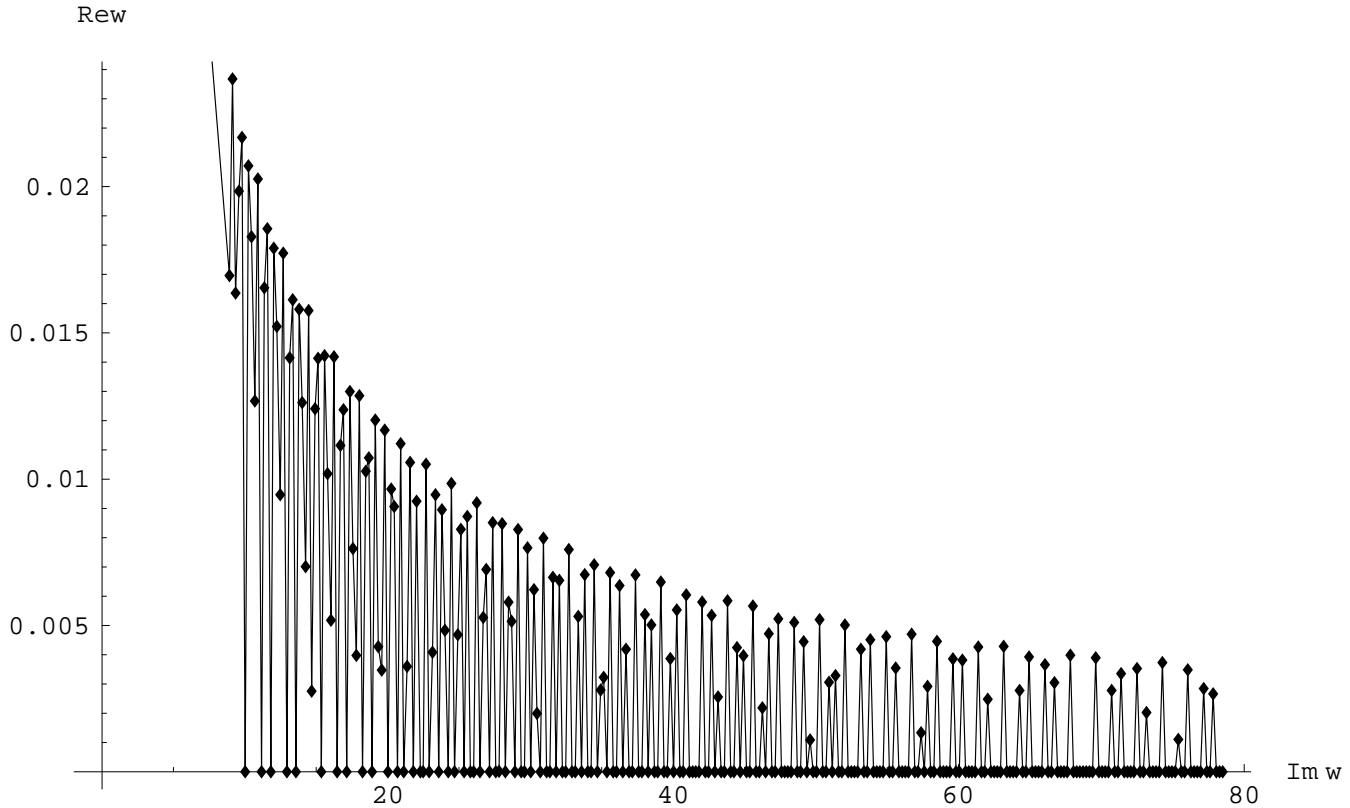


Figure 4.3: Real part of highly damping quasi-normal frequencies as a function of imaginary part for Schwarzschild-de Sitter black hole ($l = 1$ electromagnetic perturbations, $\Lambda M^2 = 0.02$). The frequencies are measured in inverse units of the black hole mass.

the field is neglected, we can consider the charged scalar field. The late-time tails of the charged scalar hair were studied for the first time by Hod [67, 68] in the context of the gravitational collapse. Quasi-normal modes of the charged scalar field for various black holes were studied for the first time in [69]. Quasi-normal modes of the charged massive scalar field for Reissner-Nordström black holes were considered in [70]. Decay of the charged Dirac field in the Reissner-Nordström background was studied in [71]. The decay law for the late-time tails of the charged massive Dirac field also was found for Reissner Nordström [72] and Kerr-Newman [73] black holes. Yet, the calculations of the quasi-normal modes in the above papers were limited by the third order WKB accuracy. The WKB accuracy does not allow to study the quasi-normal modes of the near extremal charged black holes. Namely, the decay rate of charged fields in the near extremal Reissner-Nordström background is the same within the WKB accuracy.

The numerical study of quasi-normal frequencies of the charged fields (both scalar and Dirac) in the Kerr-Newman-de Sitter background was done in [22] within a much more accurate Frobenius method (see sec. 3.4.5, 3.4.6). We have shown that for not very large value of Q , the charged field decays quicker than the neutral one. For the near extremal value of Q , the charged field decays slower than the neutral one (see fig. 4.5).

Let us summarise briefly what happens if a black hole has charge and rotation. We measure all the quantities in units of the size of the event horizon.

- As we know from previous sections, the presence of the cosmological constant decreases the absolute values of the real and imaginary parts of ω .

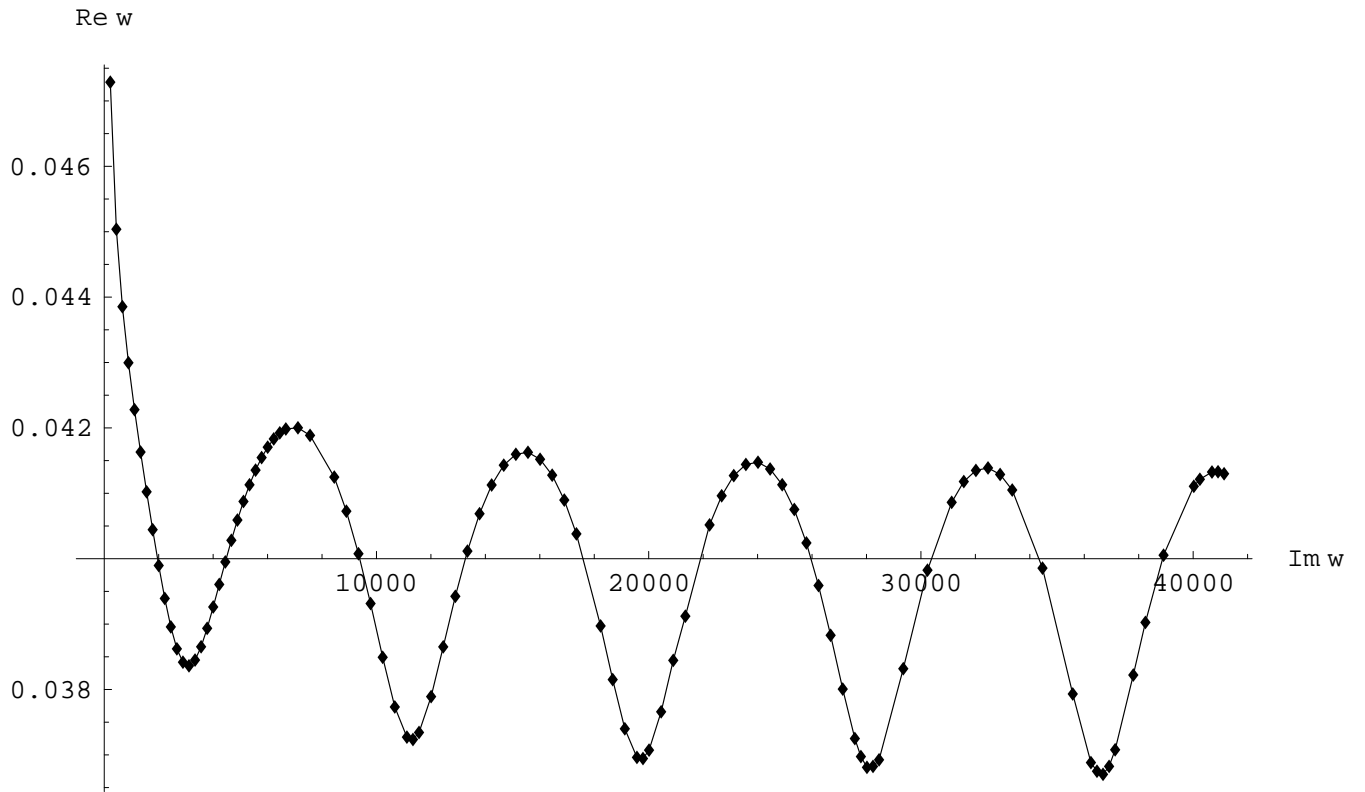


Figure 4.4: Real part of highly damping quasi-normal frequencies as a function of imaginary part ($l = 2$ metric perturbations of the Schwarzschild-de Sitter black hole, $\Lambda M^2 = 0.02$). The frequencies are measured in inverse units of the black hole mass.

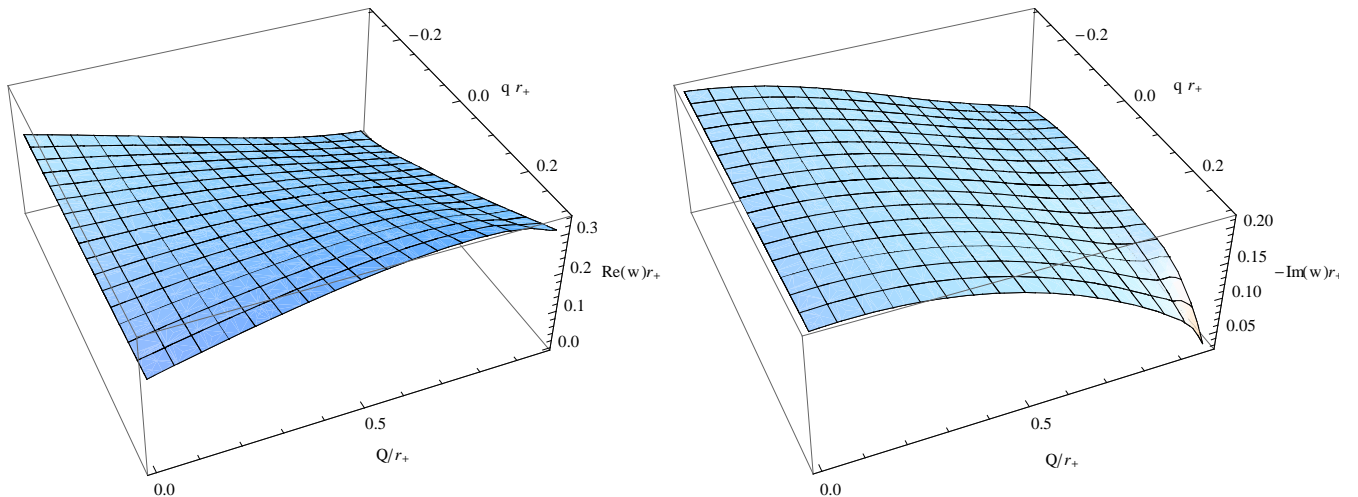


Figure 4.5: Real part and imaginary part of the fundamental quasi-normal frequency of charged (q) scalar field ($l = 0$) for the charged (Q) black hole.

- We already know, that as the multipole number l increases, the real part of ω grows, while the imaginary part of ω approaches a constant.
- Metric perturbations decay slower than any field perturbations of the same l .
- The dependance of ω on charge of the field q and of the black hole Q is shown on figure 4.5
 - If $qQ > 0$, the real part of ω monotonically grows as the field charge q increases. It grows also as the black hole charge Q increases, attains some maximum value at a large (close to extremal) value of Q , and then decreases.
 - If $qQ < 0$, the real part of ω decreases when either the black hole charge or the field charge increases.
 - The imaginary part of ω has more difficult behavior, in most cases decreasing its absolute value as qQ grows.
- The influence of the rotation parameter depends significantly on the projection of the field momentum on the axis of the black hole rotation m . We will consider this dependance later for the massive scalar field in the Kerr background (see sec. 6.3). Qualitatively the same behavior was observed for Kerr black holes, projected on the brane (see sec. 5.3.1).

Chapter 5

Perturbations of higher-dimensional black holes

5.1 Stability and quasi-normal modes of Reissner-Nordström-de Sitter black holes

Last years higher-dimensional black holes have attracted considerable interest in the context of the string theory and higher-dimensional brane-world models [74, 75, 76, 77, 78, 79]. Some of such models allow compactification radius of extra dimensions to be of macroscopic size [80, 81]. That is why the extra dimensions are important if we study small black holes. Such black holes could be produced at the next-generation particle colliders, probably at energies of order $\sim 1\text{TeV}$ [82, 83, 84, 85].

Being an important characteristic of a black hole, its quasi-normal spectrum can be used in future experiments to find number of extra dimensions and other parameters of the theory. That is why we study quasi-normal spectrum of black holes within different scenarios with various possible numbers of extra dimensions.

When a black hole is much smaller than the size of extra dimensions, it can be described by D -dimensional Einstein theory. The D -dimensional generalisation of the Schwarzschild metric was done by Tangherlini [86].

Let us consider the D -dimensional Reissner-Nordström-de Sitter black hole, which is described by the line element

$$ds^2 = f(r)dt^2 - \frac{dr^2}{f(r)} - r^2 d\Omega_d^2, \quad (5.1)$$

where $d\Omega_d$ is the line element of d -sphere, $d = D - 2$, $f(r) = 1 - X + Z - Y$. The dimensionless quantities X , Y , Z are defined as

$$X = \frac{dM\mathcal{A}_d}{4\pi r^{d-1}}, \quad Y = \frac{2\Lambda r^2}{d(d+1)}, \quad Z = \frac{Q^2}{r^{2d-2}},$$

where $\mathcal{A}_d = \frac{2\pi^{(d+1)/2}}{\Gamma((d+1)/2)}$ is the area of a unit d -sphere, M is the black hole mass, Q is the black hole charge and Λ is the cosmological constant.

Perturbations of the Einstein-Maxwell equations can be reduced to the wave-like form (2.10). The corresponding effective potential depends on their transformation law under rotations on the d -sphere (2.15). Thus, there are three types of perturbations described by three effective potentials:

tensor (V_T), vector (V_V) and scalar (V_S) type. The explicit form of the potentials was derived in [58]

$$V_T(r) = \frac{f(r)}{r^2} \left(\lambda + d + \frac{f'(r)rd}{2} + \frac{f(r)d(d-2)}{4} \right), \quad (5.2)$$

$$V_V(r) = \frac{f(r)}{r^2} \left(\lambda + d \pm \sqrt{X^2 \frac{(d^2-1)^2}{4} + 2Z\lambda d(d-1)} \times \frac{d(d-2)(1-Y) + Zd(5d-2) - X(d^2+2)}{4} \right), \quad (5.3)$$

$$V_S(r) = f(r) \frac{U_{\pm}}{64r^2 H_{\pm}^2} \quad (5.4)$$

where

$$H_+ = 1 - \frac{d(d+1)}{2} \delta X,$$

$$H_- = \lambda + \frac{d(d+1)}{2} (1 + \lambda \delta) X,$$

$$U_+ = [-4d^3(d+2)(d+1)^2 \delta^2 X^2 - 48d^2(d+1)(d-2)\delta X - 16(d-2)(d-4)] Y - \delta^3 d^3 (3d-2)(d+1)^4 (1 + \lambda \delta) X^4 + 4\delta^2 d^2 (d+1)^2 \{ (d+1)(3d-2)\lambda \delta + 4d^2 + d - 2 \} X^3 + 4\delta(d+1) \{ (d-2)(d-4)(d+1)(\lambda + d^2)\delta - 7d^3 + 7d^2 - 14d + 8 \} X^2 + \{ 16(d+1)(-4\lambda + 3d^2(d-2))\delta - 16(3d-2)(d-2) \} X + 64\lambda + 16d(d+2),$$

$$U_- = [-4d^3(d+2)(d+1)^2 (1 + \lambda \delta)^2 X^2 + 48d^2(d+1)(d-2)\lambda(1 + \lambda \delta) X - 16(d-2)(d-4)\lambda^2] Y - d^3(3d-2)(d+1)^4 \delta(1 + \lambda \delta)^3 X^4 - 4d^2(d+1)^2 (1 + \lambda \delta)^2 \{ (d+1)(3d-2)\lambda \delta - d^2 \} X^3 + 4(d+1)(1 + \lambda \delta) \{ \lambda(d-2)(d-4)(d+1)(\lambda + d^2)\delta + 4d(2d^2 - 3d + 4)\lambda + d^2(d-2)(d-4)(d+1) \} X^2 + 64\lambda^3 + 16d(d+2)\lambda^2 - 16\lambda \{ (d+1)\lambda(-4\lambda + 3d^2(d-2))\delta + 3d(d-4)\lambda + 3d^2(d+1)(d-2) \} X.$$

Here we defined $\lambda = (l+d)(l-1)$ through the multipole number $l = 2, 3, 4, \dots$. The value δ is a dimensionless constant

$$2\lambda\delta = \sqrt{1 + \frac{16\lambda Z}{(d+1)^2 X^2}} - 1.$$

Note, that the effective potential for tensor-type perturbations coincides with the potential for a test scalar field (3.65) for $l \geq 2$. Vector-type and scalar-type metric perturbations are coupled to perturbations of the electromagnetic field. For neutral ($Q = 0$) black holes the type “+” potentials are reduced to the effective potential for the test Maxwell field and for the type “-” V_V and V_S describe pure vector-type and scalar type metric perturbations respectively.

It was proven analytically that the black hole is stable against tensor-type and vector-type gravitational perturbations [58]. The effective potential of the scalar type (5.4) is not positive definite, having a negative gap for small l . Since the effective potential has an extremely complicated form, the appropriate ansatz for the S -deformation technique (see sec. 2.3.2) was not found. That is why, the black hole stability against scalar-type perturbations was not proven analytically.

The stability of higher dimensional Schwarzschild-de Sitter black holes was proven numerically in [20]. We have shown in time domain that the gravitational perturbations of scalar type decay for arbitrary black hole mass and Λ -term (see figs. 5.1,5.2).

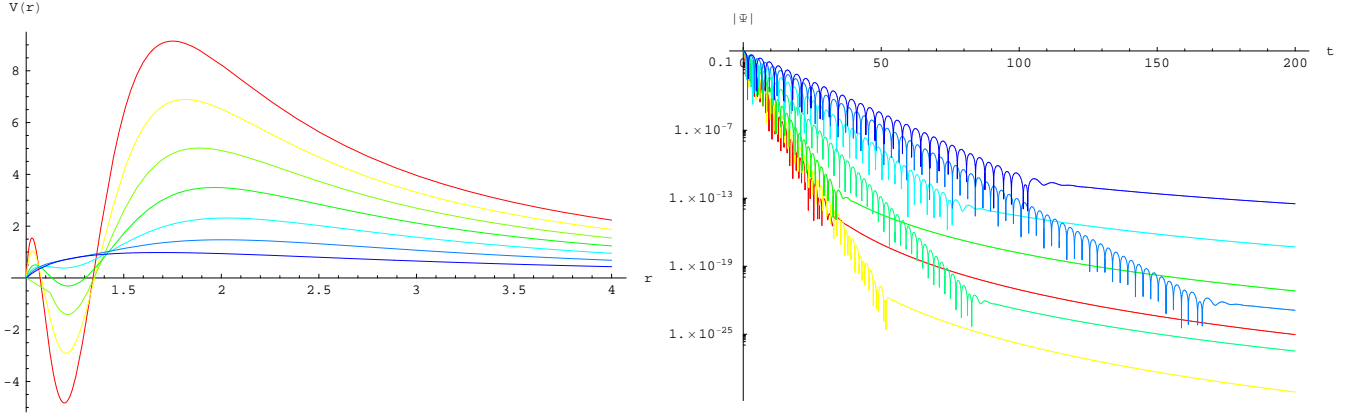


Figure 5.1: Effective potentials and time-domain profiles for scalar-type gravitational perturbations, $D = 5$ (blue) ... $D = 11$ (red) ($l = 2$, $Q = 0$, $\Lambda = 0$). For higher D both the peak and the negative gap of the potential increase. Profile for higher D decays quicker. All quantities are measured in units of the event horizon r_+ .

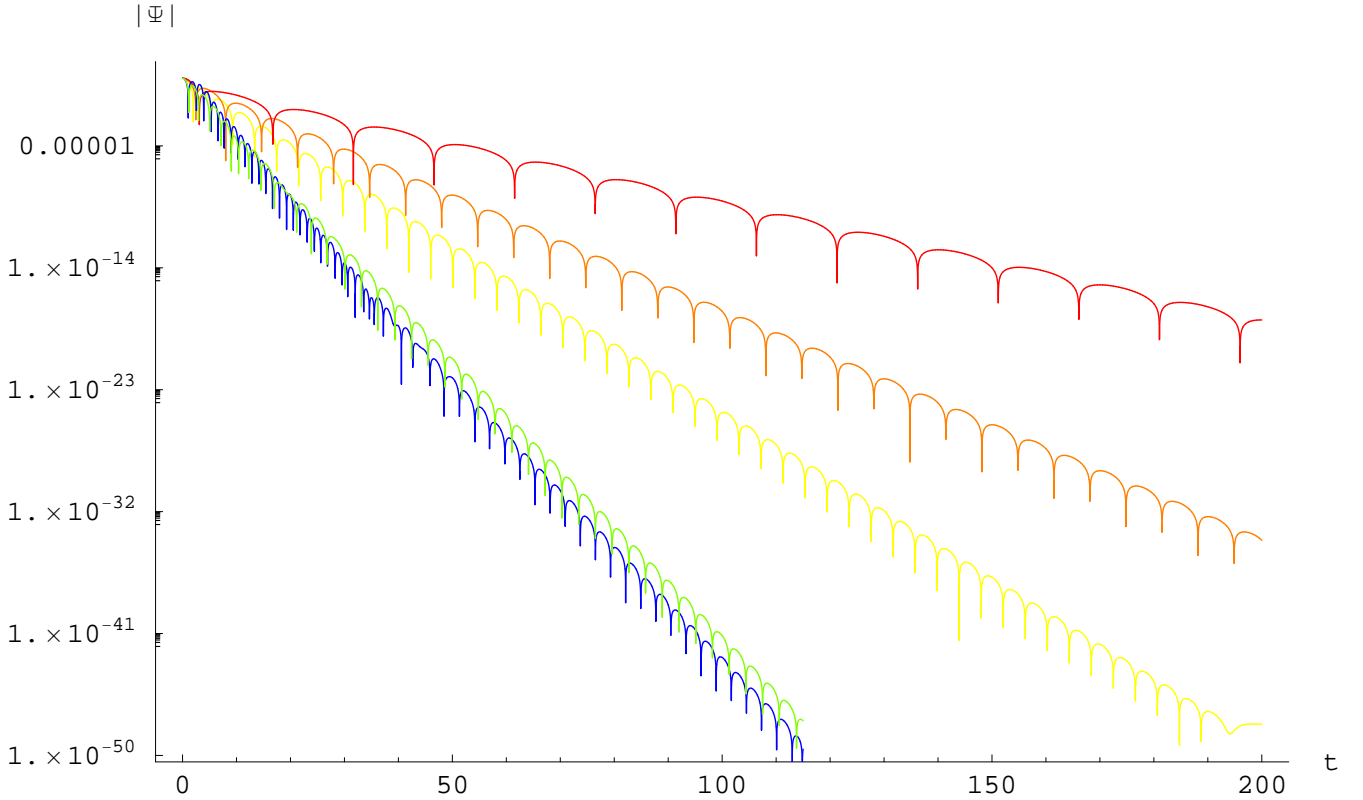


Figure 5.2: Time-domain profiles for scalar-type gravitational perturbations of 11-dimensional Schwarzschild-de Sitter black hole ($Q = 0$, $D = 11$, $\rho = r_+/r_\infty$) for $\rho = 0.3$ (blue), $\rho = 0.5$ (green), $\rho = 0.7$ (yellow), $\rho = 0.8$ (orange), $\rho = 0.9$ (red). Profile for higher ρ decays slower. All quantities are measured in units of the event horizon r_+ .

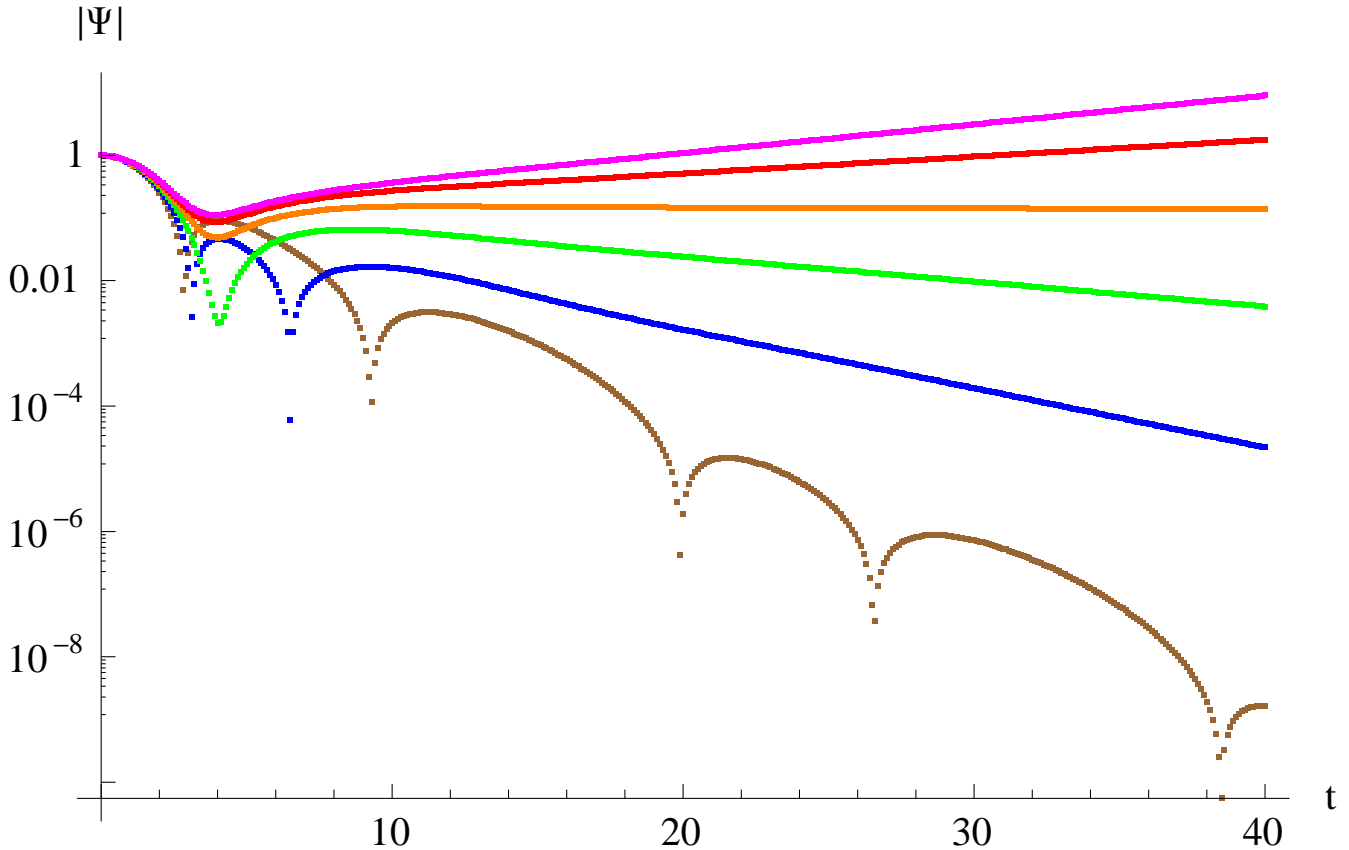


Figure 5.3: Time-domain profile for gravitational perturbations of scalar type “-” of the Reissner-Nordström-de Sitter black hole ($D = 11$, $\rho = r_+/r_\infty = 0.8$, $l = 2$) for various values of the black hole charge $q = Q/Q_{ext}$: $q=0.4$ (brown) $q=0.5$ (blue) $q=0.6$ (green) $q=0.7$ (orange) $q=0.8$ (red) $q=0.9$ (magenta). The smaller q , the slower growth of the profile is.

Also we studied the quasi-normal modes for all types of gravitational perturbations of D -dimensional spherically symmetric black holes. Since for the observational purposes only the dominant quasi-normal frequency is essential we were limited by the fundamental mode ($l = 2$) only. However, using the WKB approximation, we are able to find the large l formula for any given black hole parameters.

The dependance of the quasi-normal modes on the Λ -term is qualitatively the same as for the four-dimensional black holes: both real and imaginary parts of the quasi-normal frequency decrease their absolute values as the cosmological constant grows (see fig. 5.2). We also observe that the real and imaginary parts of the quasi-normal frequency are non-monotonic functions of the black hole charge, in most cases decreasing their absolute values as Q grows.

In [27] we have shown for the first time that Reissner-Nordström-de Sitter black holes are gravitationally unstable for large values of the electric charge and cosmological constant in $D \geq 7$ space-time dimensions. On the figure 5.3 we see the time-domain profiles for the linear gravitational perturbations of scalar type “-” (5.4) of the near extremal Reissner-Nordström-de Sitter black hole in $D = 11$ dimensions. For sufficiently small values of the black hole charge we observe usual picture of the quasi-normal ringing. Then, as the black hole charge increases, a purely imaginary (non-oscillating) mode becomes dominant, decreasing its decay rate until the threshold point of instability is reached. After crossing the instability point we observe the growing non-oscillating mode (see sec. 2.3.2). Its growth rate increases as the black hole charge grows. Therefore, we

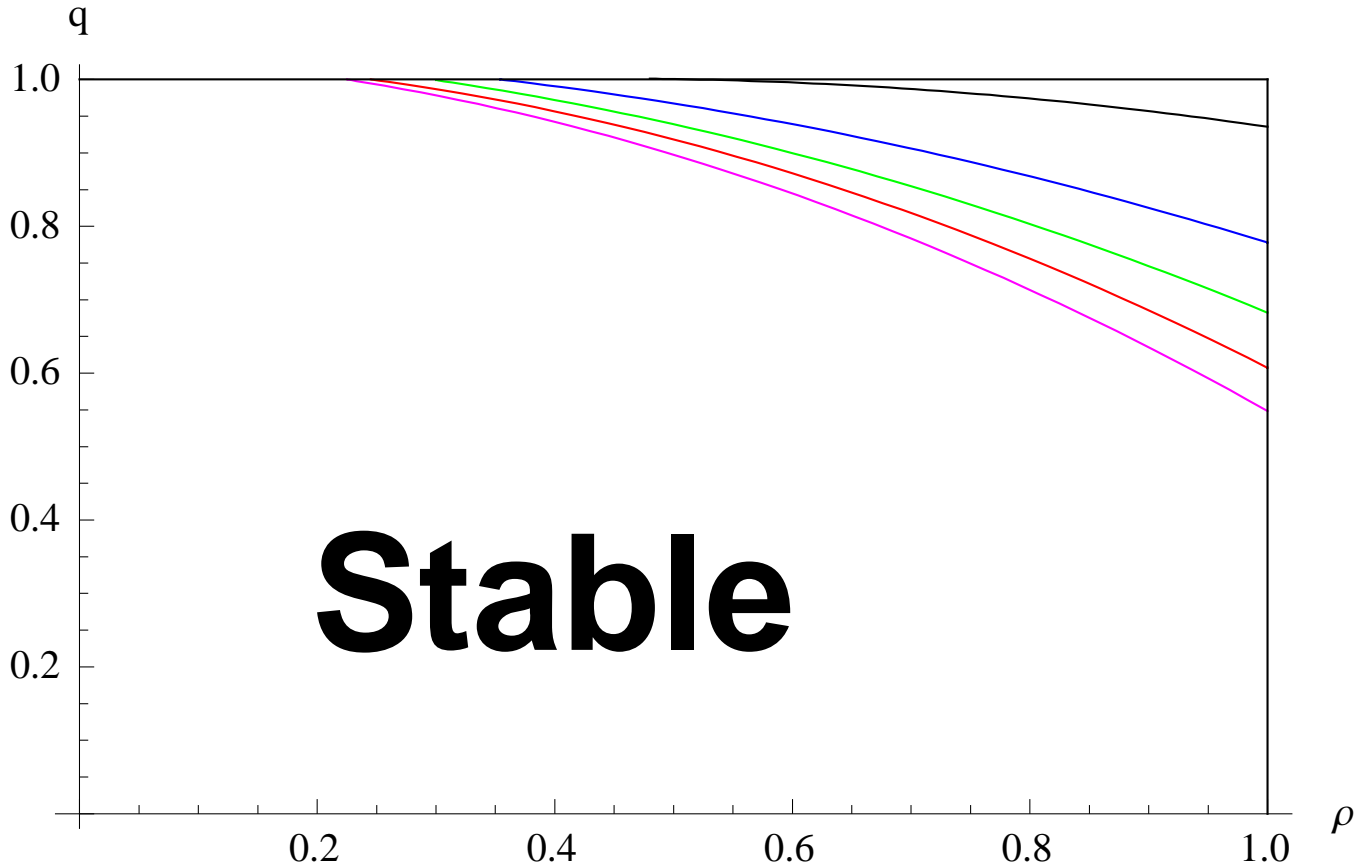


Figure 5.4: The parametric region of instability in the right upper corner of the square ($\rho = r_+/r_\infty$, $q = Q/Q_{ext}$) for $D = 7$ (top, black), $D = 8$ (blue), $D = 9$ (green), $D = 10$ (red), $D = 11$ (bottom, magenta).

conclude that exactly at the threshold point of instability there is some static solution ($\omega = 0$) of the perturbation equation. The static solution at the threshold point of instability was observed also in time-domain for the black strings (see sec. 6.4).

The parametric region of instability is shown on the figure 5.4. The larger number of space-time dimensions D is, the bigger region of instability we observe. Though the region of instability increases with D , the charged black holes in the asymptotically flat space-time are stable at least for $D \leq 11$. The instability occurs if *both* the black hole charge and the cosmological constant are large enough.

5.2 (In)stability of D -dimensional black holes in the Gauss-Bonnet theory

Higher dimensional quantum gravity implies corrections to classical general relativity. The dominant order correction to the Lagrangian is called the Gauss-Bonnet term [87]. This term is squared in curvature and vanishes for $D = 4$. The effective action is given by

$$S = \frac{1}{16\pi G_D} \int d^D x \sqrt{-g} (R + \alpha(R_{abcd}R^{abcd} - 4R_{cd}R^{cd} + R^2)), \quad (5.5)$$

where α is a positive coupling constant, $[\alpha] = L^2$.

The spherically symmetric black hole solution, which satisfies the corresponding equations of motion, is described by the line element (5.1) with

$$f(r) = 1 + \frac{r^2}{\alpha(D-3)(D-4)}(1 - q(r)), \quad q(r) = \sqrt{1 + \frac{\alpha(D-2)(D-3)(D-4)M\mathcal{A}_{D-2}}{2\pi r^{D-1}}}, \quad (5.6)$$

which is reduced to the Tangherlini metric [86] in the limit of $\alpha \rightarrow 0$.

Quasi-normal modes and late-time tails of the test scalar field for black holes in the Gauss-Bonnet theory were studied in [88, 89].

The quantum corrections imply that the effective potential for tensor-type gravitational perturbations (V_T) does not coincide with the potential for the test scalar field [90]. The effective potentials for vector-type (V_V) and scalar-type (V_S) gravitational perturbations were found in [91]. They are given by the formulae

$$V_T(r) = f(r) \frac{(D-2)(c+1)}{r^2} \left(3 - \frac{B(r)}{A(r)} \right) + \frac{1}{\sqrt{r^{D-2}A(r)q(r)}} \frac{d^2}{dr_*^2} \sqrt{r^{D-2}A(r)q(r)}, \quad (5.7)$$

$$V_V(r) = f(r) \frac{(D-2)c}{r^2} A(r) + \sqrt{r^{D-2}A(r)q(r)} \frac{d^2}{dr_*^2} \frac{1}{\sqrt{r^{D-2}A(r)q(r)}}, \quad (5.8)$$

$$V_S(r) = \frac{f(r)U(r)}{64r^2(D-3)^2A(r)^2q(r)^8(4cq(r) + (D-1)R(q(r)^2 - 1))^2}, \quad (5.9)$$

where we used the following dimensionless quantities

$$\begin{aligned} A(r) &= \frac{1}{q(r)^2} \left(\frac{1}{2} + \frac{1}{D-3} \right) + \left(\frac{1}{2} - \frac{1}{D-3} \right), \\ B(r) &= A(r)^2 \left(1 + \frac{1}{D-4} \right) + \left(1 - \frac{1}{D-4} \right), \\ R &= \frac{r^2}{\alpha(D-3)(D-4)}, \\ c &= \frac{l(l+D-3)}{D-2} - 1, \quad l = 2, 3, 4, \dots, \end{aligned}$$

$$\begin{aligned}
U(r) = & 5(D-1)^6 R^2(1+R) - 3(D-1)^5 R((D-1)R^2 + 24c(1+R))q(r) + \\
& + 2(D-1)^4(24c(D-1)R^2 + 168c^2(1+R) - (D-1)R^2(-3 + 5R + 7D(1+R)))q(r)^2 + \\
& + 2(D-1)^4 R(-184c^2 + (D-1)(13 + D)R^2 + c(-84 + 44R + 84D(1+R)))q(r)^3 + \\
& + (D-1)^3(384c^3 - 48c(2 + D(3D-5))R^2 + 192c^2(-11 + D + (-15 + D)R) + \\
& + (D-1)R^2(-3(7 + 55R) + D(26 + 106R + 7D(1+R))))q(r)^4 + \\
& + (D-1)^3 R(-64c^2(D-38) + (D-1)(71 + D(7D-90))R^2 + \\
& + 16c(303 + 255R + 13D^2(1+R) - 2D(73 + 81R)))q(r)^5 + \\
& + 4(D-1)^2(96c^3(-7 + D) - 8c(D-1)(145 - 74D + 6D^2)R^2 - \\
& - 8c^2(9 - 175R + D(-58 - 34R + 11D(1+R))) + (D-1)R^2(-5(79 + 23R) + \\
& + D(5(57 + 41R) + D(-81 - 89R + 7D(1+R))))q(r)^6 - \\
& - 4(D-1)^2 R(8c^2(43 + (72 - 13D)D) + (D-1)(-63 + D(99 + D(-49 + 5D))))R^2 + \\
& + 4c(321 + 465R + D(121 - 39R + D(-123 - 107R + 17D(1+R))))q(r)^7 + \\
& + (D-1)(128c^3(-9 + D)(D-5) + 32c(D-1)(246 + D(9 + D(-55 + 8D))))R^2 + \\
& + 64c^2(D-5)(D^2 - 3 + (49 + (D-4)D)R) - \\
& - (D-1)R^2(1173 + 565R + D(-4(997 + 349R) + D(6(393 + 217R) + \\
& + D(-548 - 452R + 45D(1+R))))q(r)^8 + \\
& + (D-1)R(-64c^2(D-5)(36 + D(-13 + 3D)) + \\
& + (D-1)(635 + D(-1204 + 3D(294 + D(-92 + 9D))))R^2 - \\
& - 8c(D-5)(63 + 31R + D(127 + 191R + D(-47 + D + (-79 + D)R)))q(r)^9 + \\
& + 2(D-5)(64c^3(D-5)(D-3) + 8c(D-1)(-27 + D(141 + (-43 + D)D)))R^2 + \\
& + 8c^2(D-5)(-3 + 77R + D(D-2 + (D-18)R)) + (D-1)^2 R^2(-33(R-7) + \\
& + D(59 + 43R + D(-59 - 35R + 9D(1+R))))q(r)^{10} - \\
& - 2(D-5)R(24c^2(-11 + D)(D-5)(D-3) + (D-1)^2(-65 + D(81 + D(7D-39))))R^2 + \\
& + 12c(-7 + D)(D-5)(D-3)(D-1)(1+R)q(r)^{11} + \\
& + (D-5)^2(-1 + D)R^2(16c(26 + (D-9)D) + \\
& + (D-1)(77 - 3R + D(-18 + D + (D-2)R)))q(r)^{12} + \\
& + (D-5)^2(D-3)^2(D-1)^2 R^3 q(r)^{13}.
\end{aligned}$$

The quasi-normal modes of gravitational perturbations of Einstein-Gauss-Bonnet black holes were found in time-domain (see sec. 3.1) for the first time in [23]. Consequently, we confirm the instability of these black holes in five- and six-dimensional space-times, proven analytically in [92].

Namely, in five dimensional case scalar-type perturbations are unstable for $\alpha > 0.207r_+^2$ while in six dimensions tensor-type perturbations are unstable for $\alpha > 1.006r_+^2$. We can see on the figure 5.5 that the larger l , at the earlier times instability growth occurs, and the stronger the growth rate is. In the region near the threshold value of α , one can observe the growth only for large enough l , while perturbations of lower multipole number are not growing. For each l there is some maximal value of α for which the perturbations are not growing. In order to find the threshold value of α numerically we extrapolate this value for $l \rightarrow \infty$ (see fig. 5.6). Einstein-Gauss-Bonnet black holes in $D \geq 7$ space-times are stable.

In units of the event horizon radius, the imaginary part of fundamental quasi-normal modes decreases, when α increases, for all numbers of D and all types of perturbations. Unlike the imaginary part, the real oscillation frequency does not behave uniformly: it decreases as α grows for most cases

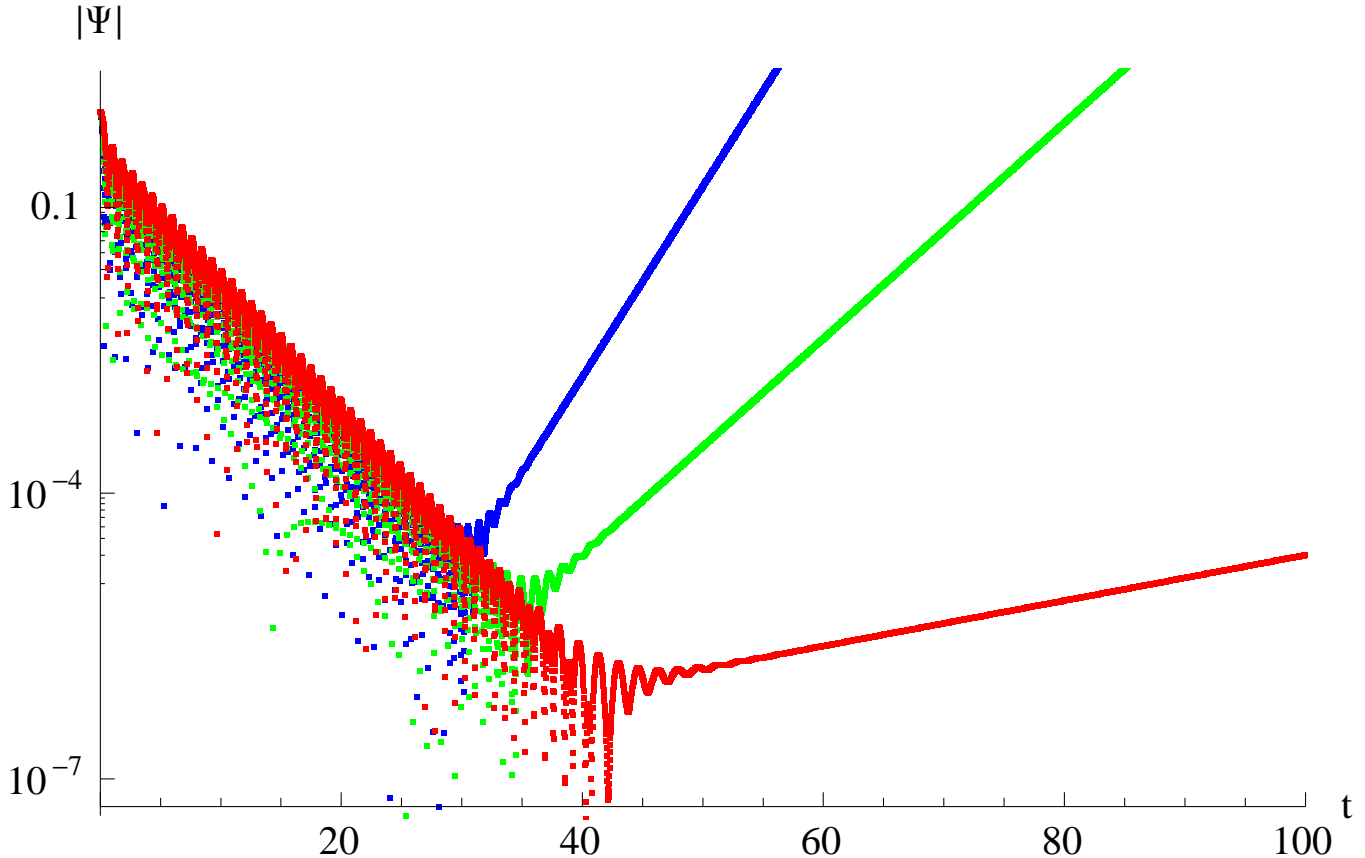


Figure 5.5: The picture of instability of tensor-type of gravitational perturbations of Gauss-Bonnet black holes, developing at large multipole numbers: $D = 6$, $l = 8$ (red), $l = 12$ (green), $l = 16$ (blue), $\alpha = 1.3$. All quantities are measured in units of the event horizon r_+ .

of tensor and vector modes. The behavior of the scalar mode is different: there are *two* competing for the domination modes at different stages of the quasi-normal ringing. This superposition of modes, also with competing excitation coefficients, makes dependence of the fundamental scalar type quasi-normal modes on α and D non-monotonic. On the figure 5.7 one can see that at the first stage the actual frequency of the dominant mode is much larger than at the second stage, while their damping rate stays almost the same.

5.3 Quasi-normal modes of brane-localised Standard Model fields

The other possible scenario is that the Standard Model particles (scalars, fermions and gauge bosons) are restricted to live on the $3 + 1$ -brane, which is embedded in the higher-dimensional bulk, while the gravitons can propagate also in the bulk. Therefore, if we study propagation of the fields near a D -dimensional black hole, we must consider the induced-on-the-brane gravitational background. If the size of extra dimensions is large, comparing to the size of the black hole, the induced background is given by the projection of the D -dimensional black hole metric onto the brane by fixing the values of the additional angular coordinates that describe the $(D - 4)$ extra spacelike dimensions [93, 94].

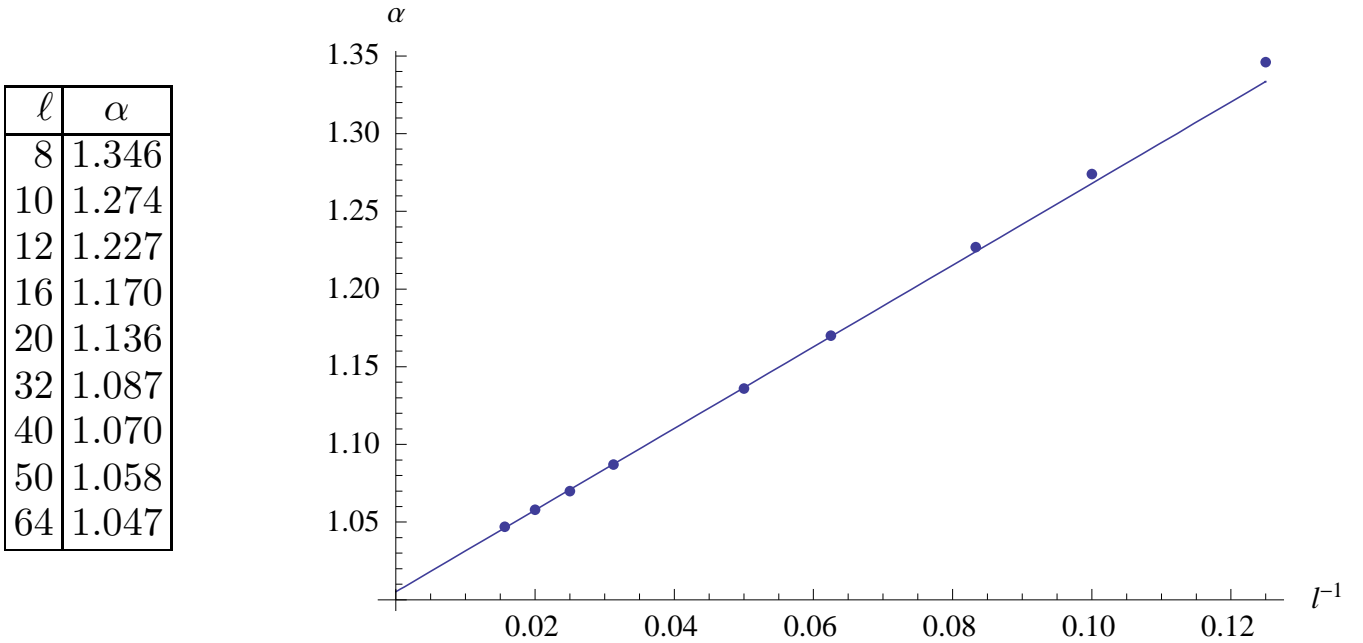


Figure 5.6: The threshold α as a function of the inverse multipole number l for tensor type of gravitational perturbations of Gauss-Bonnet black holes $D = 6$. The points $l = 16, 20, 32, 40, 50, 64$ were fit by the line $\alpha = 2.627l^{-1} + 1.005$. The theoretical result is $\alpha_t \approx 1.006$ (the value of α is measured in units of the event horizon r_+).

5.3.1 Kerr black holes

The quasi-normal ringing of brane-localised fields propagating in Schwarzschild, Reissner-Nordström and Schwarzschild-(anti) de Sitter induced gravitational backgrounds was studied in [95]. Yet, during the high-energy collisions of elementary particles resulting in the creation of black holes, it is unnatural to expect that only head-on collisions, leading to spherically symmetric black holes, would take place. Collisions with a non-vanishing impact parameter are most likely to occur, and, in addition, it is for these collisions that the black-hole production cross-section is maximised [96]. Therefore, microscopic rotating black holes should be the most generic situation, and the effect of the angular momentum of the black hole on the quasi-normal spectra of brane-localised fields is essential and cannot be neglected. This effect has been studied in [17].

The line-element, describing a higher-dimensional rotating neutral black hole, is given by the Myers-Perry solution [97]. After the projection of the Myers-Perry metric onto the brane, the brane background assumes the form [96]

$$ds^2 = \left(1 - \frac{\mu}{\Sigma r^{D-5}}\right) dt^2 + \frac{2a\mu \sin^2 \theta}{\Sigma r^{D-5}} dt d\varphi - \frac{\Sigma}{\Delta} dr^2 - \Sigma d\theta^2 - \left(r^2 + a^2 + \frac{a^2 \mu \sin^2 \theta}{\Sigma r^{D-5}}\right) \sin^2 \theta d\varphi^2, \quad (5.10)$$

where

$$\Delta = r^2 + a^2 - \frac{\mu}{r^{D-5}}, \quad \Sigma = r^2 + a^2 \cos^2 \theta. \quad (5.11)$$

The parameters μ and a are related to the mass M and the angular momentum J , respectively, of the black hole through the definitions [97]

$$M = \frac{(D-2) \pi^{(D-1)/2}}{\kappa_D^2 \Gamma[(D-1)/2]} \mu, \quad J = \frac{2Ma}{D-2}, \quad (5.12)$$

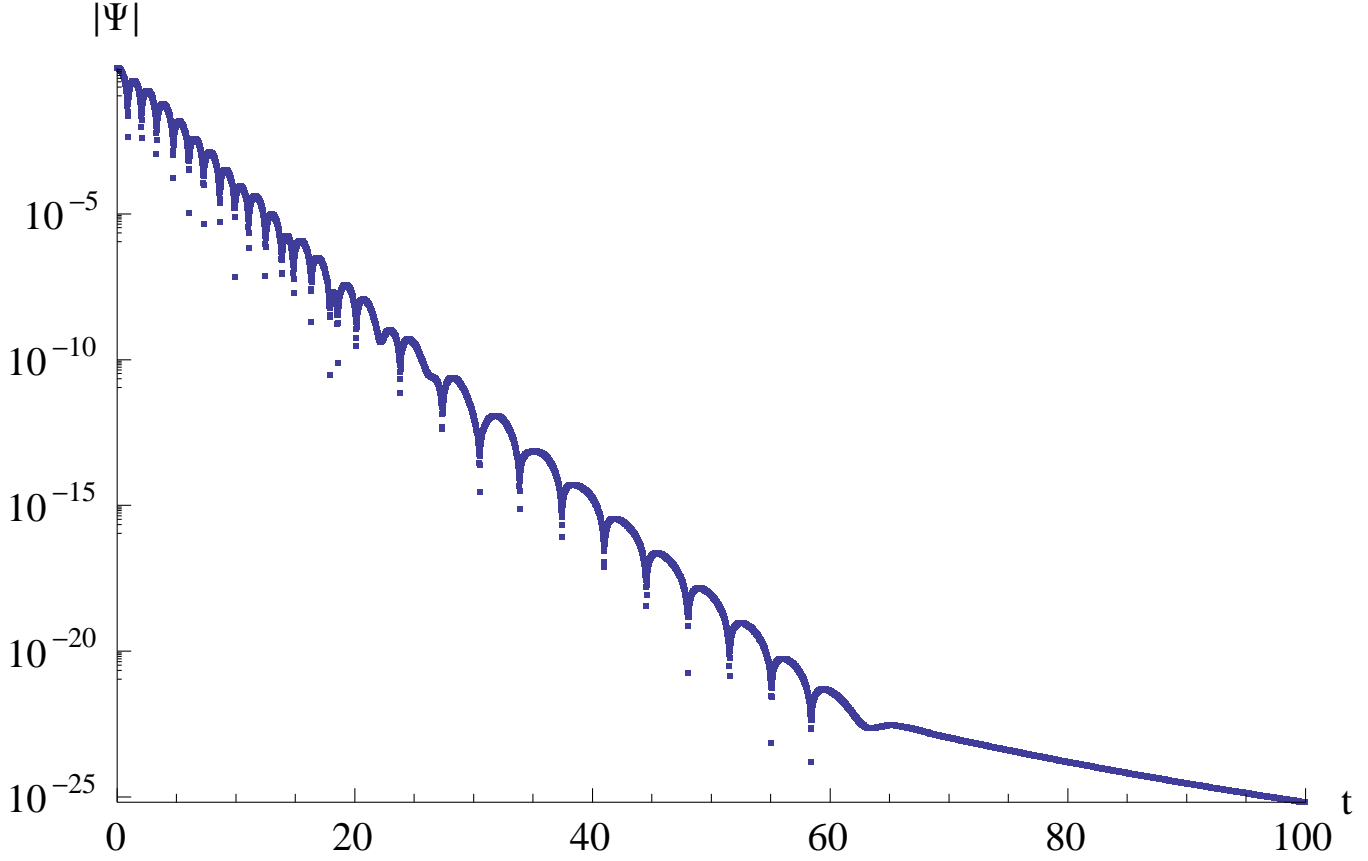


Figure 5.7: The picture of time-domain evolution for scalar-type gravitational perturbations of Gauss-Bonnet black holes $D = 10$, $l = 2$, $\alpha = 0.01$. One can see that two modes are dominating at the different stages. All quantities are measured in units of the event horizon r_+ .

where $\kappa_D^2 = 8\pi G = 8\pi/M_*^{D-2}$ is the D -dimensional Newton's constant. The radius of the event horizon r_+ parameterises the black hole mass

$$\mu = r_+^{D-5}(r_+^2 + a^2).$$

We should note here that the higher-dimensional black hole is assumed to have only one non-vanishing component of angular momentum, about an axis in the brane. This is due to the simplifying assumption that the particles that created the black hole were restricted to live on an infinitely-thin brane, therefore, during collision they had a non-vanishing impact parameter only on a 2-dimensional plane along our brane.

The equations of motion of the Standard Model fields in the background (5.10) can be reduced to the following to coupled equations for the angular

$$\begin{aligned} & \frac{1}{\sin \theta} \frac{d}{d\theta} \left(\sin \theta \frac{dS_{s,\ell}^m}{d\theta} \right) + \\ & + \left[-\frac{2ms \cot \theta}{\sin \theta} - \frac{m^2}{\sin^2 \theta} - a^2 \omega^2 \sin^2 \theta - 2a\omega s \cos \theta - s - s^2 \cot^2 \theta + 2a\omega m + \lambda \right] S(\theta) = 0, \end{aligned} \quad (5.13)$$

and radial parts

$$\Delta^s \frac{d}{dr} \left(\Delta^{1-s} \frac{dP_s}{dr} \right) + \left(\frac{K^2 - isK\Delta'}{\Delta} + 4is\omega r - \lambda \right) R(r) = 0, \quad (5.14)$$

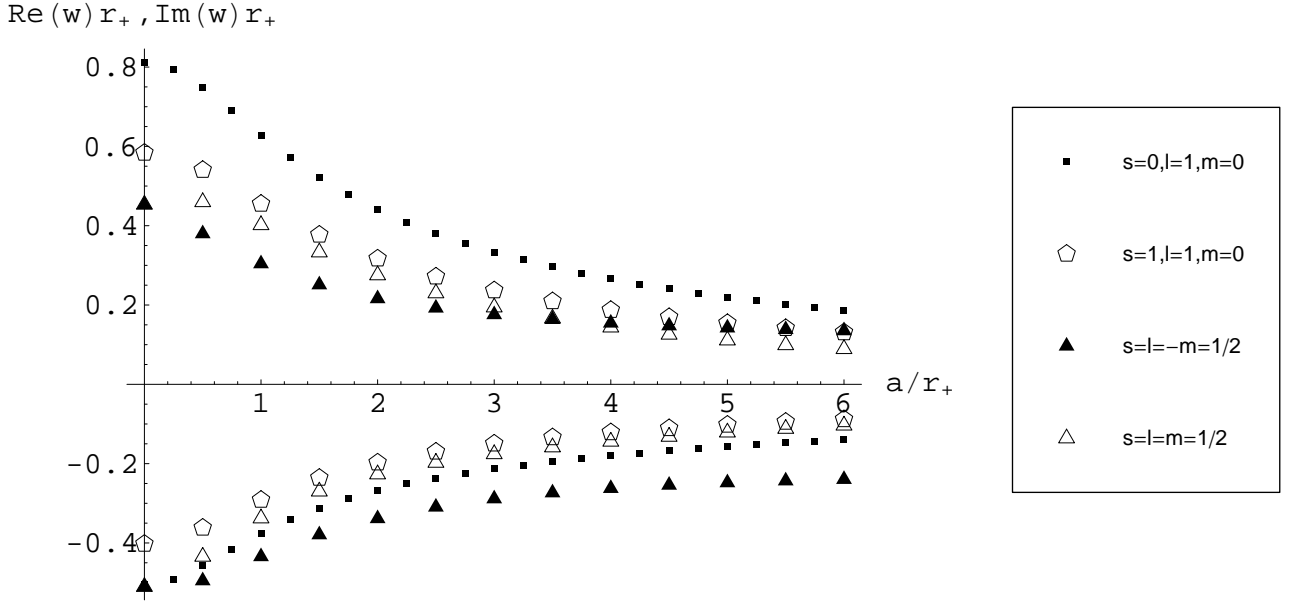


Figure 5.8: Fundamental quasi-normal modes for the 6-dimensional black hole projected on the 4-brane.

where λ is the separation constant, m is the azimuthal number, $s = 0, 1/2, 1$ for scalar, fermion and gauge boson fields respectively and K is defined as

$$K = (r^2 + a^2)\omega - am.$$

In order to solve numerically the equations (5.13) and (5.14) we use the Frobenius method. Since (3.55) coincides with (5.13) in the limit of $\alpha \rightarrow 0$, the equation for the angular part can be solved as described in the section 3.4.5. The analysis of the singular points of the equation (5.14) allows to find the Frobenius series for the function $R(r)$ [17]

$$R(r) = \frac{e^{i\omega r}}{r - r_0} \left(\frac{r - r_+}{r - r_0} \right)^{-i\beta} \sum_{i=0}^{\infty} b_i \left(\frac{r - r_+}{r - r_0} \right)^i, \quad (5.15)$$

where β is fixed (see sec. 3.4.6) as

$$\beta = \frac{K(r_+)}{\Delta'(r_+)} = \frac{\omega r_+(r_+^2 + a^2) - mar_+}{(D-5)(r_+^2 + a^2) + 2r_+^2}.$$

From the figure 5.8, one easily observes that, as a increases, the absolute values of both the real and imaginary parts of the fundamental quasi-normal frequency decrease. This makes the damping time longer and the field oscillations on the brane longer-lived. For large a one can observe that the lifetime of a fermion signal is longer for the positive value of the azimuthal number m . The same behavior was observed also for the scalar field: the field oscillation lifetime grows as m increases.

On the figure 5.9, we display a few of the higher overtones for a brane-localised gauge field (with $l = 3, m = 0$). For all higher overtones, it was found that an increase in a leads again to the decrease of the absolute values of both the real and imaginary parts.

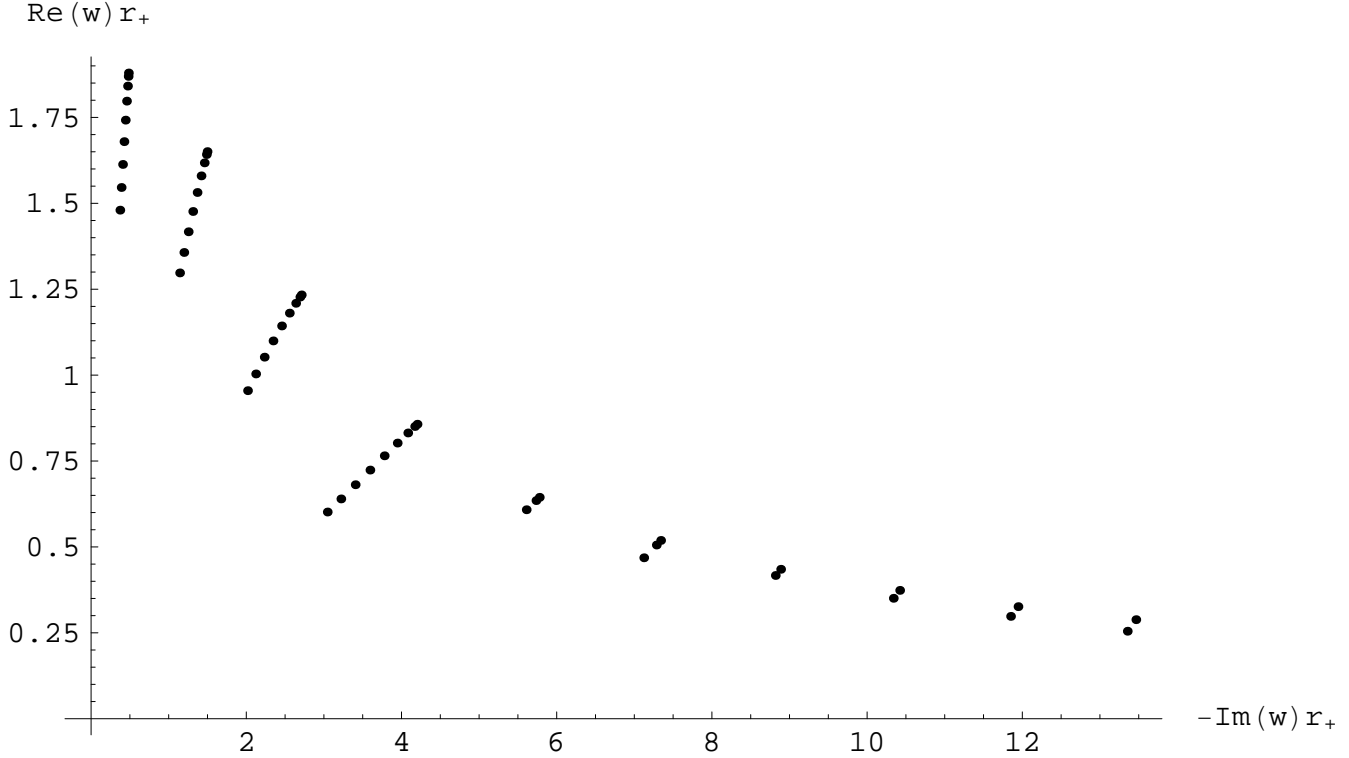


Figure 5.9: A few higher overtones of the electromagnetic field for the 6-dimensional Kerr black hole projected on the 4-brane ($l = 3$, $m = 0$) for the range $(0, r_+)$ of the angular momentum parameter a with a step of $r_+/8$.

For fixed a we find that, as D increases, the imaginary part of the quasi-normal frequency decreases while the real part changes insignificantly (see fig. 5.10). This behavior of the real part is different from the case of D -dimensional black holes, which are not projected on the brane (see sec. 5.1). For those black holes the real part of the quasi-normal frequency also grows as D increases. Therefore, we conclude that higher dimensional black holes are better oscillators than the black holes, projected on the 4-brane.

5.3.2 Gauss-Bonnet black holes

Within large extra dimensions scenarios of TeV-scale gravity, the classical space-time, induced by mini black holes, has large curvature along the transverse collision plane. Thus quantum gravity effects, and in particular higher curvature corrections to the Einstein gravity, cannot be ignored [98]. Therefore, the quantum corrections, provided by the Gauss-Bonnet theory (see sec. 5.2), must be taken into account, when mini black holes are considered.

In this context, the propagation of brane-localised Standard Model fields in the background, induced by the Gauss-Bonnet black hole, has been studied numerically for the first time in [25].

The metric induced on the brane is given by the following line element

$$ds^2 = f(r)dt^2 - f(r)^{-1}dr^2 - r^2(d\theta^2 + \sin^2\theta d\phi^2), \quad (5.16)$$

with the function $f(r)$ defined in (5.6).

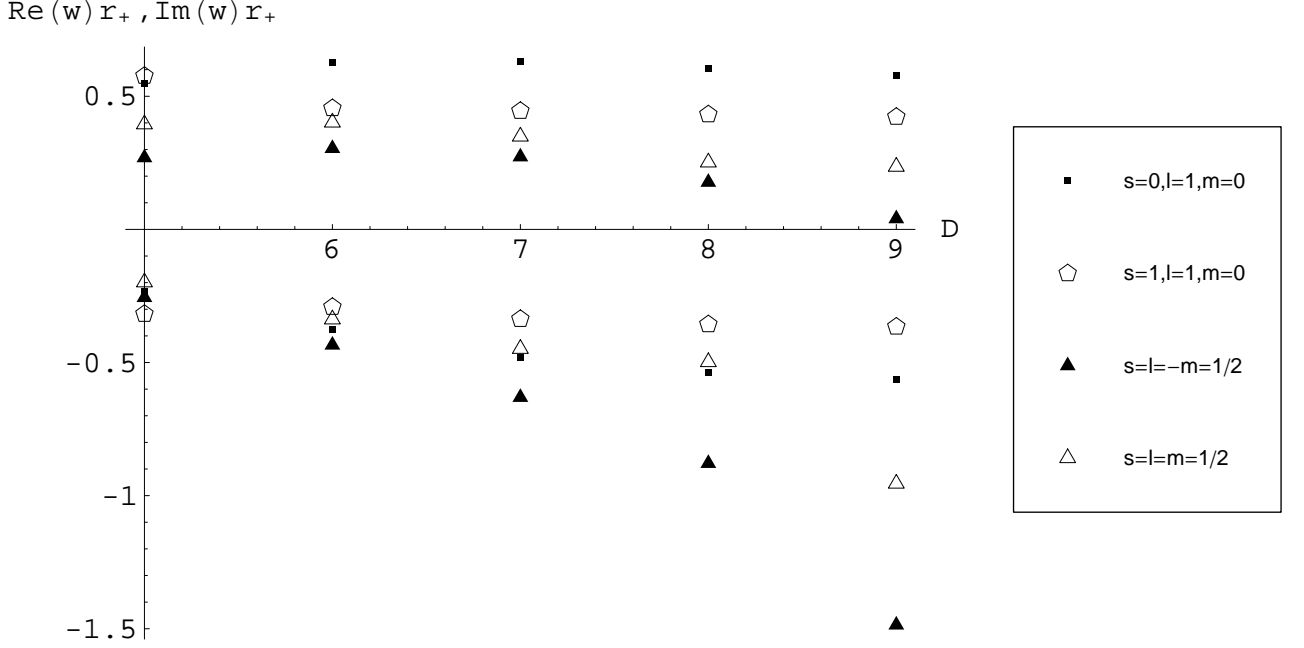


Figure 5.10: Fundamental quasi-normal modes for the higher-dimensional Kerr black hole ($a = r_+$) projected on the 4-brane.

The effective potentials for the Standard Model fields can be derived in the same way as in the Schwarzschild-de Sitter case. Their explicit form can be obtained by substituting the function $f(r)$ from (5.6) into the effective potentials for the test scalar (2.11), massless Dirac (2.13), and Maxwell (2.14) fields.

As well as for the Schwarzschild black holes, the oscillations of brane-localised Standard Model fields decay faster for higher D . On the other hand, the Gauss-Bonnet term causes the perturbations decay slower. The real part of the quasi-normal frequencies has a more complicated behavior: for $D = 5$ it decreases as α grows, but for higher-dimensional cases it starts growing first and then decreases after some value of α is reached. However, the quality factor $Q = \frac{\text{Re}(\omega)}{2\text{Im}(\omega)}$ increases as α grows for all fields and all values of D (see fig. 5.11).

As we can see in time-domain (see fig. 5.12), the late-time tails decay according to the inverse power law, which is found to be [25]

$$\Psi \propto t^{-(2l+D-1)}. \quad (5.17)$$

This law depends only on the multipole number l and the number of extra dimensions D .

Using the WKB formula, we are able to find the Gauss-Bonnet corrections to the large multipole limit

$$\begin{aligned} \omega &= \Omega_R(1 + \alpha A_1 + \dots) \left(l + \frac{1}{2} \right) - i\Omega_I(1 + \alpha B_1 + \dots) \left(n + \frac{1}{2} \right) + \mathcal{O}\left(\frac{1}{l}\right), \quad n = 0, 1, 2, \dots \\ \omega &= \Omega_R(1 + \alpha A_1 + \dots)\kappa_{\pm} - i\Omega_I(1 + \alpha B_1 + \dots) \left(n + \frac{1}{2} \right) + \mathcal{O}\left(\frac{1}{\kappa_{\pm}}\right), \quad n = 0, 1, 2, \dots \\ \Omega_R &= \frac{1}{R_0} \sqrt{\frac{D-3}{D-1}}, \quad \Omega_I = \frac{1}{R_0} \frac{D-3}{\sqrt{D-1}}, \end{aligned} \quad (5.18)$$

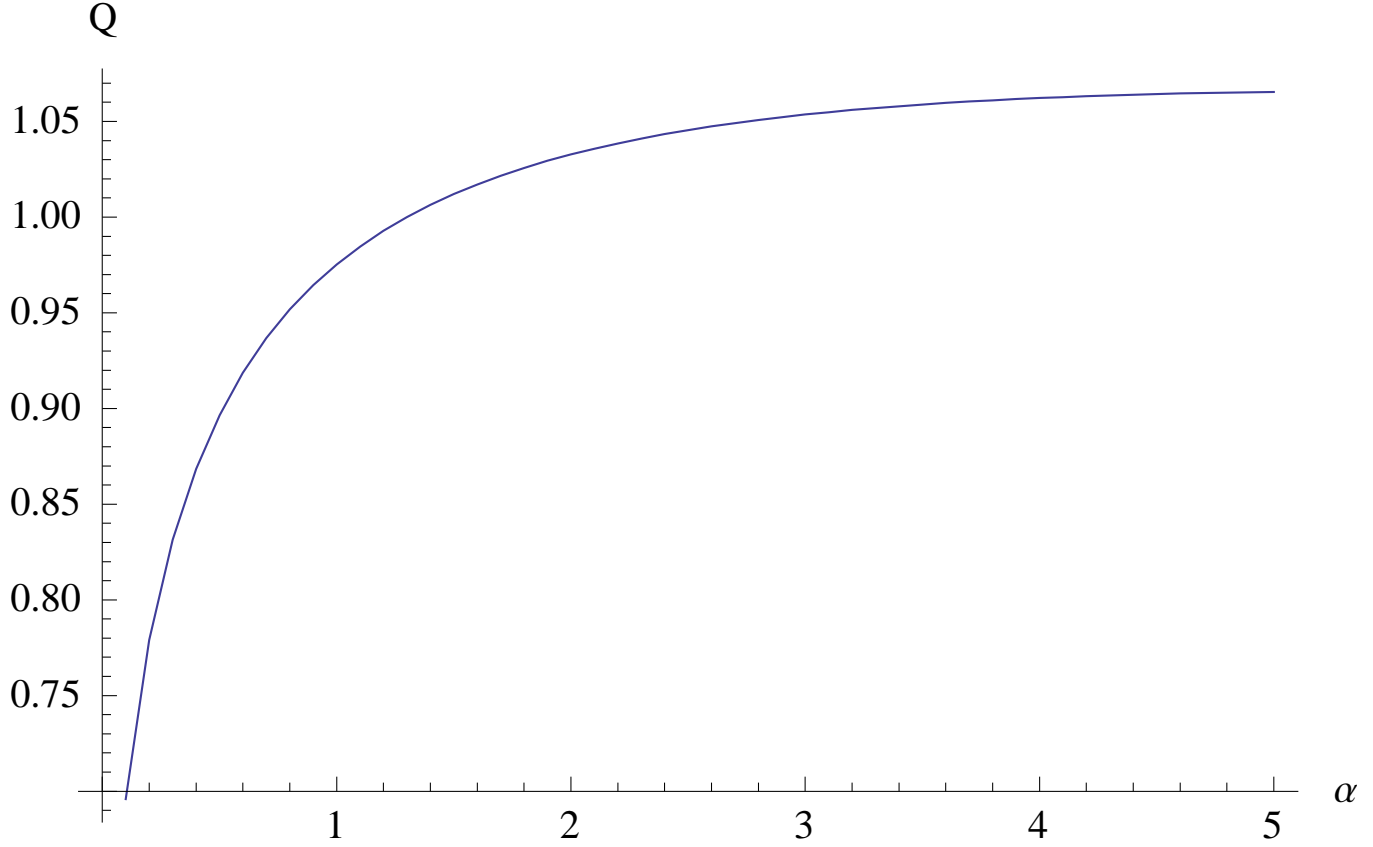


Figure 5.11: The quality factor of the scalar field localised on the 4-brane as a function of the Gauss-Bonnet parameter α ($D = 9, l = 1$).

where R_0 is the point, where the effective potential reaches its maximum for large l

$$\left(\frac{R_0}{r_+}\right)^{D-3} = \frac{D-1}{2} + \mathcal{O}\left(\frac{1}{l}\right).$$

We see that for large multipoles the quality factor also decreases as D grows

$$Q \sim \frac{\Omega_R}{\Omega_I} = \frac{1}{\sqrt{D-3}}.$$

The corrections of the first order of α are given by

$$A_1 = -\frac{1}{r_+^2} \frac{D-4}{D-1} \left(\frac{D-1}{2} - \frac{r_+^2}{R_0^2} \right) < 0,$$

$$B_1 = -\frac{1}{r_+^2} \frac{D-4}{D-1} \left(\frac{D-1}{2} + (D-2) \frac{R_0^2}{r_+^2} \right) < 0,$$

implying quicker decreasing of the absolute value of the imaginary part than decreasing of the real part. It means that the quality factor grows as α increases. Thus we conclude, that the large multipole limit resembles the main properties of the fundamental quasi-normal modes for small multipole number.

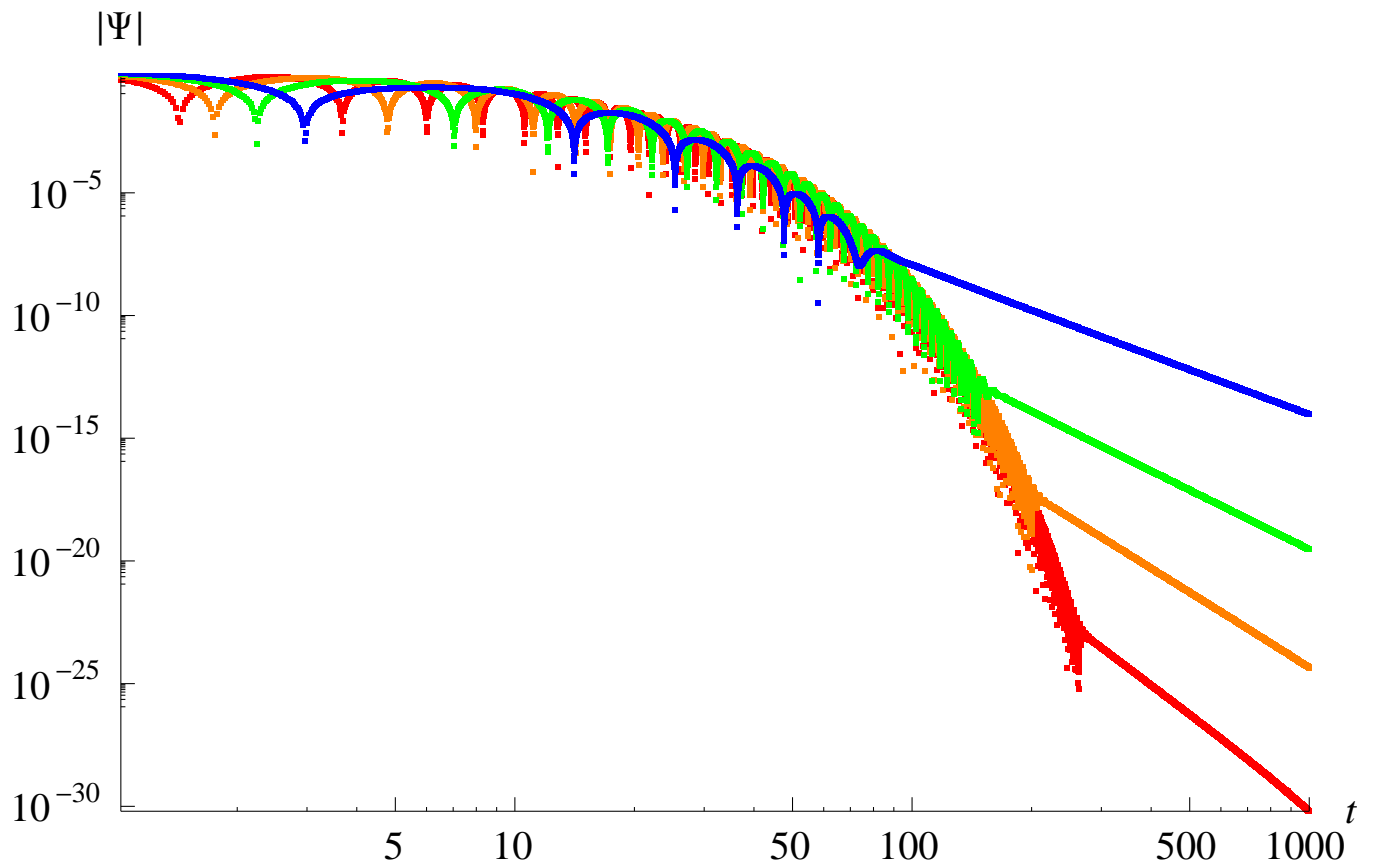


Figure 5.12: The time-domain profiles of the brane-localised massless scalar field for the Gauss-Bonnet black hole ($D = 7$, $\alpha = 5$) for $l = 0$ (blue), $l = 1$ (green), $l = 2$ (orange), $l = 4$ (red). The bigger l corresponds to the longer life of quasi-normal ringing and the quicker tail decay.

5.4 Perturbations of squashed Kaluza-Klein black holes

If the compactification radius of the extra dimensions is comparable with the size of the black holes we must take into account the size of extra dimensions. Such higher dimensional model of black holes has the asymptotic structure of the Kaluza-Klein type. The simplest example of five-dimensional black objects with the Kaluza-Klein geometry is the black string, the direct product of four-dimensional black hole and a circle. These objects look different from four-dimensional black holes only at sufficiently high energies, when Kaluza-Klein modes are excited. Therefore within these space-times we need high energy regime to see the extra dimensions. At the same time, there exist exact solutions of Kaluza-Klein black holes with squashed horizons, that look like five-dimensional squashed black holes near the event horizon, and like a Kaluza-Klein space-time at spatial infinity. Owing to the non-trivial bundle structure, the size of the extra dimension might be observed even at low energies by detecting e. g. their Hawking radiation [99].

To the best of my knowledge, quasi-normal frequencies of such black holes have been studied for the first time in [24].

5.4.1 Quasi-normal modes of the scalar field for rotating squashed Kaluza-Klein black holes

The five-dimensional rotating squashed Kaluza-Klein black hole with two equal angular momenta is described by

$$ds^2 = dt^2 - \frac{\Sigma_0}{\Delta_0} k(r)^2 dr^2 - \frac{r^2 + a^2}{4} [k(r)(d\sigma_1^2 + d\sigma_2^2) + d\sigma_3^2] - \frac{M}{r^2 + a^2} (dt - \frac{a}{2} d\sigma_3)^2, \quad (5.19)$$

with

$$d\sigma_1 = -\sin\psi d\theta + \cos\psi \sin\theta d\phi, \quad d\sigma_2 = \cos\psi d\theta + \sin\psi \sin\theta d\phi, \quad d\sigma_3 = d\psi + \cos\theta d\phi, \quad (5.20)$$

where $0 < \theta < \pi$, $0 < \phi < 2\pi$ and $0 < \psi < 4\pi$. The parameters are given by

$$\begin{aligned} \Sigma_0 &= r^2(r^2 + a^2), \\ \Delta_0 &= (r^2 + a^2)^2 - Mr^2, \\ k(r) &= \frac{(r_\infty^2 - r_+^2)(r_\infty^2 - r_-^2)}{(r_\infty^2 - r^2)^2}. \end{aligned} \quad (5.21)$$

Here M and a correspond to mass and angular momenta, respectively. Values $r = r_+$ and $r = r_-$ are outer and inner horizons of the black hole. They relate to M and a by $a^4 = (r_+ r_-)^2$, $M - 2a^2 = r_+^2 + r_-^2$. The parameter r_∞ corresponds to the spatial infinity. In the parameter space $0 < r_- \leq r_+ < r_\infty$, r is restricted within the range $0 < r < r_\infty$. The shape of black hole horizon is deformed by the parameter $k(r_+)$.

The wave equation for the massless scalar field $\Phi(t, r, \theta, \phi, \psi)$ in the background (5.19) is given by

$$\frac{1}{\sqrt{-g}} \partial_\mu \sqrt{-g} g^{\mu\nu} \partial_\nu \Phi(t, r, \theta, \phi, \psi) = 0. \quad (5.22)$$

Taking the ansatz

$$\Phi(t, r, \theta, \phi, \psi) = e^{-i\omega t} R(\rho) e^{im\phi + i\lambda\psi} S(\theta),$$

where $S(\theta)$ is the so-called spheroidal harmonics, the radial and time variables can be decoupled from angular ones, so that the final wave-like equation reads

$$\frac{d}{d\rho} \left[\Delta \frac{dR(\rho)}{d\rho} \right] + \left[\frac{\tilde{H}^2}{\Delta} + \Lambda - l(l+1) + \lambda^2 \right] R(\rho) = 0, \quad (5.23)$$

where l is the non-negative integer multipole number, $|m| < l$ and $|2\lambda| < 2l$ are integers,

$$\tilde{H}^2 = \frac{Mr_\infty^2(\rho + \rho_0)^4}{H^4(r_\infty^2 + a^2)^2} \left[\omega - \frac{\lambda a H^2 (r_\infty^2 + a^2)}{\rho_0 r_\infty^3} \right]^2, \quad (5.24)$$

$$\Lambda = \frac{4\rho_0^2 r_\infty^6 (\rho + \rho_0)^2}{H^2 (r_\infty^2 + a^2)^4} \omega^2 - \frac{4\lambda^2 (\rho + \rho_0)^2}{r_\infty^2 + a^2}, \quad (5.25)$$

$$H^2 = \frac{\rho + \rho_0}{\rho + \frac{a^2}{r_\infty^2 + a^2} \rho_0}. \quad (5.26)$$

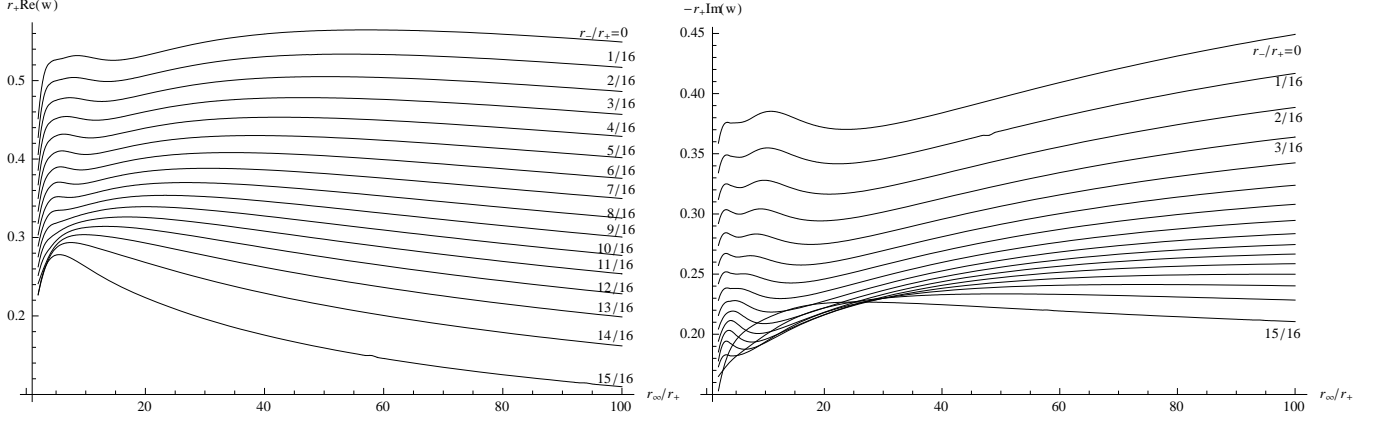


Figure 5.13: Real and imaginary part of the fundamental quasi-normal frequency of the test scalar field ($l = 0$) for rotating squashed Kaluza-Klein black holes.

The radial coordinate ρ is given by

$$\rho = \rho_0 \frac{r^2}{r_\infty^2 - r^2}, \quad (5.27)$$

with

$$\begin{aligned} \rho_0^2 &= \frac{k_0}{4}(r_\infty^2 + a^2), \\ k_0 &= k(r = 0) = \frac{(r_\infty^2 + a^2)^2 - Mr_\infty^2}{r_\infty^4}. \end{aligned} \quad (5.28)$$

Note that the three parameters ρ_0 and $\rho_\pm = \rho_0 r_\pm^2 / (r_\infty^2 - r_\pm^2)$ can define the metric (5.19) if $r_\infty < \infty$. In some papers they are used to parameterise the black hole, instead of the parameters r_∞, r_\pm .

The quasi-normal modes have been found with Frobenius method (see sec. 3.4), using the following expansion [24]

$$R = \left(\frac{r^2 - r_+^2}{r^2 - r_-^2} \right)^{-i\beta} e^{i\rho\Omega} \rho^{i\nu-1} \sum_{n=0}^{\infty} a_n \left(\frac{r^2 - r_+^2}{r^2 - r_-^2} \right)^n, \quad (5.29)$$

where β, ν and Ω are chosen in order to eliminate the singularities at $r = r_+$ and $r = r_\infty$. The sign of α and Ω is chosen in order to remain them in the same complex quadrant as ω .

The fundamental quasi-normal modes are presented on the figure 5.13. One can see that the real oscillation frequency exerts some irregular growth (with local minimums) when r_∞ is increasing until some moderately large values of r_∞ . At larger r_∞ the growth of $\text{Re}(\omega)$ changes into monotonic decay. The imaginary part of ω that determines the damping rate also has some initial irregular growth when r_∞ increases, but at larger r_∞ the two scenarios are possible: either monotonic decay (for large values of r_-) or monotonic growth (for small and moderate r_-). Thus, for a given mass and angular momentum of the black hole, one can learn the size of extra dimension r_∞ from values of quasi-normal modes of the emitted radiation.

5.4.2 Gravitational quasi-normal modes for non-rotating squashed Kaluza-Klein black holes

In the previous subsection, we have considered the scalar field in the background of squashed Kaluza-Klein black holes. However, the tensor perturbations are more interesting from the point of view of the stability and possibility to observe gravitational waves from black holes.

The metric of the uncharged non-rotating squashed Kaluza-Klein black hole is a particular case of the metric (5.19)

$$ds^2 = F(\rho)d\tau^2 - \frac{G(\rho)^2}{F(\rho)}d\rho^2 - 4\rho^2G(\rho)^2d\sigma^+d\sigma^- - \frac{r_\infty^2}{4G(\rho)^2}(d\sigma^3)^2, \quad (5.30)$$

where we have defined $\tau = 2\rho_0 t/r_\infty$ and

$$F(\rho) = 1 - \frac{\rho_+}{\rho}, \quad G(\rho)^2 = 1 + \frac{\rho_0}{\rho}, \quad r_\infty^2 = 4\rho_0(\rho_+ + \rho_0).$$

Here, we have used a basis

$$d\sigma^\pm = \frac{1}{2}(d\sigma^1 \mp id\sigma^2).$$

Since the space-time has the symmetry $SU(2) \times U(1)$, the metric perturbations can be classified by eigenvalues J, M for $SU(2)$ and K for $U(1)$. Here we consider only zero modes $J = M = 0$. Even in this case, since $d\sigma^\pm$ carry eigenvalues $K = \pm 1$, each component could have different eigenvalue K . It is important to recognise that the components with different K are decoupled. That is why we have the master equations for each K . To obtain master equations, we choose the gauge condition as

$$h_{3+} = h_{3-} = h_{+-} = h_{tt} = h_{t3} = 0. \quad (5.31)$$

As is shown in [100], the perturbation equations for the $|K| = 2$ mode can be reduced to the wave equation for h_{++} with the effective potential in the form

$$V_2 = \frac{-(\rho_+ - \rho)}{16\rho^3\rho_0(\rho_+ + \rho_0)(\rho + \rho_0)^3} \left[64\rho^5 + 256\rho^4\rho_0 - 32\rho^3\rho_0(\rho_+ - 11\rho_0) + 9\rho_+\rho_0^3(\rho_+ + \rho_0) \right. \\ \left. + 8\rho^2\rho_0(2\rho_+^2 - 5\rho_+\rho_0 + 25\rho_0^2) + \rho\rho_0^2(20\rho_+^2 - 9\rho_+\rho_0 + 35\rho_0^2) \right]. \quad (5.32)$$

Similarly, the perturbation equations for the $|K| = 1$ mode can be reduced to the wave equation for $h_{\rho+}$ with the effective potential

$$V_1 = \left(1 - \frac{\rho_+}{\rho} \right) \left[\frac{1}{\rho_+\rho_0} + \frac{7(-\rho_+ + \rho)}{16(\rho + \rho_0)^3} + \frac{17\rho_+ - 19\rho}{8\rho(\rho + \rho_0)^2} + \frac{9(-3\rho_+ + 7\rho)}{16\rho^2(\rho + \rho_0)} + \frac{\rho_+ - \rho}{\rho_+^2\rho + \rho_+\rho\rho_0} \right. \\ \left. - \frac{8(\rho_+ - \rho)^2\rho}{(\rho_+ - 2\rho)(\rho_+\rho_0 - \rho(\rho + 2\rho_0))^2} - \frac{2(\rho_+ + 2\rho)}{(\rho_+ - 2\rho)(\rho_+\rho_0 - \rho(\rho + 2\rho_0))} \right]. \quad (5.33)$$

Finally, for the $K = 0$ mode, we obtain the wave equation for h_{33} with the effective potential

$$V_0 = \frac{-(\rho_+ - \rho)}{16\rho^3(\rho + \rho_0)^3(4\rho + 3\rho_0)^2} \left[256\rho_+\rho^4 + 64\rho^3(17\rho_+ + 2\rho)\rho_0 + 48\rho^2(32\rho_+ + 11\rho)\rho_0^2 \right. \\ \left. + 60\rho(13\rho_+ + 12\rho)\rho_0^3 + 9(9\rho_+ + 35\rho)\rho_0^4 \right]. \quad (5.34)$$

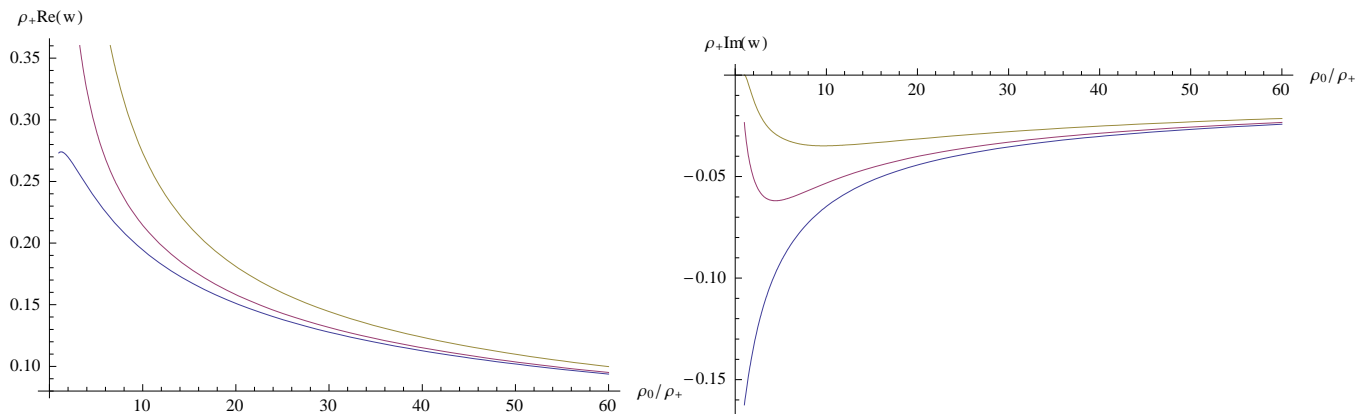


Figure 5.14: Real and imaginary parts of the fundamental quasi-normal frequency for metric perturbations ($M = J = 0$) $|K| = 0$ (blue), $|K| = 1$ (red), $|K| = 2$ (yellow) of squashed Kaluza-Klein black holes. Higher values of K correspond to higher oscillation frequency and slower damping.

The fundamental quasi-normal modes calculated with 6th order WKB method (see sec. 3.3) are presented on the figure 5.14. The real part of ω decreases for higher values of ρ_0 . The absolute value of imaginary part has maximum for $K \neq 0$. For not large values of ρ_0 the quasi-normal modes of such Kaluza-Klein black hole perturbations are longer lived. Their behavior for small values of ρ_0 in time-domain looks like massive field tails (see chapter 6), which occur at much earlier time.

It is important to note, that if we know the quasi-normal frequency we can find the size of the extra dimension in the considered black hole model, so that quasi-normal modes give a kind of opportunity to "look into" an extra dimension at low energies. In detail, when a dominant quasi-normal mode is measured, one can compare it with the numerically found one and find out which is the value of ρ_0 and the radius of the event horizon that corresponds to the observed quasinormal mode. In this way we can determine the parameters of the black hole and the size of the extra dimension, assuming that there exist no other Kaluza-Klein black holes with similar features. Also, we do not observe any growing mode, what supports stability of such black holes.

Chapter 6

Massive fields around black holes

6.1 Evolution of massive fields. Quasi-resonances

In the previous chapters we have considered massless fields propagating in the background of various black holes. Let us go further and study evolution of massive fields.

One should note, that a scalar field with the mass term can be interpreted as a self-interacting massless scalar field within regime of small perturbations [101]. A massless scalar field, when considered in models with extra dimensions of Randall-Sundrum type [77, 78], gains a large effective mass due to the Kaluza-Klein momentum. Also, the effective mass is acquired by a massless scalar field in the vicinity of the magnetised black holes [102].

Let us start from the consideration of a test massive scalar field in the D -dimensional Schwarzschild background, given by the metric (5.1) with

$$f(r) = 1 - \left(\frac{r_+}{r}\right)^{D-3}.$$

The Klein-Gordon equation,

$$\frac{1}{\sqrt{-g}} \frac{\partial}{\partial x^a} g^{ab} \sqrt{-g} \frac{\partial \Phi(x)}{\partial x^b} = -\mu^2 \Phi(x), \quad (6.1)$$

which governs the massive scalar field evolution in the curved background, can be reduced to the wave-like equation (2.10) with the effective potential

$$V(r) = f(r) \left(\mu^2 + \frac{l(l+D-3)}{r^2} + \frac{(D-4)(D-2)}{4r^2} f(r) + \frac{D-2}{2r} f'(r) \right), \quad (6.2)$$

where μ is the field mass and $l = 0, 1, 2, \dots$ is the multipole number.

One can see, that the potential (6.2) does not vanish at the spatial infinity. It changes the behavior of the eigenfunction Q_ω (2.10), so that

$$r_\star \rightarrow +\infty : \quad Q_\omega \propto \exp(i\chi r_\star) \quad (6.3)$$

where $\chi = \sqrt{\omega^2 - \mu^2}$ (see sec. 3.4.7).

Repeating the calculations of the section 2.3.2, instead of (2.27) we find [12]

$$\operatorname{Re}(\chi) |Q_\omega(r_\star = \infty)|^2 + \operatorname{Re}(\omega) |Q_\omega(r_\star = -\infty)|^2 + 2\operatorname{Re}(\omega)\operatorname{Im}(\omega) \int_{-\infty}^{\infty} |Q_\omega(r_\star)|^2 dr_\star = 0. \quad (6.4)$$

Since $\text{Re}(\chi)$ has the same sign as $\text{Re}(\omega)$, the unstable modes do not oscillate (see sec. 6.4).

For some values of the black hole mass M and the scalar field mass μ purely real frequencies were observed. Such oscillations have infinitely long lifetime and were called quasi-resonances [57]. Indeed, for massive fields quasi-normal frequencies are not required to be complex. Let us suppose that for some parameters we have $\text{Im}(\omega) = 0$, so that $\text{Re}(\chi) = 0$, implying

$$Q_\omega(r_\star = -\infty) = 0. \quad (6.5)$$

It means, that there is no wave at the event horizon and, because $\text{Re}(\chi) = 0$, no energy transmission to the spatial infinity. That is why such oscillations do not decay. The situation is similar to the standing waves on a fixed string. The requirement for χ to be imaginary, bounds the purely real frequencies by the field mass, what was pointed out in [12],

$$\omega_{QRM} < \mu. \quad (6.6)$$

The phenomenon of quasi-resonance exists since the effective potential is not zero at the spatial infinity. If the potential vanishes at $r_\star \rightarrow \pm\infty$ the condition $\text{Im}(\omega) = 0$ does not satisfy (2.27). Thus, for instance, there is no quasi-resonances in the spectrum of the massive scalar field in the Schwarzschild-de Sitter background.

6.2 Quasi-normal spectrum of the massive scalar field around Schwarzschild black holes

The quasi-normal modes of the massive scalar field around 4-dimensional Schwarzschild, Kerr [103] and Reissner-Nordström black holes [70] and of the massive Dirac field in the 4-dimensional Schwarzschild background [104] were calculated within the 3rd order WKB approach. Yet, the WKB formula, used for the calculations, is valid only for small field mass. For large mass of the field the WKB approach needs modifications (see sec. 3.3), that were not taken into account in the earlier research [70, 103, 104].

The quasi-normal spectrum of the massive scalar field for Reissner-Nordström black holes were studied for the first time by the more accurate Frobenius method by Ohashi and Sakagami [57]. They have found the quasi-resonances and supposed that they appear in a limiting situation and quasi-normal modes can disappear when the field mass exceeds a certain value. We found [12] that after reaching a quasi-resonance only one quasi-normal frequency disappears. The higher overtones remain in the spectrum for any finite field mass.

The quasi-normal spectrum of massive scalar fields in D -dimensional Schwarzschild background was studied for the first time in [18] within Frobenius method.

On the figure 6.1 one can see, that increasing of the field mass gives rise to decreasing of the imaginary part of the quasi-normal mode until reaching the vanishing damping rate. When some threshold values of μr_+ are exceeded, the particular quasi-normal modes “disappear”. The larger field mass is, the more first overtones share this destiny. The disappearing of a finite number of modes implies that for large field mass some higher overtone becomes a fundamental frequency, having the longest lifetime among the rest of the modes. Nevertheless, the quasi-normal spectrum remains infinite for any finite field mass.

The behavior of the fundamental mode depends qualitatively on the number D . For $D = 4, 5$, the fundamental mode behaves like higher overtones: decreases its imaginary part, reaches quasi-resonance for some value of μ , and disappears. For $D \geq 6$ we observe qualitatively different picture

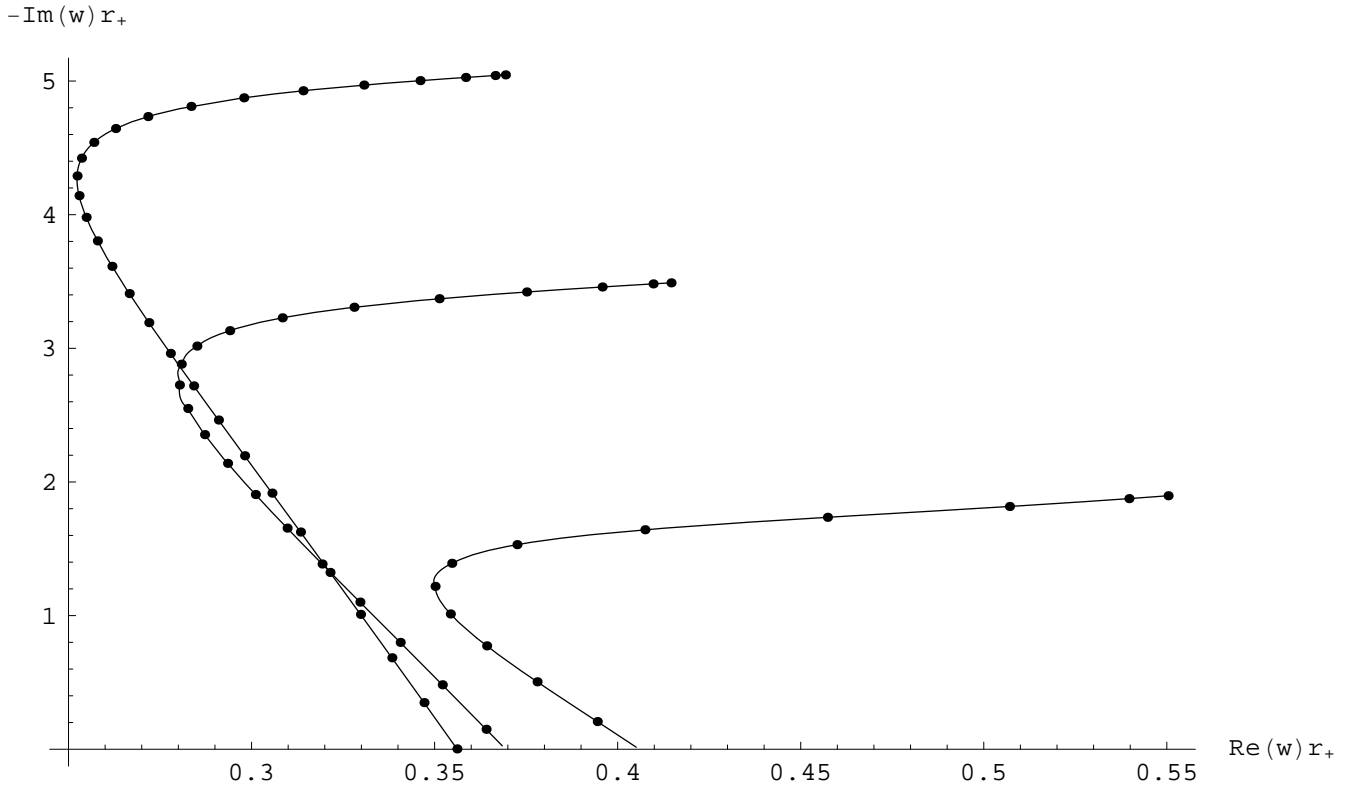


Figure 6.1: Three higher quasi-normal modes ($l = 0$) of the Schwarzschild black hole ($D = 6$) for the massive scalar field of various μ . The frequency for $\mu = 0$ has the largest imaginary part. The points were plotted with the step of $\Delta\mu r_+ = 1/2$. Solid lines mark the same overtone number.

(see fig. 6.2). As μ grows the imaginary part of the fundamental mode tends to zero asymptotically while the real part approaches μ (see fig. 6.3).

This property of the fundamental frequency behavior for large D leads to another remarkable fact. Since for high field mass the imaginary part of the fundamental mode tends to zero only asymptotically (see fig. 6.2), and the imaginary part of higher overtones reaches zero for some finite value of μr_+ (see fig. 6.3), there are some values of μr_+ for which the imaginary parts of two overtones are the same. After one of these values is reached the overtones can be distinguished only by their real part and the quasi-normal ringing has two dominant frequencies in its spectrum. Thus one could observe the superposition of that two frequencies at late times of the quasi-normal ringing.

The dependance on the field mass is qualitatively the same for all multipole numbers (see fig. 6.3). Since the real part of the quasi-normal frequency of higher l is larger, the quasi-resonances are reached for larger μ in order to satisfy the constraint (6.6).

It was shown both analytically and numerically [12, 18] that asymptotically high overtones do not depend on the field mass and satisfy the same formula as for the massless case

$$\omega_n = \frac{f'(r_+)}{4\pi} \left(\pm \ln(3) - 2\pi i \left(n + \frac{1}{2} \right) \right) = T_{Hawking} \left(\pm \ln(3) - 2\pi i \left(n + \frac{1}{2} \right) \right).$$

It is important to note, that despite in most cases quasi-normal modes of the fields of different spin show qualitatively the same behavior, when the field is massive, the field spin becomes crucial.

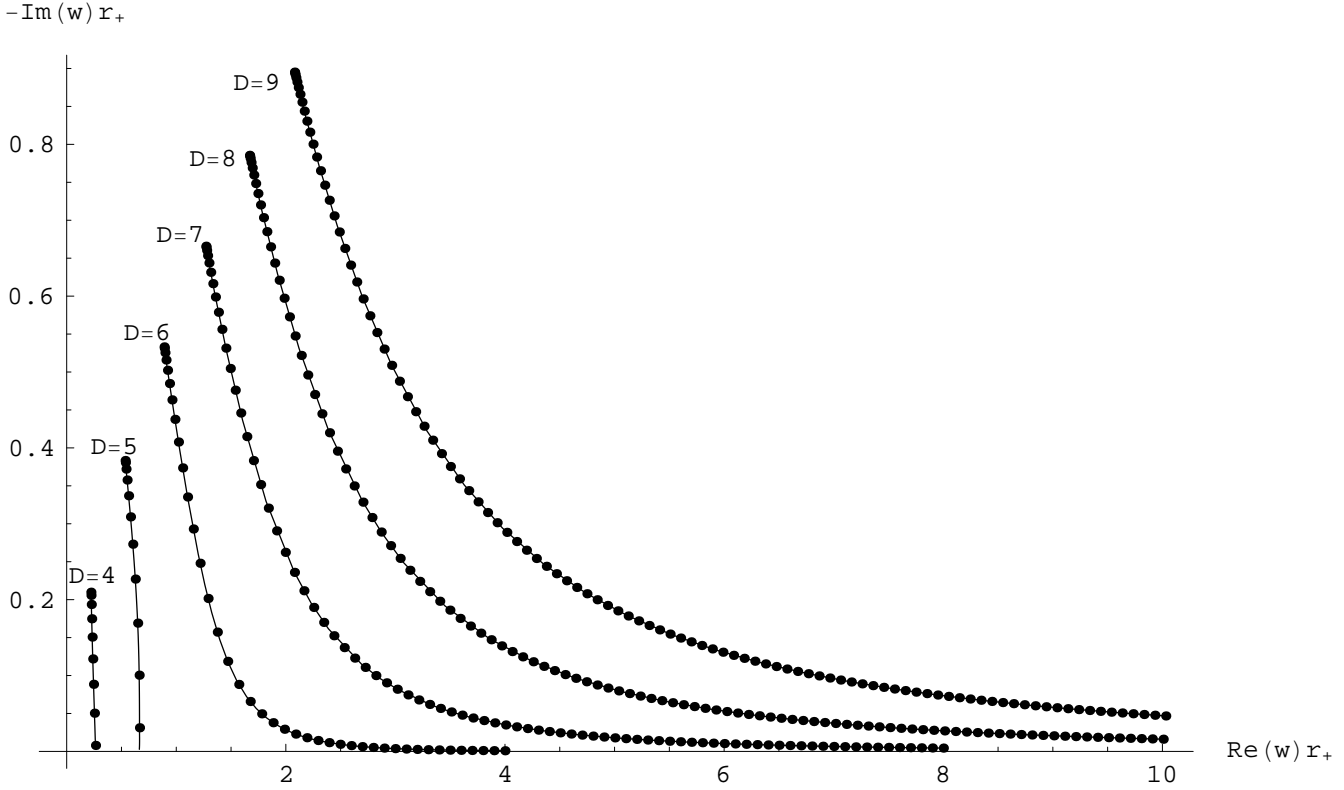


Figure 6.2: Fundamental quasi-normal frequencies for the D -dimensional Schwarzschild black hole for the massive scalar field ($l = 0$) of various μ . The frequency for $\mu = 0$ has the largest imaginary part. The points were plotted with the step of $\Delta\mu r_+ = 1/10$. Solid lines mark the same number of D .

The quasi-normal modes of the massive vector field for 4-dimensional black holes were studied in [105]. It was found that the fundamental mode shows correlation with the field mass totally different from all the remaining higher overtones. For massive scalar and massive vector fields the behavior of the fundamental frequency is qualitatively similar: the real part grows with μ , while the absolute value of the imaginary part decreases until reaching zero (quasi-resonance) and then disappears. The higher overtones have their real part decreasing to tiny values, and, the absolute value of the imaginary part is growing with μ , leading to existence of almost pure imaginary modes which just damp without oscillations.

6.3 Stability and quasi-normal modes of the massive scalar field around Kerr black holes

Analysis of the quasi-normal spectrum allows also to prove stability of massive fields in the Kerr background numerically [14]. The stability was proved analytically only for high field mass [106]:

$$\mu \geq \frac{|m|a}{2Mr_+} \sqrt{1 + \frac{2M}{r_+} + \frac{a^2}{r_+^2}}. \quad (6.7)$$

Re(ω) r_+ , Im(ω) r_+

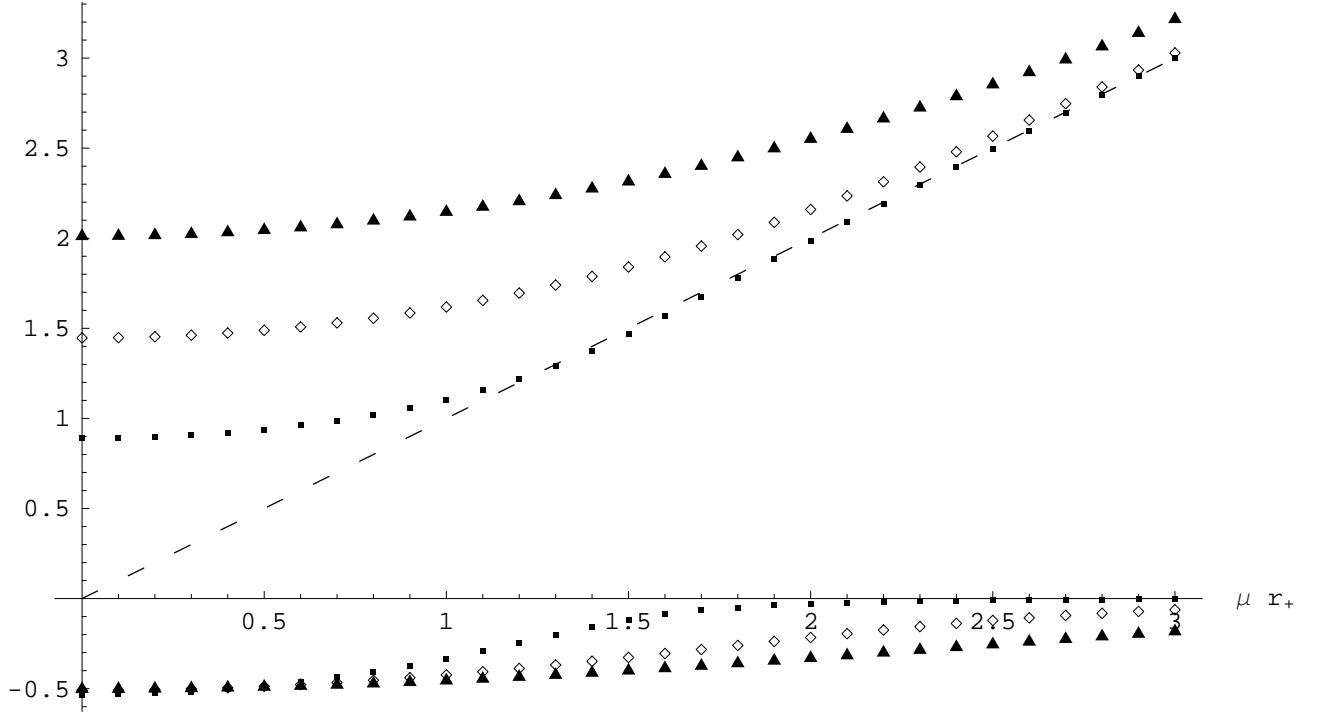


Figure 6.3: Fundamental quasi-normal frequencies of the Schwarzschild black hole ($D = 6$) for the massive scalar field as function of the field mass μ for $l = 0, 1, 2$ (represented as dots, rhombuses and triangles respectively). The dashed line corresponds to $\text{Re}(\omega) = \mu$.

Strictly speaking, because the azimuthal number appears in the righthand side, for any finite field mass one could find such kind of perturbations, that is not proven to be stable. In practice, the numerical proof is reduced to checking that there is no growing mode in the quasi-normal spectrum for small field mass and high enough value of m [14].

The Kerr metric is described by (3.53), if we put $Q = 0$, $\Lambda = 0$. The Klein-Gordon equation for the massive scalar field (6.1) in this background, after substituting the ansatz

$$\Phi(t, r, \theta, \phi) = e^{-i\omega t} e^{im\phi} R(r) S(\theta),$$

allows to separate variables. The radial part satisfies

$$\frac{d}{dr} \left(\Delta_r \frac{dR(r)}{dr} \right) + \left(\frac{K^2}{\Delta_r} - \lambda - \mu^2 r^2 \right) R(r) = 0, \quad (6.8)$$

where λ is the separation constant,

$$\Delta_r = r^2 + a^2 - 2Mr, \quad K = \omega(r^2 + a^2) - am. \quad (6.9)$$

The angular part

$$\frac{1}{\sin \theta} \frac{d}{d\theta} \left(\sin \theta \frac{dS(\theta)}{d\theta} \right) + \left(-\frac{m^2}{\sin^2 \theta} - a^2 \omega^2 \sin^2 \theta - a^2 \mu^2 \cos^2 \theta + 2am\omega + \lambda \right) S(\theta) = 0 \quad (6.10)$$

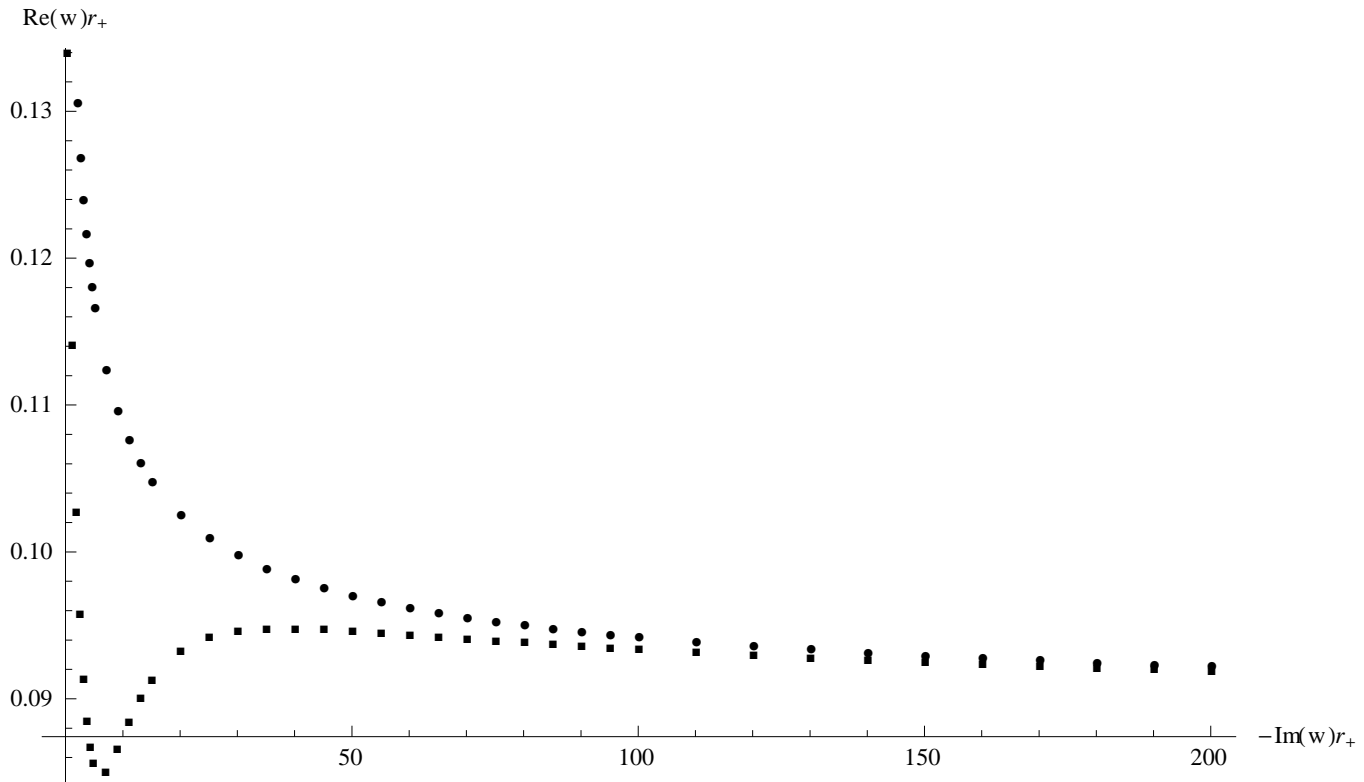


Figure 6.4: High overtones of the Schwarzschild black hole for the massive scalar field ($D = 4$, $l = 0$) for $\mu r_+ = 0.6$ (dots) and $\mu r_+ = 6.0$ (boxes).

is equivalent to (5.13) up to the redefinition of variables and can be solved as described in the section 3.4.5.

The appropriate Frobenius series for (6.8) are given by

$$R(r) = \exp(i\chi r) \left(\frac{r}{r_+} - \frac{a^2}{r_+^2} \right)^{i\sigma-1} \left(\frac{rr_+ - r_+^2}{rr_+ - a^2} \right)^{-i\alpha} \sum_{k=0}^{\infty} a_k \left(\frac{rr_+ - r_+^2}{rr_+ - a^2} \right)^k, \quad (6.11)$$

where $\chi = \sqrt{\omega^2 - \mu^2}$.

The coefficients a_k of (6.11) satisfy the three-term recurrence relation (3.41), which allows to find the spectrum numerically and prove, that it does not contain unstable modes [14].

We can see that despite the lifetime of the quasi-normal oscillation increases monotonously as the azimuthal number m grows, its imaginary part remains bounded (see fig. 6.5) and, thereby, does not show any tendency to instability. Therefore, we conclude that the formula (6.7) implies stability for the large field mass.

The dependance of the quasi-normal frequency on the field mass μ is qualitatively the same as for the Schwarzschild case: larger μ leads to considerable decreasing of the damping rate and finally to the quasi-resonances (see sec. 6.2).

The dependance on the rotation parameter a is more complicated. For $m = 0$ the imaginary part of quasi-normal frequencies decreases its absolute value as a grows, while the real part increases, reaches maximum and then decreases.

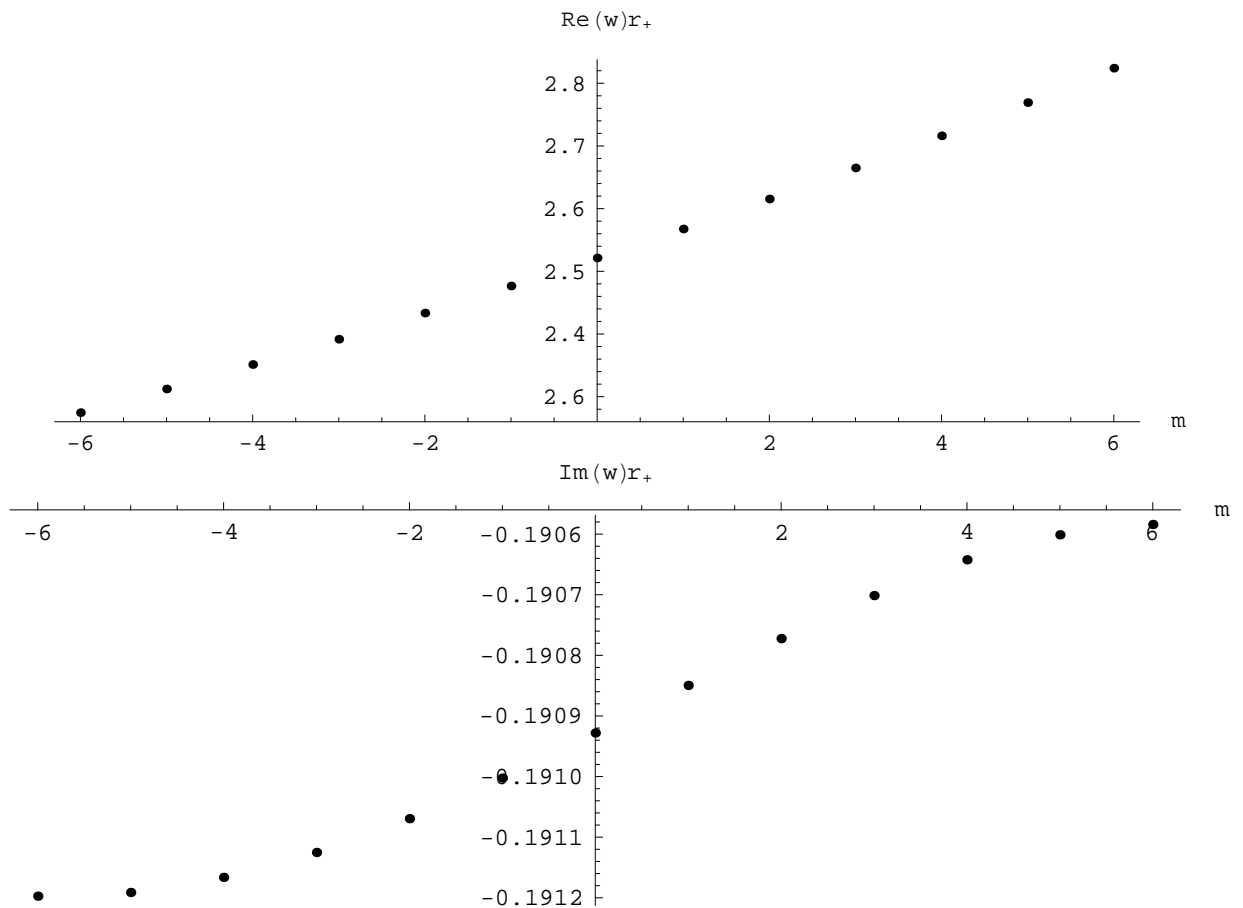


Figure 6.5: The fundamental quasi-normal frequency of Kerr black holes for the massive scalar field as a function of azimuthal number m for $l = 6$, $a = 0.15r_+$, $\mu r_+ = 0.2$.

6.4 Quasi-normal modes of black strings and the Gregory-Laflamme instability

Unlike four dimensional Einstein gravity, which allows existence of black holes, higher dimensional theories, such as the brane-world scenarios and string theory, allow existence of a number of “black” objects: higher dimensional black holes, black strings and branes, black rings and saturns and others. In higher than four dimensions we lack the uniqueness theorem, so that stability may be the criteria which will select physical solutions among this variety of solutions.

According to the brane-world scenarios, if the matter localised on the brane undergoes gravitational collapse, a black hole with the horizon extended to the transverse extra direction will form. This object looks like a black hole on the brane, but is, in fact, a black string in the full D -dimensional theory. Such black strings suffer from the so-called Gregory-Laflamme instability [107, 108], which is the long-wavelength gravitational instability of the scalar type of the metric perturbations. The threshold values of the wave vector k at which the instability appears were found in [109].

The evolution of the spherically symmetric linear perturbations of D -dimensional black strings in time and frequency domains was studied in [26]. For the first time the quasi-normal modes and time-domain profiles were studied in the stable sector. Also the appearance of the Gregory-Laflamme instability was shown in the time domain.

Let us note, that the equations for gravitational perturbations contain the Kaluza-Klein momentum. The contribution of this momentum in the corresponding effective potential looks like the mass term.

For the static black string in $D \geq 5$ space-time dimensions, the background metric can be written as

$$ds^2 = g_{\mu\nu} dx^\mu dx^\nu = f(r) dt^2 - \frac{dr^2}{f(r)} - r^2 d\Omega_{D-3}^2 - dz^2, \quad (6.12)$$

where

$$f(r) = 1 - \left(\frac{r_+}{r}\right)^n, \quad n = D - 4.$$

and $d\Omega_{D-3}^2$ is the line element on a unit $(D - 3)$ -sphere.

The z -direction is periodically identified by the relation $z = z + 2\pi R$. Let us study the $(D - 3)$ -spherically symmetric perturbations, which we can write in the following form

$$\delta g_{\mu\nu} = e^{ikz} a_{\mu\nu}(t, r), \quad k = \frac{m}{R}, \quad m \in \mathbb{Z}.$$

The perturbed vacuum Einstein equations have the form

$$\delta R_{\mu\nu} = 0. \quad (6.13)$$

The perturbations can be reduced to the form, where the only non-vanishing components of $a_{\mu\nu}$ are

$$a_{tt} = h_t, \quad a_{rr} = h_r, \quad a_{zz} = h_z, \quad a_{tr} = \dot{h}_v, \quad a_{zr} = -ikh_v.$$

The linearised Einstein equations give a set of coupled equations determining the four radial profiles above. However, we may eliminate h_v , h_r and h_t from these equations in order to produce a single second order equation for h_z :

$$\ddot{h}_z = f(r)^2 h_z'' + p(r) h_z' + q(r) h_z, \quad (6.14)$$

where

$$\begin{aligned} p(r) &= \frac{f(r)^2}{r} \left(1 + \frac{n}{f(r)} - \frac{4(2+n)k^2 r^2}{2k^2 r^2 + n(n+1)(r_+/r)^n} \right), \\ q(r) &= -k^2 f(r) \frac{2k^2 r^2 - n(n+3)(r_+/r)^n}{2k^2 r^2 + n(n+1)(r_+/r)^n}. \end{aligned}$$

Defining

$$h_z(t, r) = \frac{r^{-(n-1)/2}}{2k^2 r^2 + n(n+1)(r_+/r)^n} \Psi(t, r),$$

we can reduce the equation (6.14) to the wave-like equation

$$\left(\frac{\partial^2}{\partial t^2} - \frac{\partial^2}{\partial r_\star^2} + V(r) \right) \Psi = 0, \quad (6.15)$$

where $dr_\star = \frac{dr}{f(r)}$ is the tortoise coordinate. Here, the effective potential $V(r)$ is given by

$$V(r) = \frac{f(r)}{4r^2} \frac{U(r)}{(2k^2 r^2 + n(n+1)(r_+/r)^n)^2},$$

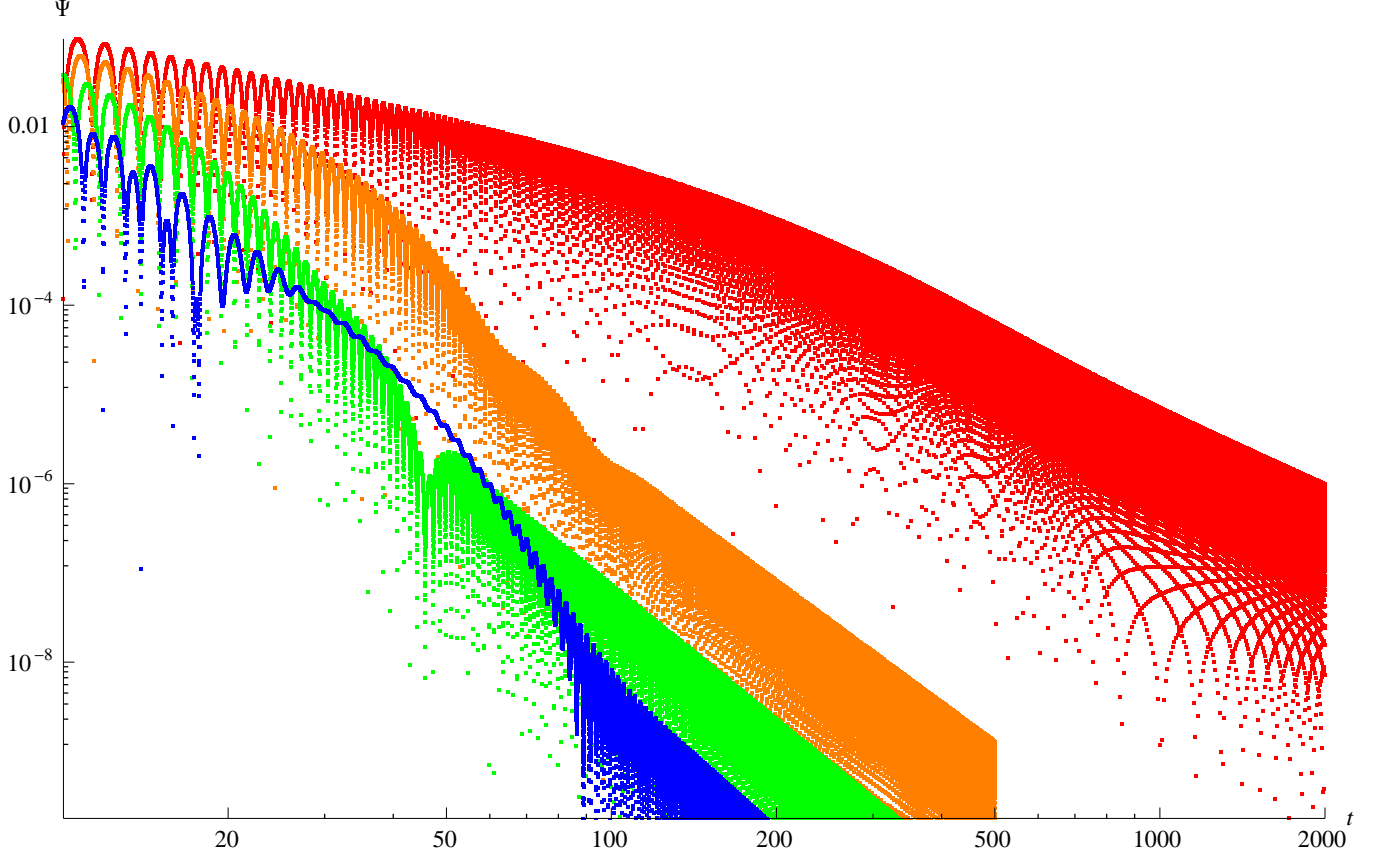


Figure 6.6: Time-domain profiles of black string perturbations for $kr_+ = 2.5$: $n = 2$ (red, top), $n = 3$ (orange), $n = 4$ (green), $n = 5$ (blue, bottom). Late-time decay of perturbations for $n \geq 3$ is $\Psi \propto t^{-(n+6)/2} \sin(kt)$.

where

$$\begin{aligned}
 U(r) = & 16k^6 r^6 + 4k^4 r^4 (n+5)(3f(r) - 2n + 3nf(r)) - \\
 & -4k^2 r^2 n(n+1) (n(n+5) + f(r)(2n^2 + 7n + 9)) \left(\frac{r_+}{r}\right)^n - \\
 & -n^2(n+1)^3 (f(r) - 2n + nf(r)) \left(\frac{r_+}{r}\right)^{2n}.
 \end{aligned}$$

One can see that k plays the role of the effective mass. At asymptotically late time we observe power-law damped tails, which have the oscillation frequency equal to k (see fig. 6.6), resembling asymptotical behavior of massive fields near Schwarzschild black holes (see sec. 6.5). The behavior of the first overtone is qualitatively similar to that of the fundamental mode for massive fields of higher-dimensional Schwarzschild black holes (see sec. 6.2).

- For $D = 5$ ($n = 1$), as k grows, the imaginary part of the first overtone quickly decreases and vanishes for some threshold value of k , while its real part stays smaller than the threshold value. After the threshold value of k is reached, the first overtone “disappears”.

- For $D \geq 6$ ($n \geq 2$), the imaginary part of the first overtone becomes small for large k , while the real part asymptotically approaches k .

Even though the first overtone of the spherically symmetric black strings behaves similarly to the fundamental mode of massive fields near higher-dimensional Schwarzschild black holes, the other modes have completely different behavior. The fundamental mode of black string perturbations

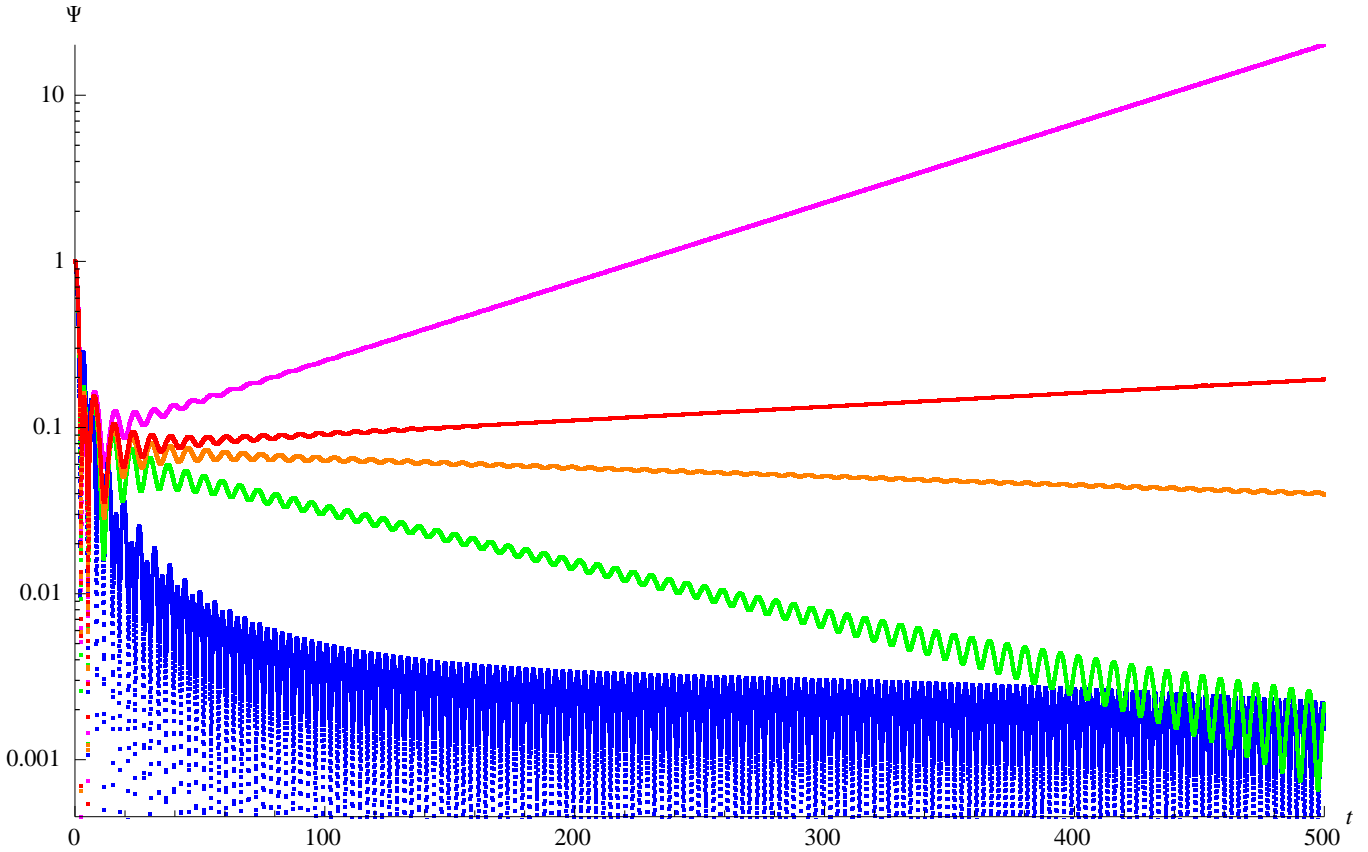


Figure 6.7: Time-domain profiles of black string perturbations for $n = 1$ $kr_+ = 0.84$ (magenta, top), $kr_+ = 0.87$ (red), $kr_+ = 0.88$ (orange), $kr_+ = 0.9$ (green), $kr_+ = 1.1$ (blue, bottom). We can see two concurrent modes: for large k the oscillating one dominates, near the critical value of k the dominant mode does not oscillate, for unstable values of k the dominant mode grows. The plot is logarithmic, so that straight lines correspond to an exponential growth or decay.

is purely imaginary. It grows for small values of k , leading to instability of the black string (see fig. 6.7). At moderately large values of k , sufficiently far from instability, the profile has the same form as that for massive fields, yet, when approaching the instability point, the real oscillation frequency and the decay rate decrease considerably. After crossing the instability point we observe, that starting from some tiny values, $\text{Im}(\omega) > 0$ are slowly increasing (while $\text{Re}(\omega) = 0$). Therefore we can conclude, that there is some static solution $\omega = 0$ of the wave equation, which shows itself exactly in the threshold point of instability.

6.5 Late-time tails of massive fields

The late-time behavior of black hole perturbations was studied for the first time by R. Price, who showed that perturbations of the massless scalar and gravitational fields decay as $\propto t^{-(2l+3)}$ at asymptotically late time [110, 111]. In [112] Bičák found that the scalar massless field in the Reissner-Nordström background decays as $\propto t^{-(2l+2)}$ for $|Q| < M$ and as $\propto t^{-(l+2)}$ for the extremal black hole charge $|Q| = M$. For Schwarzschild-de Sitter and Reissner-Nordström-de Sitter black holes, instead of power-law tails, the exponential tails were found [36].

In higher dimensional space-times the late-time behavior depends also on the number of extra

dimensions. It was found that massless scalar and vector fields, and gravitational perturbations of higher-dimensional Schwarzschild black holes have the decay law $\propto t^{-(2l+D-2)}$ for odd D [113] and $\propto t^{-(2l+3D-8)}$ for even $D > 4$ [114]. The same late-time behavior was observed for odd-dimensional Gauss-Bonnet black holes [89]. The late-time tails of the brane localised Standard Model fields were studied in [25]. Their late-time decay law is $\propto t^{-(2l+D-1)}$.

One should note that the late-time decay of perturbations within the full non-linear gravity does not agree with the linearised theory in dimensions higher than four. If we consider a massless scalar field and take into account the back reaction of the field upon the metric, the late-time decay rate becomes smaller, coinciding with the linearised theory prediction only in four dimensions [115].

The late-time behavior of massive fields is qualitatively different from massless ones: at late time the decay profile is *oscillatory* inverse power law tail. Also, the field mass implies different behavior at the intermediate late time ($1 \ll t/M < (\mu M)^{-3}$) and at the asymptotically late time ($t/M > (\mu M)^{-3}$).

For a massive scalar field with mass μ in the background of the Schwarzschild black hole, the perturbations decay as $\propto t^{-(l+3/2)} \sin(\mu t)$ at intermediate late time [101] and as $\propto t^{-(5/6)} \sin(\mu t)$ at asymptotically late time [116, 117]. The same behavior at asymptotically late time was found also for the massive scalar field perturbations of the dilaton black hole [118] and the Kerr black hole [119] and for the massive Dirac field in the Schwarzschild background [72].

For higher dimensional Schwarzschild black holes the intermediate late-time behavior of the massive scalar field is found to be $\propto t^{-(l+(D-1)/2)} \sin(\mu t)$ [120].

The late-time behavior of the massive vector field was studied both numerically and analytically for the first time in [15]. At intermediate late time the decay law depends on the polarisation, being either $\propto t^{-(l+1/2)} \sin(\mu t)$, or $\propto t^{-(l+3/2)} \sin(\mu t)$, or $\propto t^{-(l+5/2)} \sin(\mu t)$. At the asymptotical late time the behavior is the same, as for other massive fields, $\propto t^{-(5/6)} \sin(\mu t)$. Therefore, we conclude that the asymptotically late-time decay law *does not depend* on the spin of the field.

The late-time decay law for massless perturbations, the intermediate and asymptotically late-time behavior of massive field perturbations for various spins in asymptotically flat backgrounds are presented in the following table.

perturbations	massless	massive (intermediate)	massive (asymptot.)
$s = 0$ ($4D$ Schw.)	$t^{-(2l+3)}$	$t^{-(l+3/2)} \sin(\mu t)$	$t^{-(5/6)} \sin(\mu t)$
$s = 1$ ($4D$ Schw.)	$t^{-(2l+3)}$	$\{t^{-(l+1/2)}, t^{-(l+3/2)}, t^{-(l+5/2)}\} \sin(\mu t)$	$t^{-(5/6)} \sin(\mu t)$
$s = 2$ ($4D$ Schw.)	$t^{-(2l+3)}$		
$s = 0$ ($4D$ Kerr)	$t^{-(2l+3)}$	$t^{-(l+3/2)} \sin(\mu t)$	$t^{-(5/6)} \sin(\mu t)$
$s = 0$ ($4D$ R-N)	$t^{-(2l+2)}$		
$s = 0$ (odd D)	$t^{-(2l+D-2)}$	$t^{-(l+(D-1)/2)} \sin(\mu t)$	
$s = 0$ (even D)	$t^{-(2l+3D-8)}$	$t^{-(l+(D-1)/2)} \sin(\mu t)$	
on a 4-brane	$t^{-(2l+D-1)}$		

Chapter 7

Quasi-normal modes of black holes, whose metrics are unknown analytically

7.1 Numerical methods

Black holes are compact objects. Therefore, it is natural to expect that their quasi-normal ringing, being the property of the black hole, at least in the dominant order, does not depend on what happens at large distance from the black hole.

It turns out that the dominating frequencies depend mostly on the black hole solution behavior in some region near the event horizon. Thus one can find them in frequency domain, even if the behavior of the solution at large distance is not known.

Two qualitatively different examples were considered in this context: the scalar hairy black hole in the anti-de Sitter background and the Einstein-Aether black hole in the asymptotically flat background. In both types of the background the behavior of the solution at large distance is not important [28]:

- For an asymptotically anti-de Sitter background we usually require Dirichlet boundary conditions at spatial infinity. The most significant part of the metric perturbations stays, thereby, near the black hole. That is why the solution behavior at this region causes dominant influence on the quasi-normal spectrum [13].

- For the asymptotically flat case the searching of the quasi-normal modes can be reduced to the scattering problem. Therefore, the quasi-normal frequencies are determined mainly by the form of the effective potential near its peak [16, 19].

In order to calculate quasi-normal frequencies for the asymptotically anti-de Sitter background one can use the Horowitz-Hubeny method, described in the section 3.5. It is clear that if $s(z)$, $t(z)$ and $u(z)$ in (3.71) are series which converge at the spatial infinity ($z = 1$) quickly enough, then y_n is still possible to calculate because it depends insignificantly on higher terms of the series. In order to find series expansion for $s(z)$, $t(z)$ and $u(z)$, one can use equations which define the black hole solution. We can always do this because $s(z)$, $t(z)$ and $u(z)$ can be explicitly expressed in terms of the metric coefficients and their derivatives.

Thus, the quasi-normal modes could be found without solving the equations for the black hole. It is enough to find series expansions for the metric coefficients near the horizon. It is important to note that one can control the precision of the eigenfrequencies ω by requiring the convergence of the found result with respect to increasing of the number of expansion terms of all the series [13].

For asymptotically flat black hole solutions it is convenient to use the WKB method (see sec. 3.3), where the asymptotic solutions of the wave equation near the event horizon and near spatial

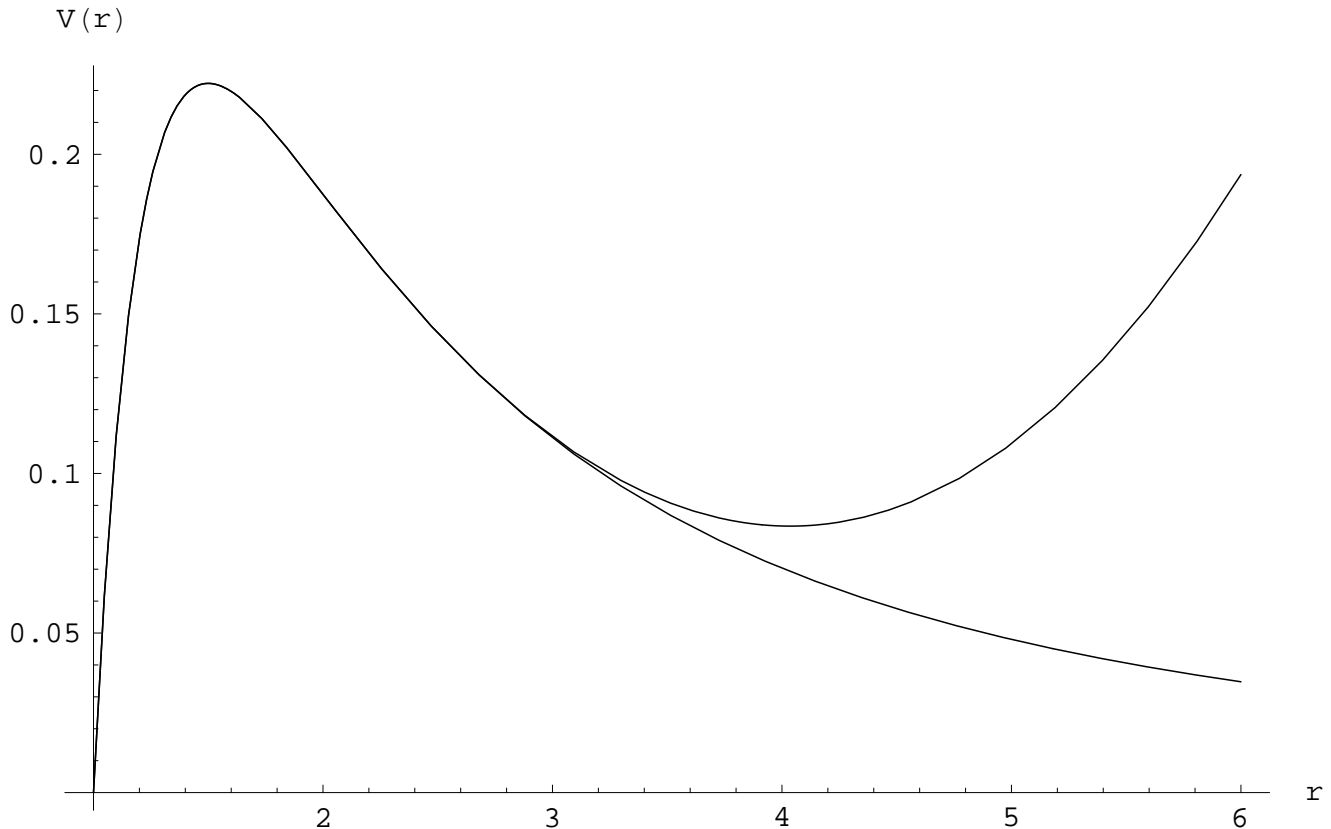


Figure 7.1: The effective potential for electromagnetic perturbations near the Schwarzschild black hole ($r_+ = 1$, $l = 2$) and the same potential interpolated numerically near its maximum.

infinity are matched with Taylor expansion near the peak of the potential. We conclude therefore that the low-damping quasi-normal modes are determined mainly by the behavior of the effective potential near its peak.

This statement was checked by considering the potential for the Schwarzschild black hole and also two other potentials, which lay closely to the Schwarzschild potential near its maximum, but have very different behavior far from the black hole. These two potentials are chosen in the following way. We choose some points near the maximum of the effective potential. The first potential is an interpolation of these points by cubic splines (see fig. 7.1). The second potential is a fit for the points by a ratio of polynomial functions.

Since the WKB formula contains the value of the effective potential and its derivatives at the potential peak, we find that the results obtained with the help of all three potentials lay very close if the interpolation and the fit were made with the appropriate precision [16]. Despite the higher derivatives of our interpolation potential are not defined, we are able to evaluate them step by step by interpolating in the same way the first and all the consequent derivatives of the potential. It turns out that the interpolation potential is very sensitive to numerical errors. Therefore, to calculate the quasi-normal modes with the appropriate precision, one must calculate the values of the potential with very high accuracy. In fact, for the practical purposes one can use fitting of the potential which does not accumulate the numerical error.

To test the accuracy of this approach one can use the fact that the sixth order WKB formula gives a smaller relative error than the third order one (see sec. 3.3). Since the higher WKB order depends on the higher derivatives of the effective potential, that are more sensitive to the interpolation or

fitting accuracy, the higher order WKB formula should give some random values, if the accuracy is not enough.

The independence of the quasi-normal modes on the behavior of the effective potential at large distance, being inspired by the WKB formula, is not related with the WKB method. However, since the WKB formula depends only on the potential near its peak, we are unable to prove the statement within the described approach. That is why, it is important to check the results with a different method. In order to do this, we have found in time domain the quasi-normal modes of gravitational perturbations of black holes in the Einstein-Aether theory. The calculated frequencies show an excellent agreement with the WKB results [19].

7.2 Quasi-normal modes of the scalar hairy black hole

Since the paper of J. Bekenstein [121], it is well-known that black hole can not have scalar hair within minimal coupling. However, as have been found in [122, 123], there is a possibility of dressing a four-dimensional black hole in anti-de Sitter space-time with a non-minimally coupled classical scalar field. In [124] the results were extended for higher dimensional configurations. Despite we live in the de Sitter universe, black holes in the anti-de Sitter background attracted considerable interest due to the AdS/CFT correspondence [6]. In this context, the quasi-normal ringing of massive non-minimally coupled scalar field to the black hole in the anti-de Sitter background was studied for the first time in [13].

We consider the spherically symmetric solution

$$ds^2 = N(r)e^{2\delta(r)} dt^2 - N(r)^{-1} dr^2 - r^2 (d\theta^2 + \sin^2 \theta d\varphi^2) \quad (7.1)$$

of the action, which describes a self-interacting scalar field ϕ with non-minimal coupling to gravity:

$$S = \int d^4x \sqrt{-g} \left[\frac{1}{2} (R - 2\Lambda) - \frac{1}{2} (\nabla\phi)^2 - \frac{1}{2} \xi R\phi^2 - \frac{\mu^2\phi^2}{2} \right], \quad (7.2)$$

where R is the Ricci scalar, Λ is the cosmological constant, ξ is the coupling constant, and

$$(\nabla\phi)^2 = \nabla_a\phi\nabla^a\phi.$$

In order to simplify the equations of motion we use the following conformal transformation

$$\bar{g}_{ab} = (1 - \xi\phi^2)g_{ab}. \quad (7.3)$$

After the transformation, the action takes the form

$$S = \int d^4\bar{x} \sqrt{-\bar{g}} \left(\frac{1}{2} (\bar{R} - 2\Lambda) - \frac{1}{2} (\bar{\nabla}\Phi)^2 - U(\Phi) \right), \quad (7.4)$$

where we define

$$\Phi = \int d\phi \sqrt{\frac{(1 - \xi\phi^2) + 6\xi^2\phi^2}{(1 - \xi\phi^2)^2}}, \quad U(\Phi) = \frac{\frac{\mu^2\phi^2}{2} + \Lambda\xi\phi^2(2 - \xi\phi^2)}{(1 - \xi\phi^2)^2}. \quad (7.5)$$

The metric takes the following form

$$d\bar{s}^2 = \bar{N}(\bar{r})e^{2\bar{\delta}(\bar{r})} dt^2 - \bar{N}(\bar{r})^{-1} d\bar{r}^2 - \bar{r}^2 (d\theta^2 + \sin^2 \theta d\varphi^2), \quad (7.6)$$

where

$$\begin{aligned}\bar{r} &= (1 - \xi\phi^2)^{\frac{1}{2}} r, \\ \bar{N} &= N (1 - \xi\phi^2 - \xi r\phi\phi')^2 (1 - \xi\phi^2)^{-2}, \\ \bar{N}e^{2\bar{\delta}} &= Ne^{2\delta} (1 - \xi\phi^2).\end{aligned}$$

Varying the action, one can find the following equations of motion [123]

$$\frac{d(\bar{r}\bar{N})}{d\bar{r}} = 1 - \Lambda\bar{r}^2 - \bar{r}^2 \left(\frac{\bar{N}}{2} \left(\frac{d\Phi}{d\bar{r}} \right)^2 + U(\Phi) \right), \quad (7.7a)$$

$$\frac{d\bar{\delta}}{d\bar{r}} = \frac{\bar{r}}{2} \left(\frac{d\Phi}{d\bar{r}} \right)^2, \quad (7.7b)$$

$$0 = \bar{N} \frac{d^2\Phi}{d\bar{r}^2} + \left(\bar{N} \frac{d\bar{\delta}}{d\bar{r}} + \frac{d\bar{N}}{d\bar{r}} + \frac{2\bar{N}}{\bar{r}} \right) \frac{d\Phi}{d\bar{r}} - \frac{dU}{d\Phi}. \quad (7.7c)$$

In order to obtain the series expansion for the metric coefficients (7.6), we have to impose some boundary conditions, which are associated with the black hole parameters. We are using the following parameters. The event horizon radius \bar{r}_+ can be chosen arbitrary in order to fix length scale. This choice defines the boundary condition for \bar{N} : $\bar{N}(\bar{r}_+) = 0$. In order to measure all dimensional values in units of \bar{r}_+ , we choose $\bar{r}_+ = 1$. The value $\bar{\delta}(\bar{r}_+)$ is chosen arbitrary in order to fix time scale. In order to introduce the boundary conditions in the same point we impose $\bar{\delta}(\bar{r}_+) = 0$, what differs from Winstanley's $\bar{\delta}(\infty) = 0$. The last parameter $\phi(\bar{r}_+) = Q$ can be associated with the scalar charge of the black hole.

Spherically symmetric perturbation equation for

$$\delta\Phi = e^{-i\omega t} \frac{Q_\omega(r)}{r}$$

takes the wave-like form (2.21), where the perturbation potential is given by [122]:

$$V(\bar{r}) = \frac{\bar{N}e^{2\bar{\delta}}}{\bar{r}^2} \left((1 - (U + \Lambda)\bar{r}^2) \left(1 - \bar{r}^2 \left(\frac{d\Phi}{d\bar{r}} \right)^2 \right) - \bar{N} + 2\bar{r}^3 \frac{dU}{d\Phi} \frac{d\Phi}{d\bar{r}} + \bar{r}^2 \frac{d^2U}{d\Phi^2} \right). \quad (7.8)$$

The tortoise coordinate is given by

$$\frac{d\bar{r}^*}{d\bar{r}} = e^{\bar{\delta}} \bar{N}. \quad (7.9)$$

It is similar to the ordinary anti-de Sitter case:

$$\begin{aligned}\bar{r} = \bar{r}_+ &\iff \bar{r}^* = \infty, \\ \bar{r} = \infty &\iff \bar{r}^* = 0.\end{aligned}$$

This perturbation corresponds to infinitesimal changing of the black hole mass and is similar to the zero-multipole scalar perturbations near a hairless black hole. The crucial difference is that the perturbation of a scalar field due to the hair gives a first-order correction to the metric.

In order to calculate the quasi-normal modes we find the series expansions near the black hole event horizon for Φ , $\bar{\delta}$ and \bar{N} using the equations (7.7). Since \bar{N} grows at the spatial infinity, it is convenient to find the series for the function $g = \bar{N}/\bar{r}^2$ instead of \bar{N} . After the series for the metric

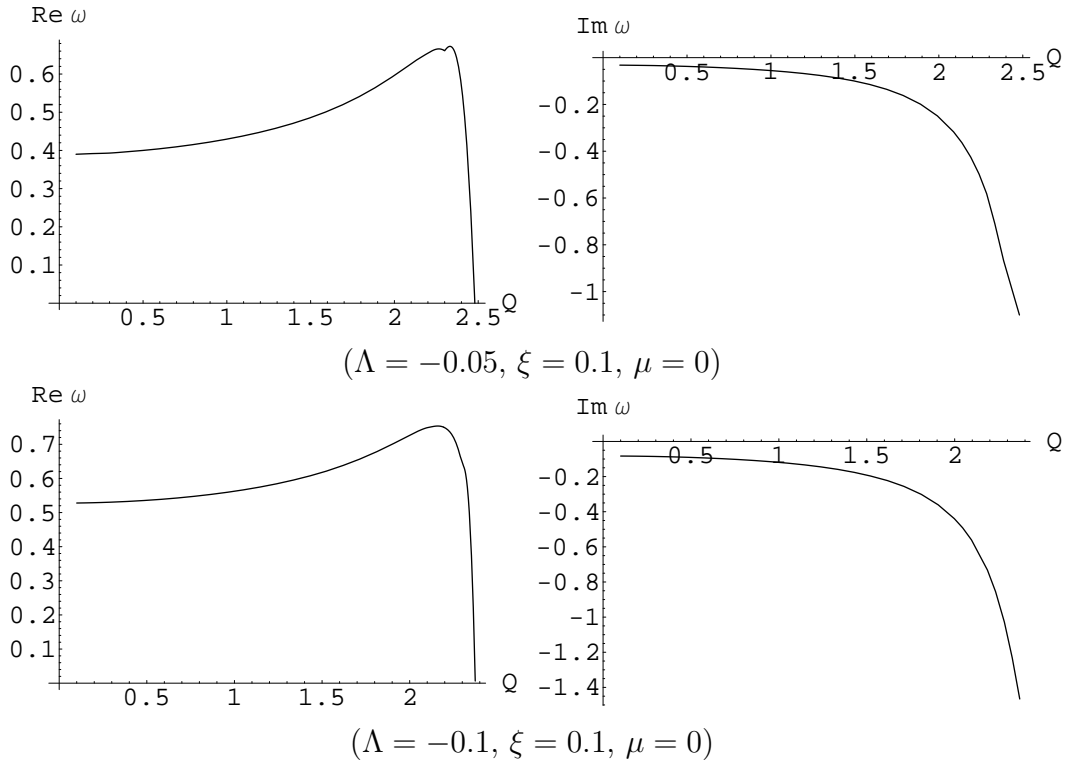


Figure 7.2: **Dependance of the real and imaginary parts of the quasi-normal frequency on Q for the scalar hairy black hole.** The imaginary part quickly decreases as the “scalar charge” Q increases. The real part reaches its maximum and then quickly falls down to zero. It vanishes for some non-critical charge $Q_0 < \xi^{-1/2}$. For $Q \geq Q_0$ the real part remains zero and the frequency is purely imaginary (within numerical precision).

functions are known one can find the series for the effective potential (7.8) and, finally, for $s(z)$, $t(z)$ and $u(z)$ in (3.71). Then we use the technique, described in the previous section.

It was found [13] that imaginary part of the quasi-normal modes changes monotonously as a function of Λ , Q and ξ . Scalar field mass μ cause imaginary part to decrease its absolute value but not to vanish. It reaches a minimum for some particular mass and then increases very rapidly (see fig. 7.5). Thus no infinitely long living oscillations appear.

Real part has more complicated behavior and depends significantly on the parameters Q and Λ (see figures 7.2 and 7.3). Other parameters, ξ and μ , change the real part within the comparable small bounds (see figures 7.4 and 7.5). For relatively large values of ξ , Λ and Q purely imaginary frequencies appear.

From the figure 7.6 we see that higher overtones tend to equidistant spacing similar to hairless black hole spectrum behavior in the anti-de Sitter background [125].

7.3 Perturbations and quasi-normal modes of black holes in the Einstein-Aether theory

General relativity is based on the local Lorentz invariance. Yet, there appeared a lot of attempts to go beyond the local Lorentz symmetry. Aether can be considered as locally preferred state of rest at each point of space-time due-to some unknown physics. Einstein-Aether theory is general relativity

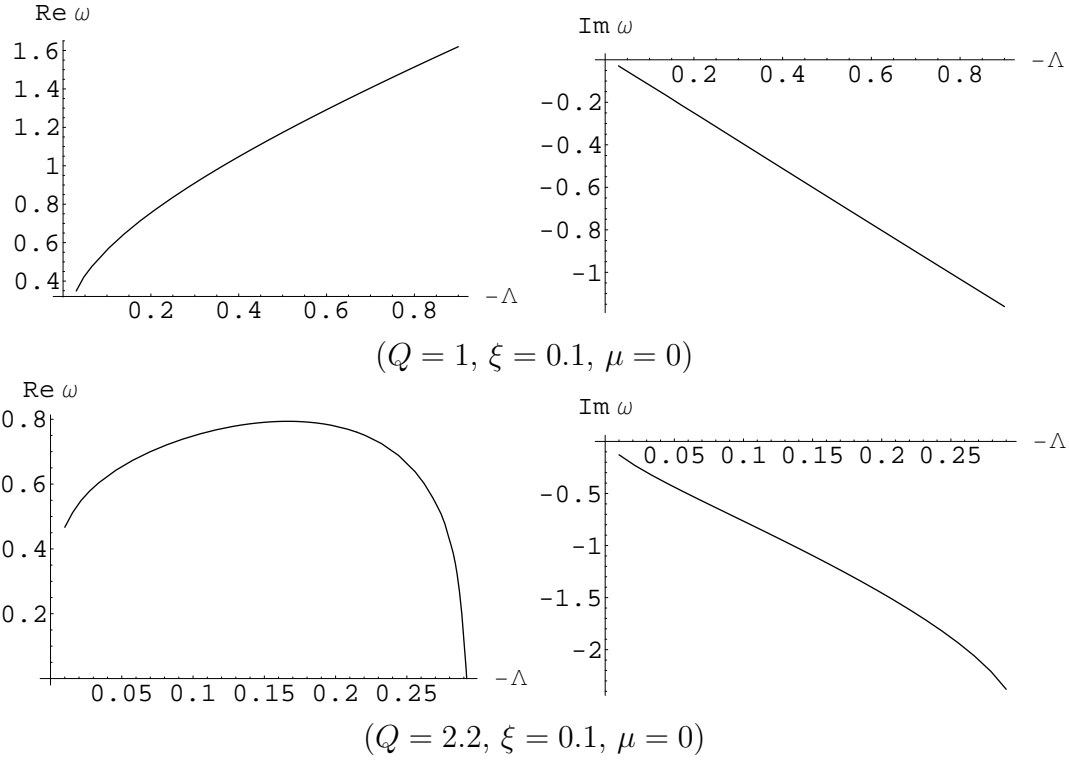


Figure 7.3: **Dependance of the real and imaginary parts of the quasi-normal frequency on Λ for the scalar hairy black hole.** The real part increases for relatively small “scalar charges” Q , but for large $Q = 2.2$ it also reaches maximum and then falls down and vanishes for $\Lambda \approx -0.292$. For larger values of Λ the real part remains zero and purely imaginary frequencies exist. The imaginary part decreases almost linearly as Λ grows.

coupled to a dynamical time-like vector field, which is called “aether”. This theory is what comes instead of usual general relativity when local Lorentz symmetry is broken. Namely, the vector field breaks local boost invariance, while rotational symmetry in the preferred frame is preserved (see [4] for review).

It is important that the significant difference between Einstein and Einstein-Aether theories should be seen in the regime of strong field, for instance in observing of the characteristic quasi-normal spectrum of black holes. Thus, existence of aether could be tested in the forthcoming experiments with new generation of gravitational antennas. In this context, the quasi-normal spectrum for test scalar and electromagnetic fields [16] and for the gravitational perturbations [19] was studied.

The solution for a black hole metric in the Einstein-Aether theory was found numerically in [126, 127]. Since the analytical solution is not known, in order to calculate the quasi-normal modes, one can apply the fitting of the effective potential as described in the section 7.1.

The Lagrangian of the full Einstein-Aether theory that forms the most general diffeomorphism invariant action of the space-time metric g_{ab} and the aether field u^a , involving no more than two derivatives, is given by

$$L = -R - K^{ab}{}_{mn} \nabla_a u^m \nabla_b u^n - \lambda(g_{ab} u^a u^b - 1), \quad (7.10)$$

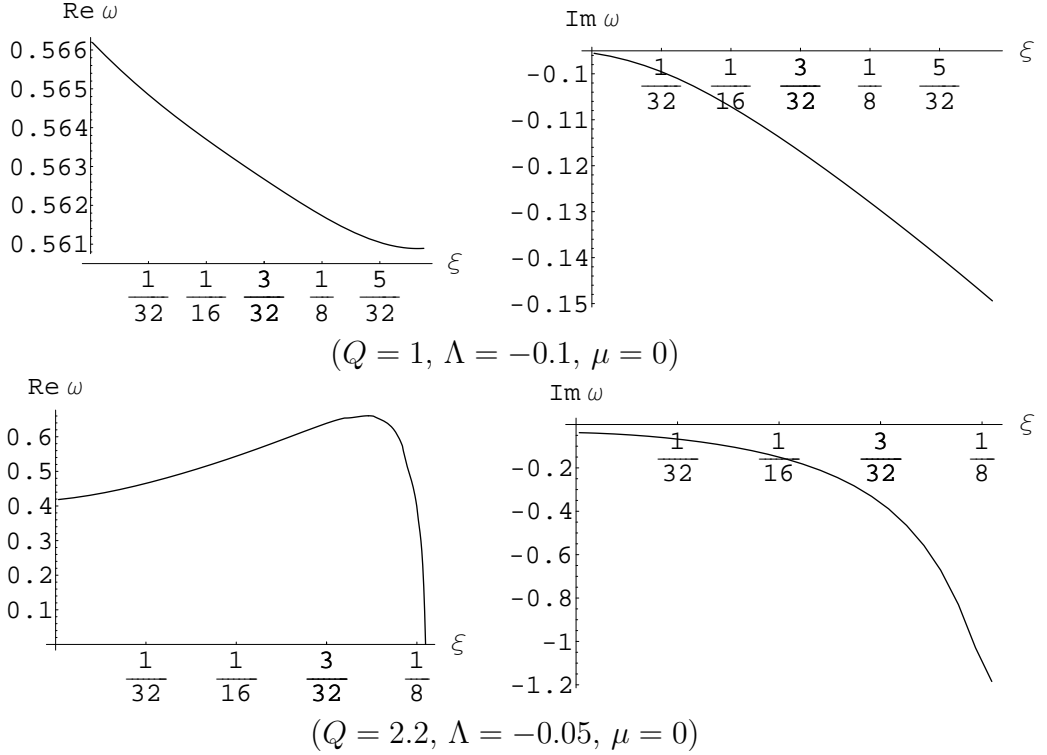


Figure 7.4: **Dependance of the real and imaginary parts of the quasi-normal frequency on $\xi < \frac{3}{16}$ for the scalar hairy black hole.** The imaginary part decreases as ξ grows. The quickness of such decreasing depends on Λ and Q . For some Λ and Q (as presented on the bottom graphic) the real part can fall down to zero and purely imaginary frequencies appear for larger ξ .

where R is the Ricci scalar, λ is a Lagrange multiplier, which provides the unit time-like constraint,

$$K^{ab}{}_{mn} = c_1 g^{ab} g_{mn} + c_2 \delta_m^a \delta_n^b + c_3 \delta_n^a \delta_m^b + c_4 u^a u^b g_{mn},$$

where c_i are dimensionless constants.

Spherical symmetry allows to fix $c_4 = 0$. Following [126, 127], we shall consider the so-called *non-reduced* Einstein-Aether theory, for which $c_3 = 0$, and we can use the field redefinition that fixes the coefficient c_2 :

$$c_2 = -\frac{c_1^3}{2 - 4c_1 + 3c_1^2},$$

so that c_1 is the free parameter.

The metric for a spherically symmetric static black hole is

$$ds^2 = N(r)dt^2 - \frac{B^2(r)}{N(r)}dr^2 - r^2 d\Omega^2, \quad (7.11)$$

where the functions $N(r)$ and $B(r)$ are given by numerical integration near the black hole event horizon.

The perturbation equations can be reduced to the wave-like form (2.10) with the effective po-

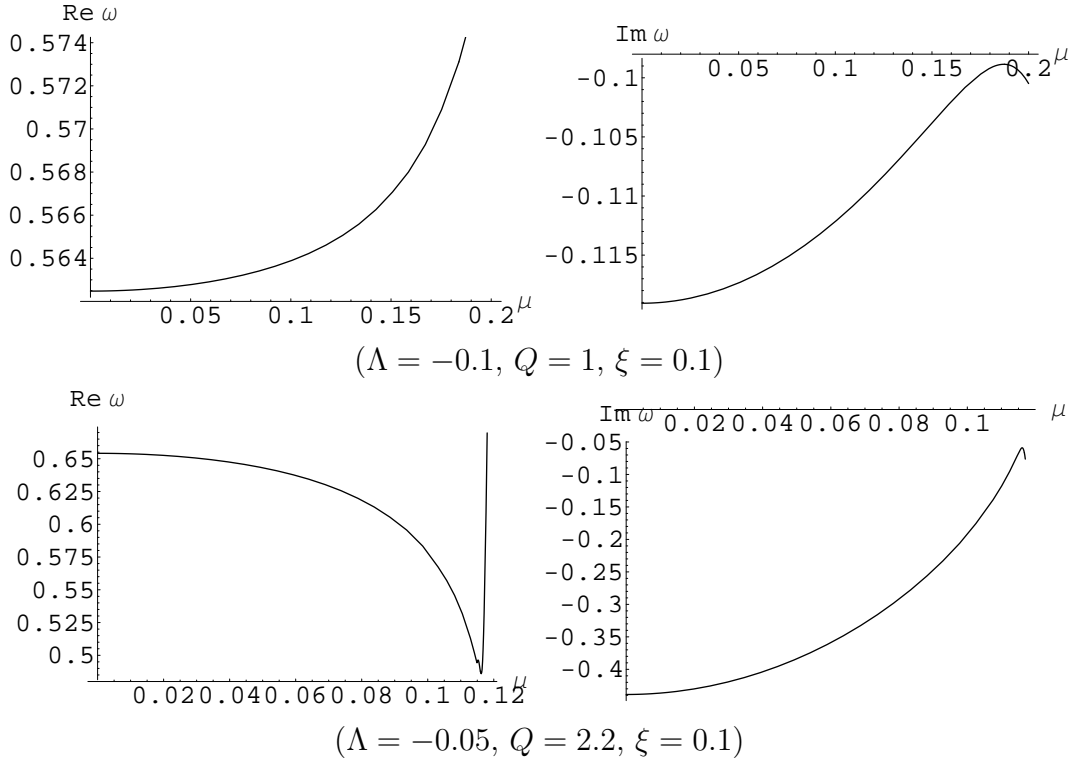


Figure 7.5: **Dependance of the real and imaginary parts of the quasi-normal frequency on μ for the scalar hairy black hole.** We consider only $0 \leq \mu^2 \leq -4\xi\Lambda$. The real part changes within comparatively small range. The imaginary part reaches its maximum remaining negative. For this value of μ the oscillations have the longest lifetime, but they still damp and we do not observe quasi-resonances. For larger scalar field masses the imaginary part of frequency decreases and the damping rate is higher.

tentials

$$V_s = N(r) \frac{l(l+1)}{r^2} + \frac{1}{r} \frac{d}{dr_*} \frac{N(r)}{B(r)}, \quad l = 0, 1, 2, \dots, \quad (7.12a)$$

$$V_e = N(r) \frac{l(l+1)}{r^2}, \quad l = 1, 2, 3, \dots, \quad (7.12b)$$

$$V_g = N(r) \frac{(l+2)(l-1)}{r^2} + \frac{2N^2(r)}{B^2(r)r^2} - \frac{1}{r} \frac{d}{dr_*} \frac{N(r)}{B(r)}, \quad l = 2, 3, 4, \dots, \quad (7.12c)$$

for scalar, Maxwell and axial gravitational perturbations respectively.

The tortoise coordinate is defined as

$$dr_* = \frac{B(r)}{N(r)} dr.$$

Note, that since the background value of aether coupling is small in comparison with the background characteristics of large black hole, the Schwarzschild metric is slightly corrected by the aether. That is why, when considering perturbations of the metric we neglect small perturbations of aether, keeping only linear perturbations of the Ricci tensor.

Since $N(r)$ and $B(r)$ are known numerically, we can use the fitting technique [16]. The fit functions for $N(r)$ and $B(r)$ were chosen as fractions of two polynomials, which are characterised

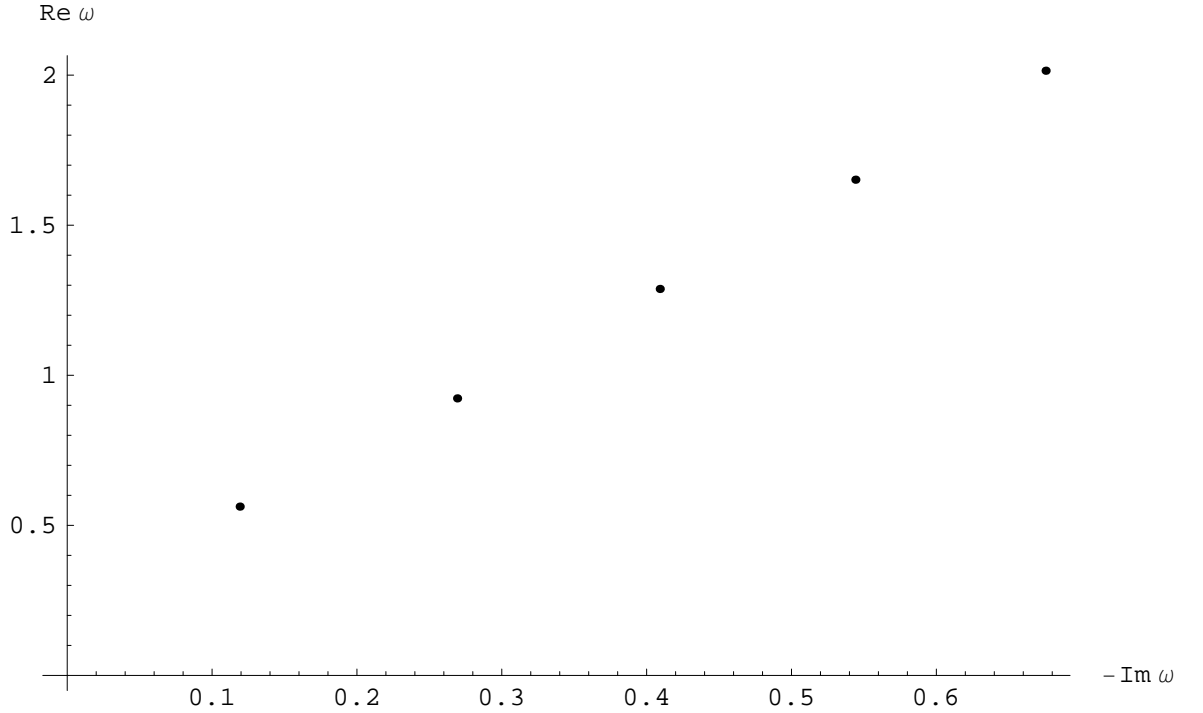


Figure 7.6: **First five quasi-normal frequencies for the scalar hairy black hole** $\Lambda = -0.1$, $Q = 1$, $\xi = 0.1$, $\mu = 0$. The high overtones approach equidistant spacing.

by the number of terms in their numerators and denominators. There is some optimal number for which the convergence of WKB series is best. Practically, in order to find optimal number of terms for $N(r)$ we search for minimal difference between third and sixth order WKB values, first for the case $B(r) = 1$. When we have found the optimal fit for $N(r)$, in a similar fashion, i.e., by looking for best WKB convergence, we are in position to find the optimal fit for $B(r)$. Quick WKB convergence shows that higher derivatives of the metric coefficients are calculated with the best accuracy.

We find that as c_1 grows, the fundamental quasi-normal frequency increases the absolute value of its real and imaginary parts. This was checked also in time-domain [19]. On the figure 7.7 we see, that for higher c_1 the oscillation period and the lifetime of the perturbations decrease. We conclude that aether, if it exists, could be indirectly observed through detection of characteristic spectrum of black holes.

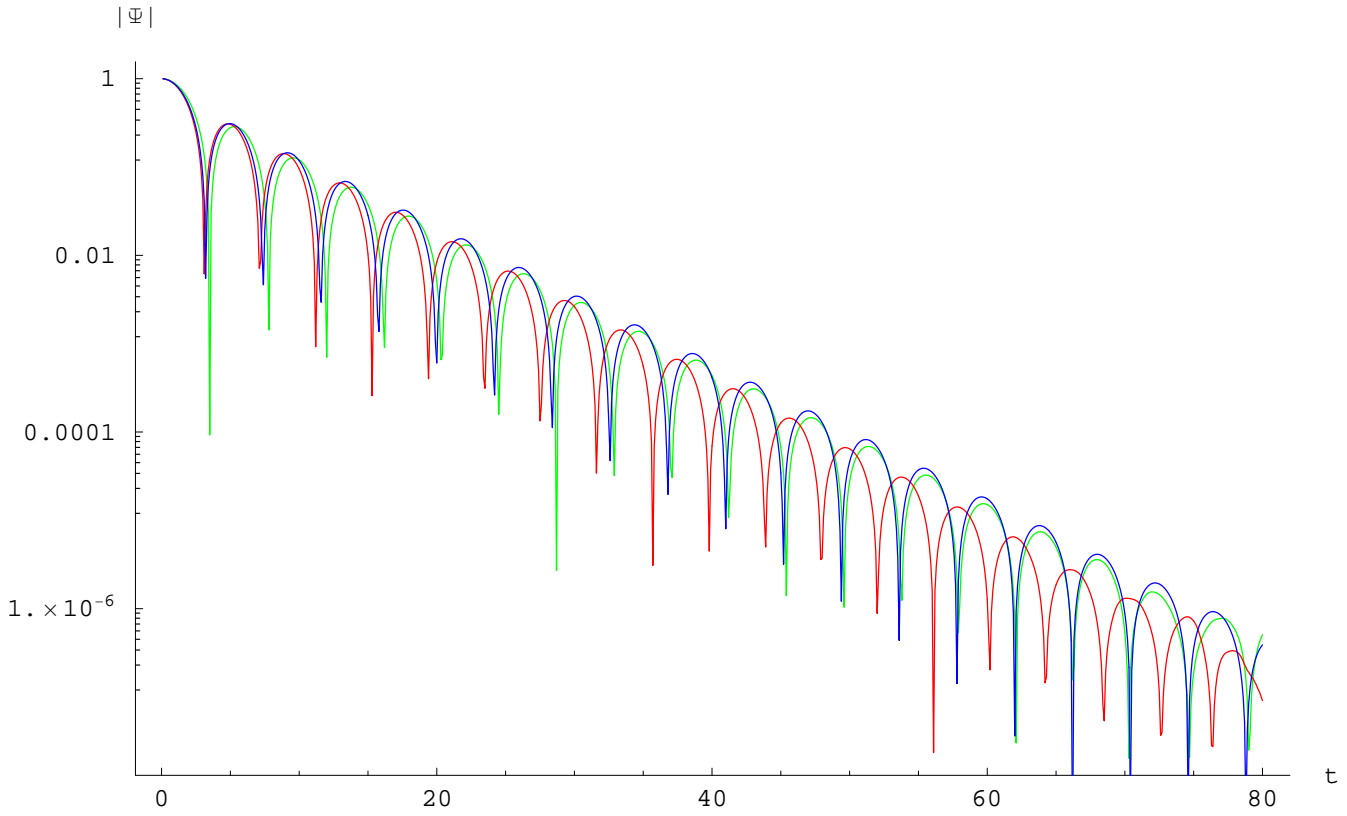


Figure 7.7: Evolution of axial gravitational perturbations ($l = 2$) in time domain for non-reduced Einstein-Aether theory, $c_1 = 0.1$ (green line) and $c_1 = 0.4$ (red line), in comparison with the Schwarzschild case $c_1 = 0$ (blue line). The higher c_1 is the quicker decay of the observed perturbations.

Chapter 8

Perturbations of Schwarzschild black holes in laboratories

8.1 Acoustic analogue of gravity

In addition to the possibility to observe quasi-normal modes of black holes with the help of a new generation of gravitational antennas, there is a window for observation of the acoustic analogue of a black hole in laboratories. This is the well-known Unruh analogue of black holes [128, 129], which are the apparent horizons appearing in a fluid with a space-dependent velocity, in the presence of sonic points. The wave, which passed through the sonic point, cannot propagate backward, mimicking thereby, the effect of the horizon at sonic points.

The dynamic of sound waves in a fluid can be described by the propagation of a scalar field in some effective background. It turns out, that steady spherically symmetric flow cannot reproduce the Schwarzschild geometry because of the equation of continuity (see [130] for review). One could construct either an acoustic analog, which is conformal to the Schwarzschild black hole,

$$ds^2 \propto r^{-3/2} \left(\left(1 - \frac{r_+}{r}\right) dt^2 - \left(1 - \frac{r_+}{r}\right)^{-1} dr^2 - r^2(d\theta^2 + \sin^2\theta d\phi^2) \right), \quad (8.1)$$

or an exact analog to the 7-dimensional black hole, projected on the 4-brane (see section 5.3)

$$ds^2 = \left(1 - \left(\frac{r_+}{r}\right)^4\right) dt^2 - \left(1 - \left(\frac{r_+}{r}\right)^4\right)^{-1} dr^2 - r^2(d\theta^2 + \sin^2\theta d\phi^2). \quad (8.2)$$

If one had a complete analogy with some known solution of the Einstein equations, say, the Schwarzschild solution, he could see, in the acoustic experiments, not only qualitative, but also, up to an experimental accuracy, exact numerical coincidence with a prototype characteristics. Namely, for quasi-normal modes, which are governed by the form of the wave equation, this numerical correspondence would mean that the effective potential of the perturbations of some hydrodynamic system coincides with an effective potential of the black hole. Fortunately, the consideration of the perturbations of a gas in de Laval nozzle [131] gives us such an opportunity of finding a system that obeys the same effective potential as a Schwarzschild black hole does [21].

8.2 de Laval nozzle

The canonical de Laval nozzle is a convergent-divergent tube, narrow in the middle. It allows to accelerate the gas until the sonic speed in its throat, reaching supersonic speeds after passing

the throat. The perturbations of the gas in de Laval nozzle can be considered as one-dimensional if the section does not change too quickly along the length of the nozzle. Let us show that the corresponding effective potential for perturbations in a canonical de Laval nozzle can be made equal to the potential for perturbations of Schwarzschild black holes, when choosing some specific form of the nozzle.

We assume that a gas in the nozzle can be described by the equations of motion for the perfect fluid and that the flow is quasi-one-dimensional. The equations of continuity, the momentum and energy conservation read respectively

$$\partial_t(\rho A) + \partial_x(\rho v A) = 0, \quad (8.3a)$$

$$\partial_t(\rho v A) + \partial_x[(\rho v^2 + p)A] = 0, \quad (8.3b)$$

$$\partial_t(\epsilon A) + \partial_x[(\epsilon + p)vA] = 0. \quad (8.3c)$$

Here ρ is the density, v is the fluid velocity, p is the pressure, A is the cross section of the nozzle, and

$$\epsilon = \frac{1}{2}\rho v^2 + \frac{p}{\gamma - 1} \quad (8.4)$$

is the energy density. The heat capacity ratio for di-atomic molecules of air is

$$\gamma = 1 + 2/n = 7/5 = 1.4 \quad (n = 5).$$

We shall assume that the flow has no entropy discontinuity. Then the fluid is isentropic

$$p \propto \rho^\gamma. \quad (8.5)$$

Instead of (8.3b), we can use the Euler equation

$$\rho(\partial_t + v\partial_x)v = -\partial_x p. \quad (8.6)$$

For isentropic fluid, (8.6) is reduced to the Bernoulli equation

$$\partial_t \Phi + \frac{1}{2}(\partial_x \Phi)^2 + h(\rho) = 0, \quad (8.7)$$

where $h(\rho) \equiv \int \rho^{-1} dp$ is the specific enthalpy and $\Phi = \int v dx$ is the velocity potential.

According to [131], the perturbation equations in such a nozzle can be reduced to

$$\left[\frac{d^2}{dx^{*2}} + \kappa^2 - V(x^*) \right] H_\omega = 0, \quad (8.8)$$

$$\kappa = \frac{\omega}{c_{s0}}, \quad (8.9)$$

$$V(x^*) = \frac{1}{g^2} \left[\frac{g}{2} \frac{d^2 g}{dx^{*2}} - \frac{1}{4} \left(\frac{dg}{dx^*} \right)^2 \right]. \quad (8.10)$$

Here $c_{s0} = \sqrt{\gamma RT/\mu}$ is the stagnation sound speed, which is used to measure x^* in meters. The variable x^* is an acoustic analogue of the tortoise coordinate which satisfies

$$x^*(x = +\infty) = +\infty, \quad x^*(x = 0) = -\infty,$$

namely,

$$x^* = c_{s0} \int \frac{c_s dx}{c_s^2 - v^2}. \quad (8.11)$$

The function H_ω represents small perturbations of the gas flow,

$$H_\omega(x) = g^{1/2} \int dt e^{i\omega(t-f(x))} \phi(t, x), \quad (8.12)$$

$$g = \frac{\rho A}{c_s}, \quad (8.13)$$

$$f(x) = \int \frac{|v| dx}{c_s^2 - v^2}. \quad (8.14)$$

The sound speed is given by

$$c_s^2 = \frac{dp}{d\rho} = \frac{\gamma p}{\rho}. \quad (8.15)$$

Since (8.8) is invariant with respect to the re-scaling of g , we can fix the coefficients in (8.13) arbitrarily:

$$g = \frac{\rho A}{2\rho^{(\gamma-1)/2}}. \quad (8.16)$$

Up to a coefficient, A can be found in terms of ρ as [21]

$$A^{-1} = (1 - \rho^{(\gamma-1)})^{1/2} \rho. \quad (8.17)$$

We find

$$g = \frac{\rho^{(1-\gamma)/2}}{2(1 - \rho^{(\gamma-1)})^{1/2}} = \frac{\rho^{(1-\gamma)}}{2(\rho^{(1-\gamma)} - 1)^{1/2}}. \quad (8.18)$$

Hence it follows that

$$\rho^{1-\gamma} = 2g^2 \left(1 \pm \sqrt{1 - g^{-2}}\right). \quad (8.19)$$

The sign in (8.19) should be chosen in order that ρ be a monotonous function with respect to the transverse coordinate. As we will show later, the function g for the Schwarzschild black hole can be chosen also monotonous in the R region, finite at the horizon and infinite at the spatial infinity. Therefore, we choose the minus sign,

$$\rho^{1-\gamma} = 2g^2 \left(1 - \sqrt{1 - g^{-2}}\right), \quad g > 1. \quad (8.20)$$

Substituting (8.19) into (8.17), we find the cross-section area as a function of g ,

$$A = \frac{\sqrt{2} \left(2g^2 \left(1 - \sqrt{1 - g^{-2}}\right)\right)^{1/(\gamma-1)}}{\sqrt{1 - \sqrt{1 - g^{-2}}}}. \quad (8.21)$$

For the steady isentropic flow, (8.7) can be rewritten as

$$\frac{v^2}{c_s^2} = \frac{2}{\gamma-1} (\rho^{1-\gamma} - 1) = \frac{2}{\gamma-1} \left(2g^2 \left(1 - \sqrt{1 - g^{-2}}\right) - 1\right). \quad (8.22)$$

Since $v = c_s$ at the event horizon, g must be finite there, and

$$g \Big|_{e.h.} = \frac{\gamma+1}{2\sqrt{2}\sqrt{\gamma-1}} = \frac{3}{\sqrt{5}} > 1. \quad (8.23)$$

This requirement fixes both constants of integration.

8.3 de Laval nozzle for the Schwarzschild black hole

Since g allows to find the cross section A and, thereby, the form of de Laval nozzle, if we find such $g(x)$ that leads to the same expression for the nozzle potential (8.8), as the effective potential for the Schwarzschild black hole [21],

$$V(r) = \left(1 - \frac{1}{r}\right) \left(\frac{l(l+1)}{r^2} + \frac{1-s^2}{r^3}\right), \quad (r_+ = 1), \quad (8.24)$$

where $l \geq s$ is the multipole integer number. The integer $s = 0, 1, 2$ describes the perturbations of fields of different spin: $s = 0$ for the test scalar field, $s = 1$ for the Maxwell field and $s = 2$ for the gravitational perturbations of axial type.

In order to find g that produces the required potential (8.24), we identify the ‘‘tortoise’’ coordinates of the black hole solution and of de Laval nozzle

$$dr^* = dx^* = \frac{\rho^{(1-\gamma)/2} dx}{1 - v^2/c_s^2} = \frac{\sqrt{2g^2(1 - \sqrt{1 - g^{-2}})} dx}{1 - \frac{2}{\gamma-1} \left(2g^2(1 - \sqrt{1 - g^{-2}}) - 1\right)}. \quad (8.25)$$

The equation (8.25) relates the real coordinate of the nozzle x and the radial coordinate of the Schwarzschild solution r . It is convenient because we are able to find the equation for $g(r)$ explicitly,

$$\frac{f(r)f'(r)g'(r) + f(r)^2g''(r)}{2g(r)} - \frac{f(r)^2g'(r)^2}{4g(r)^2} = V(r). \quad (8.26)$$

This implies that the form of de Laval nozzle is parameterised by r and $x^*(r) = r^*(r)$. Note, that as we chose the radius of the event horizon to be unity, the nozzle coordinate x is measured in the units of the radius of the event horizon.

The general solution of the equation (8.26) contains two arbitrary constants. They can be fixed in a unique way by the condition (8.23). Namely, the requirement that the solution must be finite at $r = 1$ fixes one of the constants. Then the other constant re-scales $g(r)$, and must be fixed by its value at $r = 1$. Finally, the solution of (8.26), for arbitrary l and s , that satisfies (8.23), is given by the following formula,

$$\begin{aligned} g(r) &= \frac{\gamma + 1}{2\sqrt{2}\sqrt{\gamma-1}} \sum_{n=s}^l \left(\frac{(-1)^{n+s}(l+n)!}{(n+s)!(n-s)!(l-n)!} r^{n+1} \right)^2 = \\ &= \frac{\gamma + 1}{2\sqrt{2}\sqrt{\gamma-1}} r^{2s+2} \left(\frac{\Gamma(1+l+s)_2F_1(s-l, s+l+1, 1+2s, r)}{\Gamma(1+l-s)\Gamma(1+2s)} \right)^2. \end{aligned} \quad (8.27)$$

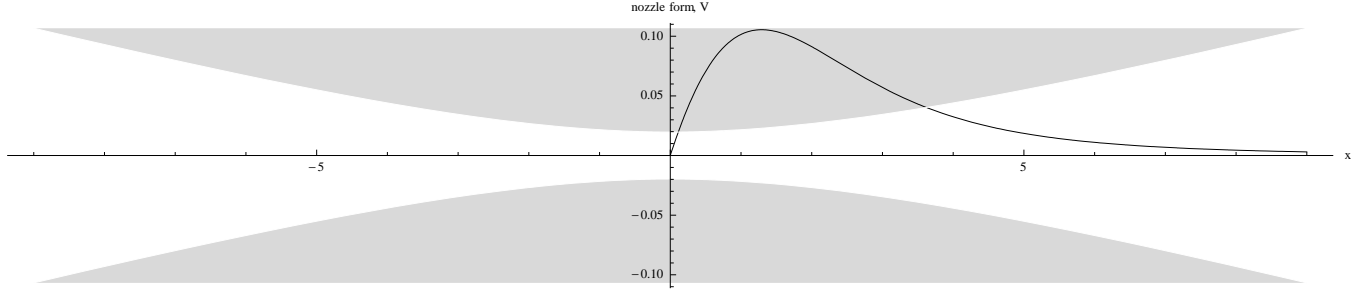
One can easily check that the above solution indeed satisfies the equation (8.23), for any fixed l and s .

The equation (8.25) allows to find the dependance of the transversal nozzle coordinate x on the parameter r ,

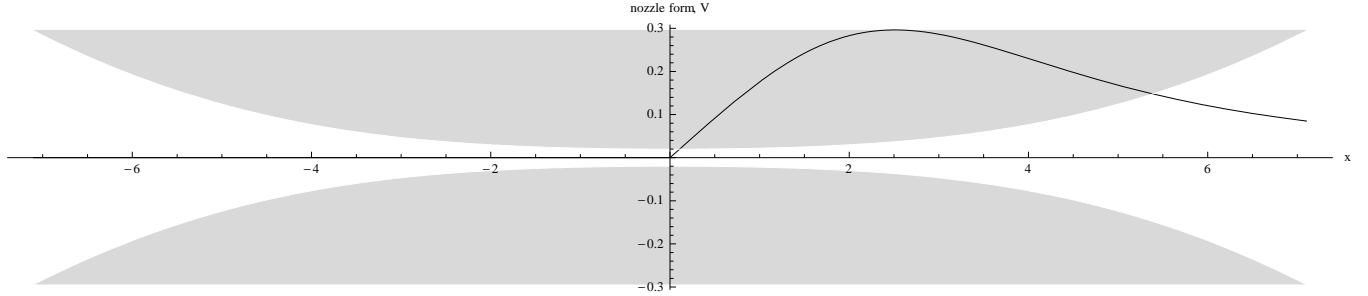
$$x = \int_1^r \frac{\left(\gamma + 1 - 4g(r)^2 \left(1 - \sqrt{1 - g(r)^{-2}}\right)\right) dr}{f(r)(\gamma - 1)\sqrt{2g(r)^2 \left(1 - \sqrt{1 - g(r)^{-2}}\right)}}. \quad (8.28)$$

The integration constant is chosen so that x vanishes at the sonic point.

$$s = l = 0$$



$$s = l = 1$$



$$s = l = 2$$

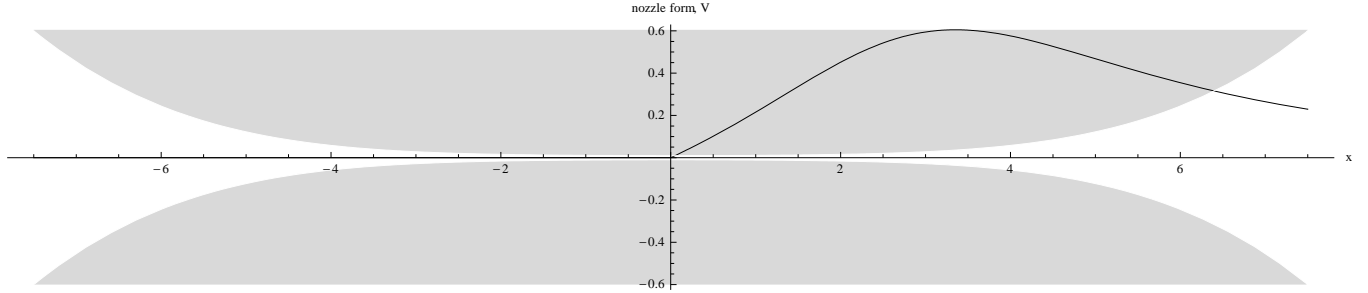


Figure 8.1: The form of de Laval nozzles and the effective potential in the nozzle coordinates.

Now we are in position to find the required form of de Laval nozzle. i.e. to find its cross-section $A(x)$. We just need to replace $g(r)$ given in (8.27) and go over to the transverse nozzle coordinate x . The radius of the de Laval nozzle as a function of the transverse coordinate x is shown in figure 8.1. Note that the canonical de Laval nozzle is diverging at the end of the flow trajectory, so that $A_{x=\infty} = \infty$. Indeed, the formula (8.27) implies divergence at least as $\sim r^2$. Nevertheless, the diverging of the nozzle still let us keep the one-dimensional representation of the motion, because x is measured in units of black hole radius, i.e. one can “pull” the nozzle along the transverse coordinate x in order to make the area of the nozzle change as slowly as one wishes. Such a “pulling” simply means that we are getting the correspondence with a larger black hole.

In a similar fashion, one can find the de Laval nozzle form for the gravitational perturbations of polar type [21]. The form of the nozzles for modeling polar and axial gravitational perturbations are very slightly different.

It should be recalled also that the *precise* acoustic analogy is only established for a scalar field. To be able to reproduce the potential $V(r)$ for fields of different spins, certainly, does not mean that one can reproduce all the characteristics of those fields in an acoustic model.

The obtained acoustic analogue for the perturbations of the Schwarzschild black holes is not limited by quasi-normal mode problems only, but allow general investigation of propagation of

fields, including such processes as scattering and tunneling of waves and particles.

Chapter 9

Summary

Let us summarise the results of this dissertation.

- We have performed the complete study of the influence of the cosmological constant on the quasi-normal spectrum of the Schwarzschild black hole for fields of various spins. We have found that the presence of the cosmological constant decreases the absolute value of the real and imaginary parts of quasi-normal frequencies. Also we have found analytically the large multipole limit for quasi-normal frequencies of Schwarzschild-de Sitter black holes (sec. 4.1).

- We have studied the behavior of high overtones for the massless Dirac and massive scalar fields in the Schwarzschild background and for the test electromagnetic field and gravitational perturbations of the Schwarzschild-de Sitter black hole. We have shown numerically that the real part of the quasi-normal frequency asymptotically approaches zero for the Dirac and electromagnetic fields, but has an oscillatory behavior for the gravitational perturbations of the Schwarzschild-de Sitter black hole. These results were confirmed later analytically (sec. 4.2). The behavior of high overtones for the massive scalar field was studied both analytically and numerically. We have shown that the asymptotical behavior does not depend on the mass of the field, coinciding with the known analytical formula for the massless scalar field (sec. 6.2).

- We have investigated the quasi-normal spectrum of the electrically charged scalar and Dirac fields in the background of the Kerr-Newman-de Sitter black hole. Special attention was paid to the influence of the electromagnetic interaction between the black hole and the test field upon the quasi-normal spectrum (sec. 4.3).

- We have studied the quasi-normal spectrum of gravitational perturbations of the neutral and electrically charged black holes in higher dimensions with a positive cosmological constant. We have considered all kinds of the perturbations and prove that higher dimensional Schwarzschild-de Sitter black holes are stable. We have shown that the higher dimensional black hole is unstable if both the black hole charge and the cosmological constant are large enough. We have found the parametrical region of the instability (sec. 5.1).

- We have considered gravitational perturbations of higher dimensional black holes in the Einstein-Gauss-Bonnet theory. We have found that the presence of the Gauss-Bonnet parameter decreases the imaginary part of quasi-normal frequencies, causing the oscillations be longer-lived. Also we have studied the developing of instability of Gauss-Bonnet black holes in five and six dimensions (sec. 5.2).

- We have found quasi-normal modes and late-time tails of the rotating black holes and the non-rotating Gauss-Bonnet black holes for the Standard Model fields localised on a 4-brane (sec. 5.3).

- We have studied quasi-normal modes of the Kaluza-Klein black holes with squashed hori-

zons. We have considered the test scalar field near rotating squashed Kaluza-Klein black holes and gravitational perturbations of non-rotating squashed Kaluza-Klein black holes (sec. 5.4).

- We have calculated the quasi-normal spectra of the massive scalar field in the backgrounds of the Tangherlini black hole (sec. 6.2), the Kerr black hole (sec. 6.3) and the scalar hairy asymptotically anti-de Sitter black hole (sec. 7.2). We have found that the massive scalar field is stable in these backgrounds and provided a comprehensive discussions about properties of their quasi-normal spectrum and quasi-resonances (sec. 6.1). Also we have studied the late-time tails for the massive vector field in the Schwarzschild background and found that the asymptotically late-time decay law does not depend on the spin of the massive field (sec. 6.5).

- We have found quasi-normal modes and tails of the gravitational perturbations of black strings. Also we have considered the developing of the long-wavelength instability of a black string in time domain (sec. 6.4).

- We have studied the influence of the local Lorentz symmetry breaking within the Einstein-Aether theory on the quasi-normal spectrum of the Schwarzschild black hole. We have found that the presence of the aether increases the absolute value of the real and imaginary parts of the fundamental quasi-normal frequency (sec. 7.3).

- We have proposed a possibility of observation of the acoustic analogue of the Schwarzschild black hole in a de Laval nozzle. We have found the particular forms of the de Laval nozzles for which the effective potentials will coincide with the effective potentials for test fields or gravitational perturbations of the Schwarzschild black hole (chapter 8).

- We have developed two new numerical tools:

- 1) the generalisation of the Nollert improvement of the Frobenius method for higher dimensional problems, which provides better convergence of the numerical procedure (sec. 3.4).

- 2) the method for the calculation of the quasi-normal frequencies of a black hole, which metric is not known analytically, but can be found as a numerical solution of a set of differential equations (sec. 7.1).

All the results reported here were obtained by us for the first time, and are, thereby, new.

Bibliography

- [1] E. E. Flanagan, (1997), [gr-qc/9804024].
- [2] P. Anninos, D. Hobill, E. Seidel, L. Smarr, and W.-M. Suen, Phys. Rev. Lett. **71**, 2851 (1993).
- [3] C. V. Vishveshwara, Nature **227**, 936 (1970).
- [4] C. Eling, T. Jacobson, and D. Mattingly, (2004), [gr-qc/0410001].
- [5] R. Emparan and H. S. Reall, Living Rev. Rel. **11**, 6 (2008), [0801.3471].
- [6] J. M. Maldacena, Adv. Theor. Math. Phys. **2**, 231 (1998), [hep-th/9711200].
- [7] G. T. Horowitz and V. E. Hubeny, Phys. Rev. **D62**, 024027 (2000), [hep-th/9909056].
- [8] G. Policastro, D. T. Son, and A. O. Starinets, JHEP **09**, 043 (2002), [hep-th/0205052].
- [9] A. Zhidenko, Class. Quant. Grav. **21**, 273 (2004), [gr-qc/0307012].
- [10] R. A. Konoplya and A. Zhidenko, JHEP **06**, 037 (2004), [hep-th/0402080].
- [11] K. H. C. Castello-Branco, R. A. Konoplya, and A. Zhidenko, Phys. Rev. **D71**, 047502 (2005), [hep-th/0411055].
- [12] R. A. Konoplya and A. V. Zhidenko, Phys. Lett. **B609**, 377 (2005), [gr-qc/0411059].
- [13] A. Zhidenko, Class. Quant. Grav. **23**, 3155 (2006), [gr-qc/0510039].
- [14] R. A. Konoplya and A. Zhidenko, Phys. Rev. **D73**, 124040 (2006), [gr-qc/0605013].
- [15] R. A. Konoplya, C. Molina, and A. Zhidenko, Phys. Rev. **D75**, 084004 (2007), [gr-qc/0602047].
- [16] R. A. Konoplya and A. Zhidenko, Phys. Lett. **B644**, 186 (2007), [gr-qc/0605082].
- [17] P. Kanti, R. A. Konoplya, and A. Zhidenko, Phys. Rev. **D74**, 064008 (2006), [gr-qc/0607048].
- [18] A. Zhidenko, Phys. Rev. **D74**, 064017 (2006), [gr-qc/0607133].
- [19] R. A. Konoplya and A. Zhidenko, Phys. Lett. **B648**, 236 (2007), [hep-th/0611226].
- [20] R. A. Konoplya and A. Zhidenko, Nucl. Phys. **B777**, 182 (2007), [hep-th/0703231].
- [21] E. Abdalla, R. A. Konoplya, and A. Zhidenko, Class. Quant. Grav. **24**, 5901 (2007), [0706.2489].
- [22] R. A. Konoplya and A. Zhidenko, Phys. Rev. **D76**, 084018 (2007), [0707.1890].

- [23] R. A. Konoplya and A. Zhidenko, Phys. Rev. **D77**, 104004 (2008), [0802.0267].
- [24] H. Ishihara, M. Kimura, R. A. Konoplya, K. Murata, J. Soda and A. Zhidenko, Phys. Rev. **D77**, 084019 (2008), [0802.0655].
- [25] A. Zhidenko, Phys. Rev. **D78**, 024007 (2008), [0802.2262].
- [26] R. A. Konoplya, K. Murata, J. Soda, and A. Zhidenko, Phys. Rev. **D78**, 084012 (2008), [0807.1897].
- [27] R. A. Konoplya and A. Zhidenko, (2008), [0809.2822].
- [28] A. Zhidenko, (2007), [0705.2254].
- [29] D. R. Brill and J. A. Wheeler, Rev. Mod. Phys. **29**, 465 (1957).
- [30] F. Mellor and I. Moss, Phys. Rev. **D41**, 403 (1990).
- [31] T. Regge and J. A. Wheeler, Phys. Rev. **108**, 1063 (1957).
- [32] H. Kodama and A. Ishibashi, Prog. Theor. Phys. **110**, 701 (2003), [hep-th/0305147].
- [33] S. Chandrasekhar, *The Mathematical Theory of Black Holes* (Oxford University Press, New York, 1983).
- [34] H.-P. Nollert, Class. Quant. Grav. **16**, R159 (1999).
- [35] C. Gundlach, R. H. Price, and J. Pullin, Phys. Rev. **D49**, 883 (1994), [gr-qc/9307009].
- [36] P. R. Brady, C. M. Chambers, W. Krivan, and P. Laguna, Phys. Rev. **D55**, 7538 (1997), [gr-qc/9611056].
- [37] P. R. Brady, C. M. Chambers, W. G. Laarakkers, and E. Poisson, Phys. Rev. **D60**, 064003 (1999), [gr-qc/9902010].
- [38] P. K. Kovtun and A. O. Starinets, Phys. Rev. **D72**, 086009 (2005), [hep-th/0506184].
- [39] H. Kodama and A. Ishibashi, (2003), [gr-qc/0312012].
- [40] E. Berti, V. Cardoso, J. A. Gonzalez, and U. Sperhake, Phys. Rev. **D75**, 124017 (2007), [gr-qc/0701086].
- [41] E. Abdalla and D. Giugno, Braz. J. Phys. **37**, 450 (2007), [gr-qc/0611023].
- [42] H.-J. Blome and B. Mashhoon, Phys. Lett. A **100**, 231 (1984).
- [43] V. Ferrari and B. Mashhoon, Phys. Rev. Lett. **52**, 1361 (1984).
- [44] G. Pöschl and E. Teller, Z. Phys. **83**, 143 (1933).
- [45] V. Cardoso and J. P. S. Lemos, Phys. Rev. **D67**, 084020 (2003), [gr-qc/0301078].
- [46] C. Molina, Phys. Rev. **D68**, 064007 (2003), [gr-qc/0304053].
- [47] B. Schutz and C. Will, Astrophys. J. Lett. **291**, L33 (1985).

- [48] S. Iyer and C. M. Will, *Phys. Rev. D* **35**, 3621 (1987).
- [49] R. A. Konoplya, *Phys. Rev.* **D68**, 024018 (2003), [gr-qc/0303052].
- [50] R. A. Konoplya, *Phys. Rev.* **D68**, 124017 (2003), [hep-th/0309030].
- [51] R. A. Konoplya, *J. Phys. Stud.* **8**, 93 (2004).
- [52] N. Froeman, P. O. Froeman, N. Andersson, and A. Hoekback, *Phys. Rev.* **D45**, 2609 (1992).
- [53] E. W. Leaver, *Proc. Roy. Soc. Lond.* **A402**, 285 (1985).
- [54] H.-P. Nollert, *Phys. Rev. D* **47**, 5253 (1993).
- [55] A. Rostworowski, *Acta Phys. Polon.* **B38**, 81 (2007), [gr-qc/0606110].
- [56] H. Suzuki, E. Takasugi, and H. Umetsu, *Prog. Theor. Phys.* **100**, 491 (1998), [gr-qc/9805064].
- [57] A. Ohashi and M.-a. Sakagami, *Class. Quant. Grav.* **21**, 3973 (2004), [gr-qc/0407009].
- [58] H. Kodama and A. Ishibashi, *Prog. Theor. Phys.* **111**, 29 (2004), [hep-th/0308128].
- [59] A. Ishibashi and H. Kodama, *Prog. Theor. Phys.* **110**, 901 (2003), [hep-th/0305185].
- [60] K. D. Kokkotas and B. G. Schmidt, *Living Rev. Rel.* **2**, 2 (1999), [gr-qc/9909058].
- [61] S. Hod, *Phys. Rev. Lett.* **81**, 4293 (1998).
- [62] J. F. Barbero G., *Phys. Rev.* **D51**, 5507 (1995), [gr-qc/9410014].
- [63] G. Immirzi, *Nucl. Phys. Proc. Suppl.* **57**, 65 (1997), [gr-qc/9701052].
- [64] L. Motl, *Adv. Theor. Math. Phys.* **6**, 1135 (2003), [gr-qc/0212096].
- [65] J.-l. Jing, *Phys. Rev.* **D71**, 124006 (2005), [gr-qc/0502023].
- [66] V. Cardoso, J. Natario, and R. Schiappa, *J. Math. Phys.* **45**, 4698 (2004), [hep-th/0403132].
- [67] S. Hod and T. Piran, *Phys. Rev.* **D58**, 024017 (1998), [gr-qc/9712041].
- [68] S. Hod and T. Piran, *Phys. Rev.* **D58**, 024018 (1998), [gr-qc/9801001].
- [69] R. A. Konoplya, *Phys. Rev.* **D66**, 084007 (2002), [gr-qc/0207028].
- [70] R. A. Konoplya, *Phys. Lett.* **B550**, 117 (2002), [gr-qc/0210105].
- [71] W. Zhou and J.-Y. Zhu, *Int. J. Mod. Phys.* **D13**, 1105 (2004), [gr-qc/0309071].
- [72] J. Jing, *Phys. Rev.* **D72**, 027501 (2005), [gr-qc/0408090].
- [73] X. He and J. Jing, *Nucl. Phys.* **B755**, 313 (2006), [gr-qc/0611003].
- [74] N. Arkani-Hamed, S. Dimopoulos, and G. R. Dvali, *Phys. Lett.* **B429**, 263 (1998), [hep-ph/9803315].

- [75] N. Arkani-Hamed, S. Dimopoulos, and G. R. Dvali, Phys. Rev. **D59**, 086004 (1999), [hep-ph/9807344].
- [76] I. Antoniadis, N. Arkani-Hamed, S. Dimopoulos, and G. R. Dvali, Phys. Lett. **B436**, 257 (1998), [hep-ph/9804398].
- [77] L. Randall and R. Sundrum, Phys. Rev. Lett. **83**, 3370 (1999), [hep-ph/9905221].
- [78] L. Randall and R. Sundrum, Phys. Rev. Lett. **83**, 4690 (1999), [hep-th/9906064].
- [79] E. Abdalla, B. Cuadros-Melgar, A. B. Pavan, and C. Molina, Nucl. Phys. **B752**, 40 (2006), [gr-qc/0604033].
- [80] D. Cremades, L. E. Ibanez, and F. Marchesano, Nucl. Phys. **B643**, 93 (2002), [hep-th/0205074].
- [81] C. Kokorelis, Nucl. Phys. **B677**, 115 (2004), [hep-th/0207234].
- [82] P. C. Argyres, S. Dimopoulos, and J. March-Russell, Phys. Lett. **B441**, 96 (1998), [hep-th/9808138].
- [83] T. Banks and W. Fischler, (1999), [hep-th/9906038].
- [84] S. B. Giddings and S. D. Thomas, Phys. Rev. **D65**, 056010 (2002), [hep-ph/0106219].
- [85] S. Dimopoulos and G. L. Landsberg, Phys. Rev. Lett. **87**, 161602 (2001), [hep-ph/0106295].
- [86] F. R. Tangherlini, Nuovo Cim. **27**, 636 (1963).
- [87] D. G. Boulware and S. Deser, Phys. Rev. Lett. **55**, 2656 (1985).
- [88] R. Konoplya, Phys. Rev. **D71**, 024038 (2005), [hep-th/0410057].
- [89] E. Abdalla, R. A. Konoplya, and C. Molina, Phys. Rev. **D72**, 084006 (2005), [hep-th/0507100].
- [90] G. Dotti and R. J. Gleiser, Phys. Rev. **D72**, 044018 (2005), [gr-qc/0503117].
- [91] R. J. Gleiser and G. Dotti, Phys. Rev. **D72**, 124002 (2005), [gr-qc/0510069].
- [92] M. Beroiz, G. Dotti, and R. J. Gleiser, Phys. Rev. **D76**, 024012 (2007), [hep-th/0703074].
- [93] P. Kanti and J. March-Russell, Phys. Rev. **D66**, 024023 (2002), [hep-ph/0203223].
- [94] P. Kanti and J. March-Russell, Phys. Rev. **D67**, 104019 (2003), [hep-ph/0212199].
- [95] P. Kanti and R. A. Konoplya, Phys. Rev. **D73**, 044002 (2006), [hep-th/0512257].
- [96] P. Kanti, Int. J. Mod. Phys. **A19**, 4899 (2004), [hep-ph/0402168].
- [97] R. C. Myers and M. J. Perry, Ann. Phys. **172**, 304 (1986).
- [98] V. S. Rychkov, Phys. Rev. **D70**, 044003 (2004), [hep-ph/0401116].
- [99] H. Ishihara and J. Soda, Phys. Rev. **D76**, 064022 (2007), [hep-th/0702180].

- [100] M. Kimura, K. Murata, H. Ishihara, and J. Soda, Phys. Rev. **D77**, 064015 (2008), [arXiv:0712.4202 [hep-th]].
- [101] S. Hod and T. Piran, Phys. Rev. **D58**, 044018 (1998), [gr-qc/9801059].
- [102] R. A. Konoplya and R. D. B. Fontana, Phys. Lett. **B659**, 375 (2008), [0707.1156].
- [103] L. E. Simone and C. M. Will, Class. Quant. Grav. **9**, 963 (1992).
- [104] H. T. Cho, Phys. Rev. **D68**, 024003 (2003), [gr-qc/0303078].
- [105] R. A. Konoplya, Phys. Rev. **D73**, 024009 (2006), [gr-qc/0509026].
- [106] H. R. Beyer, Commun. Math. Phys. **221**, 659 (2001), [astro-ph/0008236].
- [107] R. Gregory and R. Laflamme, Phys. Rev. Lett. **70**, 2837 (1993), [hep-th/9301052].
- [108] R. Gregory and R. Laflamme, Nucl. Phys. **B428**, 399 (1994), [hep-th/9404071].
- [109] J. L. Hovdebo and R. C. Myers, Phys. Rev. **D73**, 084013 (2006), [hep-th/0601079].
- [110] R. H. Price, Phys. Rev. **D5**, 2419 (1972).
- [111] R. H. Price, Phys. Rev. **D5**, 2439 (1972).
- [112] J. Bičák, Gen. Relativ. Gravit. **3**, 331 (1972).
- [113] V. Cardoso, S. Yoshida, O. J. C. Dias, and J. P. S. Lemos, Phys. Rev. **D68**, 061503 (2003), [hep-th/0307122].
- [114] P. Bizon, T. Chmaj, and A. Rostworowski, Phys. Rev. **D76**, 124035 (2007), [0708.1769].
- [115] P. Bizon, T. Chmaj, and A. Rostworowski, (2008), [0812.4333].
- [116] H. Koyama and A. Tomimatsu, Phys. Rev. **D64**, 044014 (2001), [gr-qc/0103086].
- [117] H. Koyama and A. Tomimatsu, Phys. Rev. **D65**, 084031 (2002), [gr-qc/0112075].
- [118] R. Moderski and M. Rogatko, Phys. Rev. **D64**, 044024 (2001), [gr-qc/0105056].
- [119] L. M. Burko and G. Khanna, Phys. Rev. **D70**, 044018 (2004), [gr-qc/0403018].
- [120] R. Moderski and M. Rogatko, Phys. Rev. **D72**, 044027 (2005), [hep-th/0508175].
- [121] J. D. Bekenstein, Ann. Phys. **82**, 535 (1974).
- [122] E. Winstanley, Found. Phys. **33**, 111 (2003), [gr-qc/0205092].
- [123] E. Winstanley, Class. Quant. Grav. **22**, 2233 (2005), [gr-qc/0501096].
- [124] E. Radu and E. Winstanley, Phys. Rev. **D72**, 024017 (2005), [gr-qc/0503095].
- [125] V. Cardoso, R. Konoplya, and J. P. S. Lemos, Phys. Rev. **D68**, 044024 (2003), [gr-qc/0305037].
- [126] C. Eling and T. Jacobson, Class. Quant. Grav. **23**, 5625 (2006), [gr-qc/0603058].

- [127] C. Eling and T. Jacobson, *Class. Quant. Grav.* **23**, 5643 (2006), [gr-qc/0604088].
- [128] W. G. Unruh, *Phys. Rev. Lett.* **46**, 1351 (1981).
- [129] W. G. Unruh, *Phys. Rev.* **D51**, 2827 (1995).
- [130] C. Barcelo, S. Liberati, and M. Visser, *Living Rev. Rel.* **8**, 12 (2005), [gr-qc/0505065].
- [131] S. Okuzumi and M.-a. Sakagami, *Phys. Rev.* **D76**, 084027 (2007), [gr-qc/0703070].